SEMINAR

I

Hybrid and Composite Structures

Structures mixtes et hybrides

Verbundtragwerke

Chairman: M. Ito, Japan

Coordinator: R. Favre, Switzerland

General Reporter: J.C. Badoux, Switzerland

Leere Seite
Blank page
Page vide

Mechanical Joints for Composite Construction

Joints mécaniques pour constructions composites

Mechanische Verbindung für Verbundkonstruktionen

Shinichi HINO
Lecturer
Yamaguchi Univ.
Ube, Japan

Toshiaki OHTA
Professor
Kyushu Univ.
Fukuoka, Japan

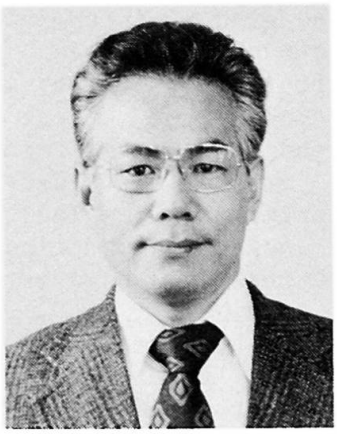

Sumio HAMADA
Professor
Yamaguchi Univ.
Ube, Japan

Fujio IMAI
Assistant
Kyushu Univ.
Fukuoka, Japan

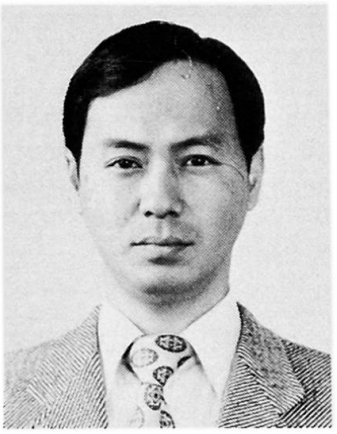

SUMMARY

A new type of composite construction in steel and concrete has attracted special interest recently, because of its economic and structural advantages. In order to find the most suitable joint structure for the above construction, several mechanical joints were investigated and a series of bending tests were carried out on composite beams and slabs with the proposed joints. In addition, an analysis of the joint on the basis of the semi-rigid connection theory is described.

RESUME

Un nouveau type de construction en acier et en béton a créé un intérêt particulier récemment, par ses avantages économiques et structurels. Pour déterminer le type le mieux approprié de ce genre de joints, divers types de joints mécaniques sont proposés, et une série d'essais à la flexion sont effectués sur des poutres et des dalles, avec les joints proposés. De plus, une analyse des joints basée sur le principe de connexion semi-rigide est décrite.

ZUSAMMENFASSUNG

Eine neue Verbundkonstruktion aus Stahl und Beton hat wegen seiner wirtschaftlichen und baulichen Vorteile eine besondere Aufmerksamkeit erregt. Um die zweckmässigste Verbindungsart zu erhalten, wurden mehrere mechanische Verbindungen untersucht und eine Reihe von Biegeversuchen an Verbundträgern und -platten durchgeführt. Eine analytische Behandlung der Stossfugen mit Hilfe der Theorie halbstarrer Verbindungen wird beschrieben.

1. INTRODUCTION

Mixed steel-concrete construction is very interesting and attractive to bridge engineers, who are eager to promote technological innovation. The advent of Düsseldorf-Flehe Bridge [1] in West Germany may be considered as one of the symbolical works in this field. Modern cable-stayed bridges are usually self-anchored as shown in Fig.1(a). For these bridges, the mixed girder system in Fig.1(c) may be more reasonable because large compressive forces act on the main girders in the vicinity of the towers (See Fig.1(b)). The joint of mixed construction needs to have a sufficient capability in transfer of bending moment, axial and shearing forces. The development of connecting methods is required for the practical application. Technological and design information about joint structures, however, is still limitted.

The purpose of this study is to provide general information with regard to the optimum method of connection for the composite structures in a broad sense. Several mechanical joints including a bolted joint applied to steel-prestressed concrete beams are investigated experimentally, and an analytical method is proposed for the bolted joint. Practical problems of the connection for the precast composite slab decks are also discussed in this paper.

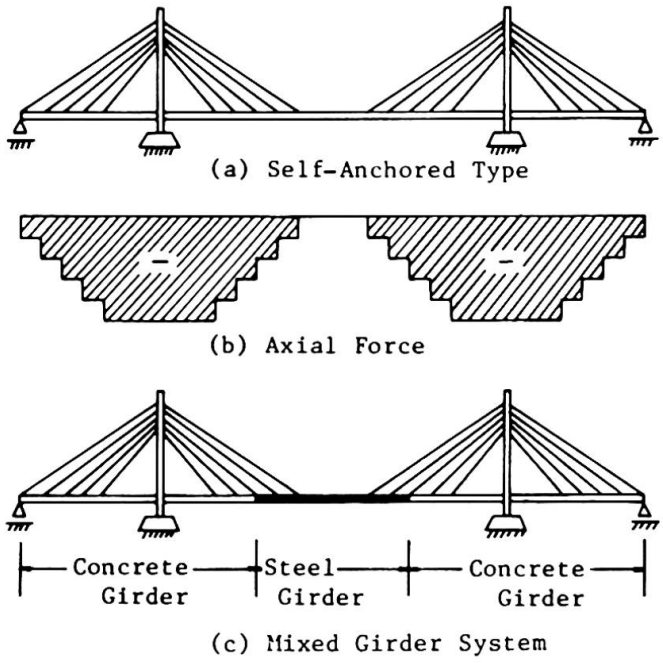

Fig.1 Cable-stayed bridge

2. MECHANICAL JOINTS APPLIED TO STEEL-PRESTRESSED CONCRETE BEAMS

2.1 General

The mechanical joints such as used in Flehe Bridge and Mosel Bridge [2] play an important role in the creative design of mixed structures. Fundamental research related to the joint of mixed structures is little presented, whereas the practical application has been extensively made in several countries.

A new mechanical joint as shown in Fig.2 is proposed herein, which can be applied to mixed steel-prestressed concrete beams subjected to bending moment. In order to investigate strength and flexural rigidity of the joint, a series of failure bending tests are carried out. Attention is also paid to slip and separation on the steel-concrete contact surface.

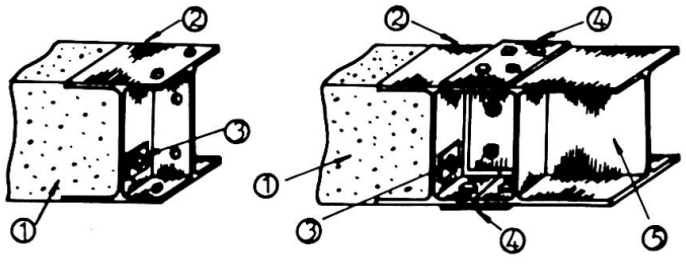

Fig.2 Mechanical joint with channel steel

2.2 Test and Discussion

Three mechanical joints were herein investigated. As shown in Fig.3, Joint-R consists of a channel steel with 3 anchor bars, Joint-S installs 6 studs

on the upper and lower plates of the channel, and the concrete of Joint-B is connected tightly to the channel with 2 H.T.bolts. Loads were transmitted through a spreader girder to the test beam in order to create two equal concentrated loads. The beams were simply supported and of 2.00 m span.

Fig.4 shows load-midspan deflection relationships. Under the loads greater than the decompression load of 35 kN, the slip on the steel-concrete contact surface in Joints-B and S increased gradually with the increase of load, which resulted in significant reduction of the flexural rigidity. However, Joint-R retained a sufficient stiffness up to almost the failure load, and the test deflections agree well with the theoretical deflections based on the elasto-plastic beam theory [3].

Cracking and ultimate moments for the test beams are given in Table 1, where theoretical values of $\overline{Mcr}$ and $\overline{Mu}$ imply the cracking and ultimate moments prescribed in Specifications for Japanese Highway Bridges [4]. Little cracks were produced in the joint concrete region of Joint-R before failure. The failure occurred due to crushing of concrete. The experimental cracking and ultimate moments agree well with the theoretical moments. For Joints-B and S, however, cracks initiated in the joint region at small loads and the test beams failed in concrete crush at the joint end. Especially, the experimental cracking moment for Joint-S was 26 % less than the theoretical cracking moment.

However, the results do not directly mean that Joints-B and S are essentially inferior to Joint-R. This difference of capability is obviously caused by the difference of resisting mechanisms which resulted from the dimensions of the joint components. Joint-S has been successfully used in Flehe Bridge and other bridges, while the similar types to Joint-B have been widely used as the connection of segmental structures. As far as authors' opinion about the results is concerned, joints combined together with Joints-R and B may be more desirable and reliable for such mixed structures from the standpoint of fatigue safety. Thus, research of the resisting mechanism and the reasonable design method of bolted joints is required for the further practical application.

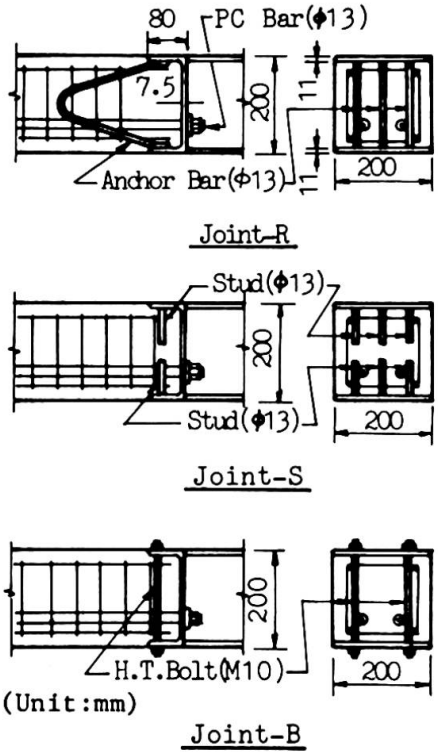

Fig.3 Details of test joints

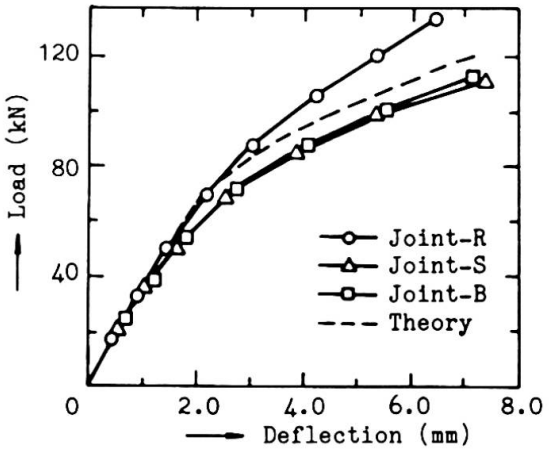

Fig.4 Comparison of load-deflection relationships

Table 1 Cracking and ultimate moments

Type of Joint	Cracking Moment (kN·m)			Ultimate Moment (kN·m)		
	Test Mcr	Theory $\overline{Mcr}$	$\frac{Mcr}{\overline{Mcr}}$	Test Mu	Theory $\overline{Mu}$	$\frac{Mu}{\overline{Mu}}$
Joint-R	20.6	20.4	1.01	54.8	52.3	1.05
Joint-S	15.6	21.0	0.74	47.0	51.5	0.91
Joint-B	20.6	21.2	0.98	49.4	51.7	0.95

3. BOLTED STEEL JOINT IN TRANSFER OF BENDING MOMENT

3.1 Test

A series of the statically and fatigue bending tests were carried out on 16 steel-reinforced concrete beams and 11 reinforced concrete beams, which were connected together by the bolted steel joint. Parameters for the joint of the present test beams were (1) tension in bolt, (2) use of mortar and bonding agent fillers on the contact surface, (3) additional reinforcement in the joint, and (4) length and thickness of the horizontal plate of the joint.

Fig.5 shows load-midspan deflection relationships for the effectively jointed beam and the corresponding monolithic beam. This beam had a rectangular section of 10 x 20 cm and a joint consisted of 9.0 x 1.0 cm holizontal steel plate, M12 bolts, bonding agent filler and longitudinally additional reinforcement. The test result shows that no significant crack occurred in joint concrete and that the flexural rigidity of the jointed beam was higher than that of the monolithic beam. Photo.1 shows the failure mode.

From the test results, it may be emphasized that the present bolted steel joint retains a sufficient capability in preserving the interconnection as well as in transfer of bending moment.

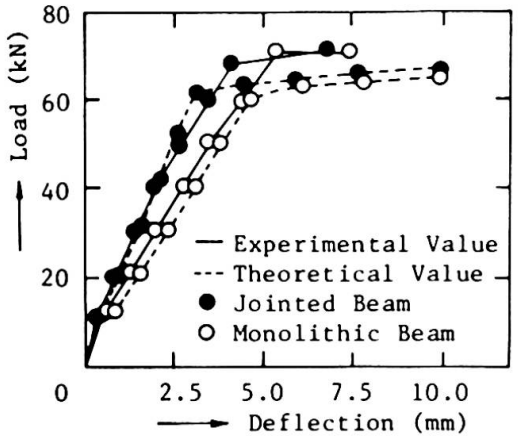

Fig.5 Comparison of load-deflection relationships

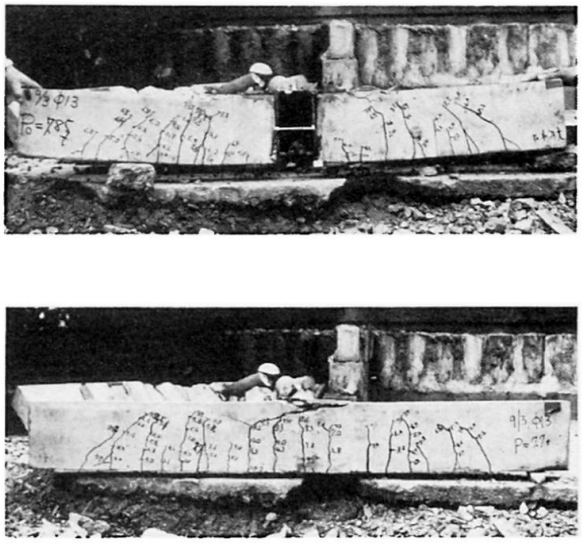

Photo.1 Failure mode of test beams

3.2 Analysis of Bolted Steel Joint (Semi-Rigid Connection Theory)

Equilibrium equations for the semi-rigid connection of the bolted joint due to the slip and separation are derived on the basis of the following assumptions.

1) The joint is a composite cantilever system consisting of upper and lower horizontal plates and of rigid concrete beam, as shown in Fig.6.

2) The beam is connected rigidly with the holizontal plates only at the bolted portions (Points A and B).

3) Elastic deformations of concrete and vertical plate are neglected for the rigid rotational deformation of the beam.

4) The end slip is expressed by F/kA_o , where F is total shear acting on the surface area (A_o) of lower holizontal plate and k is constant related to the slip.

When a concrete beam rotates rigidly as much as ϕ under bending moment M_o , the equilibrium equations of resultant forces Y_A , Z_A , M_A and Y_B , Z_B , M_B at Points A,B are expressed as (See Fig.7),

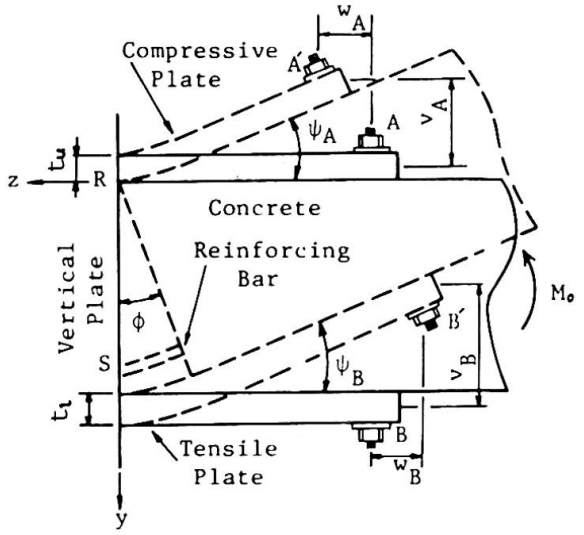

Fig.6 Idealization of bolted joint subjected to bending moment

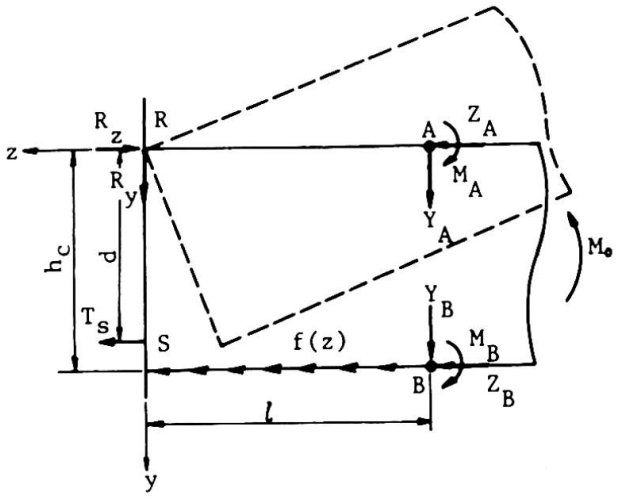

Fig.7 Forces acting on the contact surface

$$\left.\begin{aligned} &Y_A + Y_B + R_y = 0 \quad , \quad Z_A + Z_B + F + T_s - R_z = 0 \\ &M_A + M_B + (Y_A + Y_B)l + (Z_B + F)\, h_c - T_s\, d = 0 \end{aligned}\right\} \tag{1}$$

And assumning Point R as the center of the rotation, the compatibility equations for the deformation are,

$$\left.\begin{aligned} &v_A = -\,t_u\,(1-\cos\phi)/2 + l\sin\phi \quad , \quad v_B = (h_c + t_1/2)(1-\cos\phi) + l\sin\phi \\ &w_A = -\,l\,(1-\cos\phi) - t_u \sin\phi \quad , \quad w_B = -\,l\,(1-\cos\phi) + (h_c + t_1/2)\sin\phi \\ &\psi_A = \phi \qquad\qquad , \quad \psi_B = \phi \end{aligned}\right\} \tag{2}$$

Strain energies W_u and W_1 stored in upper and lower holizontal plates are, respectively,

$$\left.\begin{aligned} W_u &= \int_0^l \frac{Z_A^2}{2E_s S_s}dz + \int_0^l \frac{(M_A + Y_A z)^2}{2E_s I_s}dz \\ W_1 &= \int_0^l \frac{(Z_B + F z^2/l^2)^2}{2E_s S_s}dz + \int_0^l \frac{(M_B + Y_B z - F t_1 z^2/2l^2)^2}{2E_s I_s}dz \end{aligned}\right\} \tag{3}$$

in which E_s , S_s and I_s are modulus of elasticity, sectional area and moment of inertia of the holizontal plate, respectively.

Based on Castigliano's theorem, the deformations at Points A and B can be given as,

$$\left.\begin{aligned} v_A &= \partial W_u / \partial Y_A \;, \quad w_A = \partial W_u / \partial Z_A \;, \quad \psi_A = \partial W_u / \partial M_A \\ v_B &= \partial W_1 / \partial Y_B \;, \quad w_B = \partial W_1 / \partial Z_B \;, \quad \psi_B = \partial W_1 / \partial M_B \end{aligned}\right\} \tag{4}$$

Eqs.(1),(2) and (4) yield the semi-rigid property, K_S , equal to M_O/ϕ in the following form.

$$K_S = \frac{8E_S I_S}{l} + \frac{E_S S_S (h_C + t/2)h_C}{l} + kA_O h_C \left(\frac{5t}{12} + \frac{2h_C}{3}\right) + \frac{E_r S_r d^2}{l} \qquad (5)$$

in which the thickness t_u and t_l are equal to t ,and E_r and S_r are modulus of elasticity and sectional area of reinforcement, respectively.

Figs.8 and 9 illustrate moment-deflection relationships at the joint and moment-strain relationships of the holizontal joint plate, respectively, obtained from the test and theory. These figures also indicate that accuracy of the semi-rigid connection theory is sufficient for analysis of the deformation of the joint, and that the full-rigid connection theory considerably underestimates the deformation.

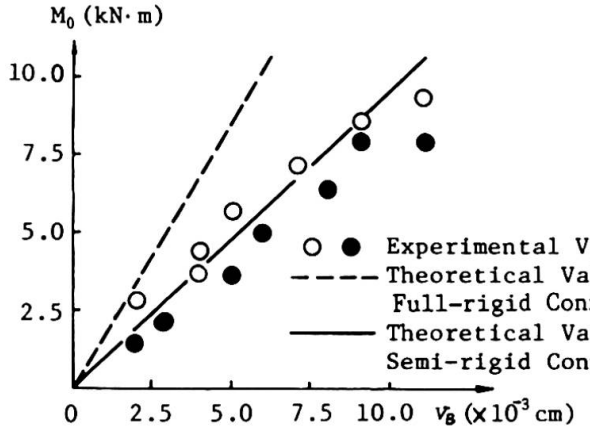

Fig.8 Comparison of moment-deflection relationships at bolted portion

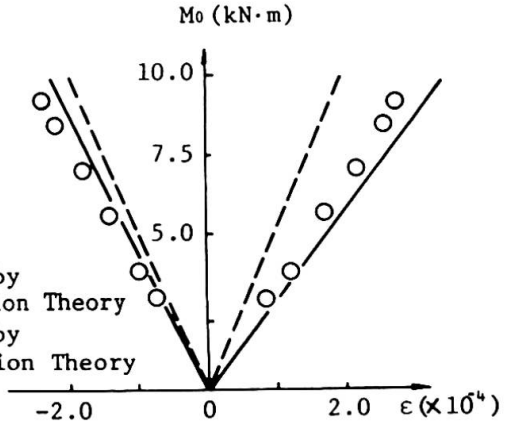

Fig.9 Comparison of moment-strain relationships of holizontal plates

4. MECHANICAL JOINTS APPLIED TO PRECAST COMPOSITE SLABS

4.1 General

A significant deterioration of concrete slab decks has been recently observed in highway bridges due to fatigue under excessive loads, and the complete replacement of these decks is often required. Precast composite slab decks are used as a conventional and quick replacement. The precast slab has a disadvantage of unfavorable discontinuous construction joints between precast and cast-in-place concrete parts. A fairly large amount of concrete is placed in the lapped portion of reinforcing bars developed from decks, as shown in Fig.10.

Two mechanical joints are proposed for connecting precast composite slab decks on the steel girder. Six composite slabs having proposed joints and a lapped joint and two corresponding monolithic slabs are tested in order to study joint capability in transfer of negative bending moment.

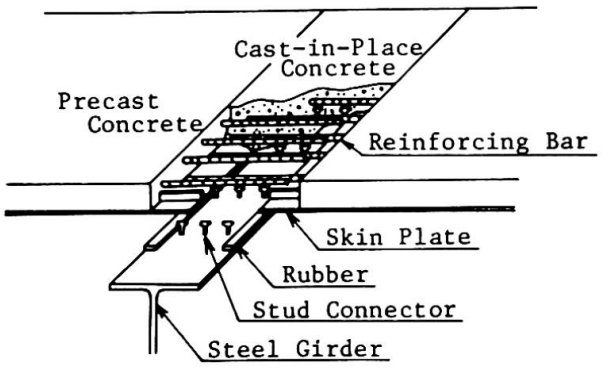

Fig.10 Existing connection of precast composite slabs on steel girder

4.2 Test and Discussion

Fig.11 illustrates details of the proposed joints. A steel joint, called Joint-CT, is spliced with the flange of steel cut T-section and main reinforcing bars are anchored to the steel and tightened with nuts. Joint-FB consists of two flat bars for anchoring main reinforcing bars. The other joint is a lapped joint, called Joint-LP, whose lap length was determined about 30 times the diameter of main reinforcing bars. Notations for the composite slabs such as Slab-CT are called after the slabs having Joint-CT. In addition to these composite slabs with joint, two corresponding monolithic slabs without joint were also tested and are called Slab-NJ.

Test slabs were loaded upside down to create negative bending in the joint. The loads were applied over the full width of the slabs simply supported at a span of 2.00 m.

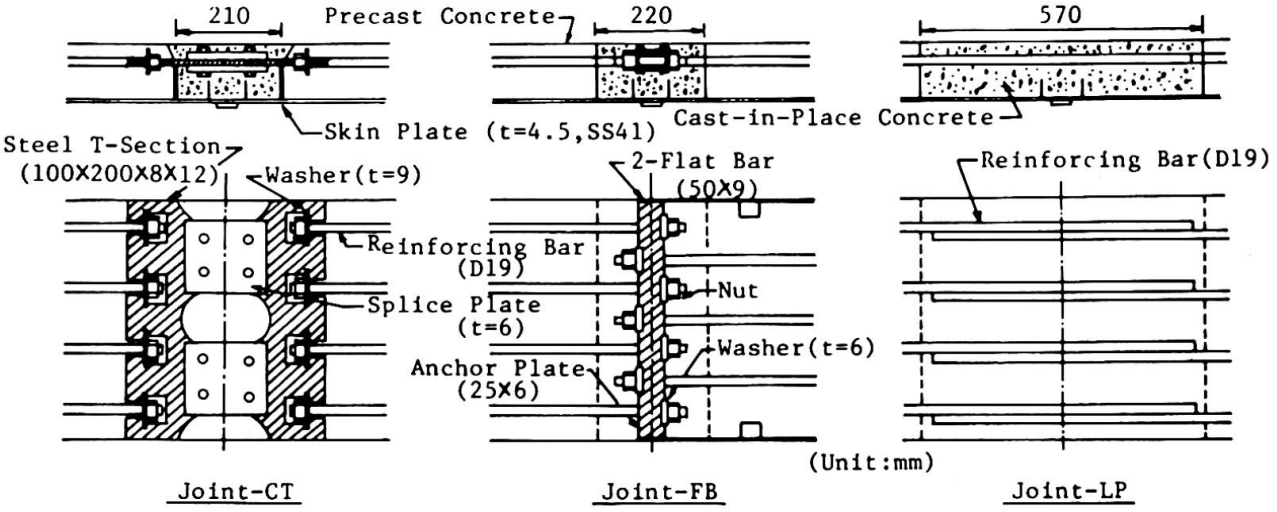

Fig.11 Details of test joints

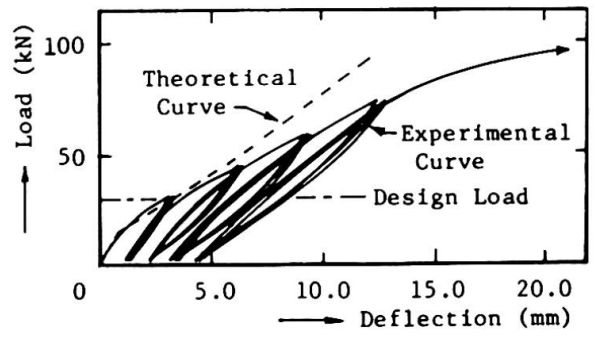

Fig.12 Load-deflection relationships for Slab-CT

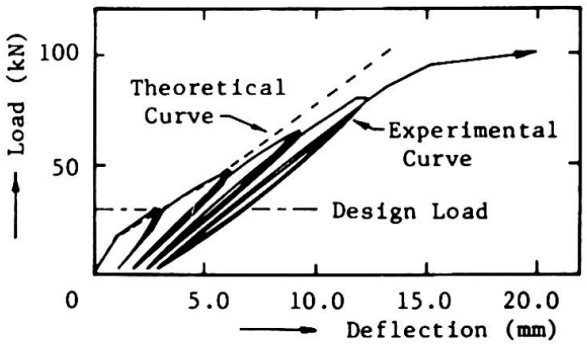

Fig.13 Load-deflection relationships for Slab-FB

Figs.12 and 13 illustrate load-midspan deflection relationships for Slabs-CT and FB obtained from test, including theoretical results. There are no significant differences in deflection among these test slabs, and the test results are close to the theoretical results under loads lower than the design load of 29.4 kN. At the design load, the maximum crack width in the joint region reached approximately 0.15 mm. But, the deflections of Slabs-CT and FB gradually increased with the number of repetitions of the maximum loads of two and three times the design load, respectively. In Joint-CT, a significant crack due to stress concentration was observed at the notch of the steel flange, in which reinforcing bars were anchored, under the loads greater than the design load. This defect must be improved in practical use.

Table 2 Comparison of ultimate moment

Type of Specimen		Ultimate Strength		$\frac{Mu}{Md}$ [1]	$\frac{Mu}{\overline{Mu}}$ [2]	$\frac{Mu}{Mun}$ [3]
		Pu(kN)	Mu(kN·m)			
CT	No.1	102.9	38.6	3.53	0.92	0.94
	No.2	105.4	39.5	3.61	0.94	0.96
FB	No.1	105.0	39.4	3.61	0.93	0.96
	No.2	105.8	39.7	3.63	0.94	0.97
LP	No.1	111.0	41.7	3.81	0.99	1.01
	No.2	118.2	44.3	4.05	1.05	1.08
NJ	No.1	108.1	40.6	3.71	0.96	0.99
	No.2	110.9	41.7	3.81	0.99	1.01

1) Md:Design Moment (=10.93kN m)
2) $\overline{Mu}$:Theoretical Ultimate Moment (=42.1kN·m)
3) Mun:Average Ultimate Moment of Specimens NJ

Ultimate strengths of all test slabs are given in Table 2, where the definition of $\overline{Mu}$ is the same as that in Table 1. All test slabs failed in a typical flexural faillure and had the ultimate moments approximately 3.5 to 4.0 times the design moment. The test values of jointed slabs were nearly equal to the values of monolithic slabs both in experiment and theory. This implies that a certain degree of the stiffness reduction at joint little affects the ultimate strength of the jointed slabs.

5.CONCLUSIONS

Mixed steel-concrete construction is expected to be one of the most attractive structural systems of the bridges, from the standpoints of structural rationality, construction cost, maintenance and repair. The joint of mixed construction needs to have a sufficient resisting capability to external forces. The development of joint structures has been desired for the further practical application.

This study provides some instructive information about several mechanical joints in transfer of bending moment. The proposed bolted steel joint is desirable and reliable for such mixed structures from the test results. Analytical equations of the bolted joint are derived on the basis of the semi-rigid connection theory. This analysis provides sufficient accuracy.

Two mechanical joints are also proposed for the precast composite slab decks in highway bridges. These joints can reduce a fair amount of joint length and can be used as a structural element.

REFERENCES

1. MODEMANN J. et al., Die neue Rheinbrücke Düsseldorf-Flehe/Neuss-Uedesheim, Der Bauingenieur, 1979.1.
2. Lehmann G. et al., Bau der Moselbrücke zwischen Kobern-Gondorf und Niederfall, Der Stahlbau, 1980.7.
3. OHTA T. et al., Elasto-Plastic Analysis of Reinforced and Prestressed Concrete Beams, Proc. JSCE, Vol.276, 1978.8.
4. Japanese Highway Association, Specifications for Highway Bridges, 1978.1.

High Strength Steel, Concrete, Hoop Composite Structure

Structure composite béton — acier à haute résistance

Verbundsystem aus Beton und hochfestem Stahl

Toshiro SUZUKI
Professor
Tokyo Inst. of Techn.
Tokyo, Japan

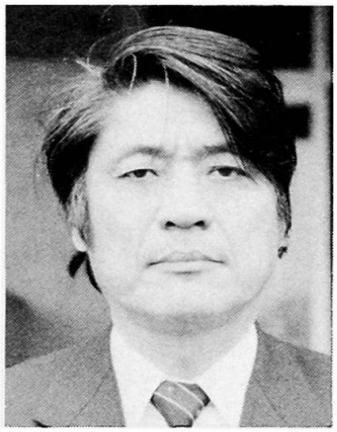

Toshiro Suzuki, born 1936, received his doctor's degree from the University of Tokyo in 1963. He was awarded the Prize from the Architectural Institute of Japan for his study on steel structure in 1981.

Katsuki TAKIGUCHI
Assoc. Prof.
Nagoya I.T.
Nagoya, Japan

Tetsumi OKAMOTO
Grad. Student
Tokyo I.T.
Tokyo, Japan

Toshikatsu ICHINOSE
Res. Assoc.
Nagoya I.T.
Nagoya, Japan

Masahiro KATO
Struct. Eng.
Sumitomo
Tokyo, Japan

Akira HANAJIMA
Struct. Eng.
Nikken Sekkei
Osaka, Japan

SUMMARY

A new steel and reinforced concrete structural system is proposed. It consists of high strength steel, concrete and hoop reinforcement. Longitudial reinforcement is not used. Experiments are carried out to study the restoring force characteristics of the proposed system. The proposed system showed a large energy dissipating capacity as well as a large deformation capacity.

RESUME

Un nouveau système structural béton-acier à haute résistance est proposé. Il est constitué d'un profilé H en acier à haute résistance et du béton renforcé d'étriers fermés. Il ne présente pas d'armature longitudinale. Les expériences ont montré que le système a de grandes capacités de dissipation d'énergie et de déformation.

ZUSAMMENFASSUNG

Eine neue Verbundbauweise für Rahmentragwerke wird vorgestellt. Die Stützen bestehen aus hochfesten H-förmigen Stahlprofilen, die mit Beton ummantelt sind, der keine Längsbewehrung enthält. Er ist nur mit einer geschlossenen Bügelbewehrung umschnürt. Die experientellen Untersuchungen zeigen, dass das System viel Energie zu dissipieren vermag und ein grosses Deformationsvermögen besitzt.

1. INTRODUCTION

The steel and reinforced concrete composite (SRC) is one of the commonly used structural systems in Japan, especially for tall buildings. About 92% of the buildings taller than 9 stories were built by SRC system during the past five years in Japan.

The objective of this study is to develop a new SRC, 'H or cross-H shaped 784MPa (80kgf/mm²) strength steel' - 'concrete' - 'hoop reinforcement' composite. Illustrative examples of the proposed structural system are shown in Fig 1. The beams are made of the H-shaped steel or the ordinary reinforced concrete. The columns and the beam-column joints are made of the proposed SRC. Unlike the customary SRC, longitudinal reinforcement is not used in the column. Experiments are carried out to study the restoring force characteristics of the proposed SRC system. Effects of the hoop reinforcement and the steel strength are discussed.

2. THE FEATURES OF THE PROPOSED 'SRC' AND THE PROBLEMS LIABLE

One feature of the proposed SRC system is the non usage of longitudinal reinforcement. When the deformed bar is used as the longitudinal reinforcement, the bond between the deformed bar and the concrete induces the inclined flexural shear cracks, which consitute the truss action together with the web reinforcement. The authors intend that the concrete should be liberated from the truss action in the proposed SRC system. The role of the longitudinal bar is replaced by the larger section of H-shaped steel. The role of the concrete is limited to the arch action to sustain the diagonal compressive force and the axial force. This would make the concrete more ductile for the compressive straining. The non-usage of the longitudinal reinforcement brings about another merit; it shall reduce the congestion of reinforcement, which leads to the better concrete placing.

Another feature of the proposed SRC structural system is the usage of high tensile strength (784MPa or 80kgf/mm²) H or cross-H shaped steel instead of normal strength steel. This might cause the following problems concerning to the deformation capacity of the column.

(a) The concrete might not be able to sustain the compressive stress enough at small ductility factor, because the yield strain of the high strength steel is large.

(b) The local buckling of compressive steel flange might occur, because the

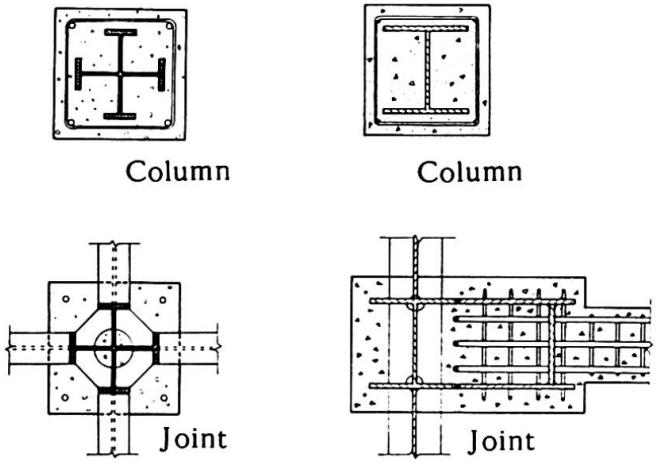

(a) Two-way steel beams (b) One-way R/C beam

Fig 1. Design Examples

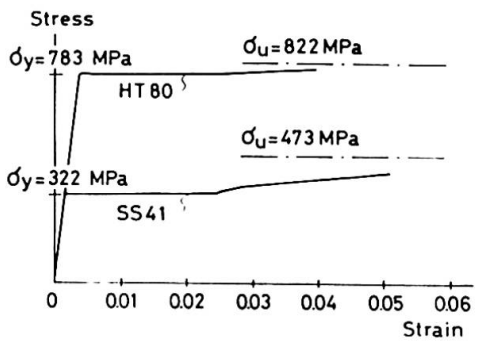

Fig 2. Stress-Strain of Steel

thickness of the steel plate should be designed thinner than that of the normal strength steel.
These problems shall be surmounted by the confinement [3] of the concrete by the hoop reinforcement within the column. On the other hand, the authors recommend that the hoop reinforcement within the beam-column joint should be curtailed as shown in Fig 1, in order to save the constructors' labor. The effect of the hoop reinforcement upon the restoring force characteristics of the columns and the beam-column joint is investigated within this paper.

The usage of high strength steel might cause another problem. The welding of high strength steel is more difficult than that of normal strength steel. The inelastic strain is apt to concentrate near the critical section, because the strain hardening of high strength steel is small and the yield zone length should be smaller. (Examples of stress strain relationships of high and normal strength steels are shown in Fig 2.) Therefore, the tensile fracture of steel flange at the critical section might be induced by the inperfection of the welding and by the inelastic strain concentration. In this paper, such effects are also to be discussed comparing the experimental results of the SRC members of various strength steels.

3. RESTORING FORCE CHARACTERISTICS OF THE COLUMN

Fifty-four SRC member specimens were tested. The variables were,
(1) amount of hoop reinforcement,
(2) the tensile strength of the H-shaped steel, and
(3) loading conditions, which include
C : monotonic Compression, B : cyclic Bending without axial force,
CB : constant Compressive force and cyclic Bending, and
CBS: constant Compressive force and cyclic Bending Shear.
The yield strength of the hoop reinforcement was not the variable; the normal strength steel was used. In this paper, only the results of the CB and CBS series testings with HT80 steel are reported. The detailed informations of the experiments is reported in the reference [4].

An example of the CB and CBS test specimens is shown in Fig 3. The compressive strength of concrete was 29.7 to 30.6 MPa. The loading and measuring system of the CB and CBS tests is shown in Fig 4. Axial force was maintained as N=500kN, which was about 20% of the calculated concentric compressive strength.

Test results of the HT80-CB series specimens are plotted in Fig 5. The second part of the specimens name '020' or '000' indicates that the spacing of the hoop reinforcement was 20mm or no hoop was used, respectively. The specimen with 20mm pitched hoop showed a stable spindle shaped hysteresis loop. Although

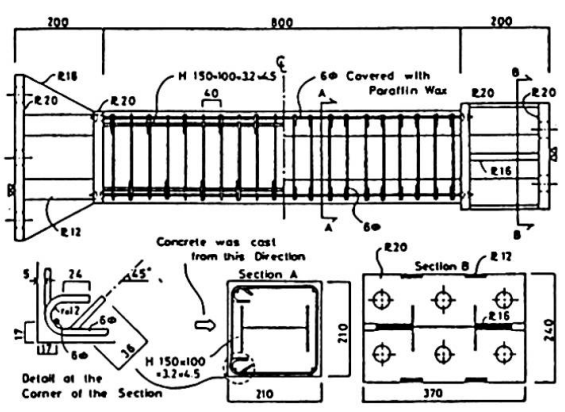

Fig 3. Specimen HT80-040-CBS-20

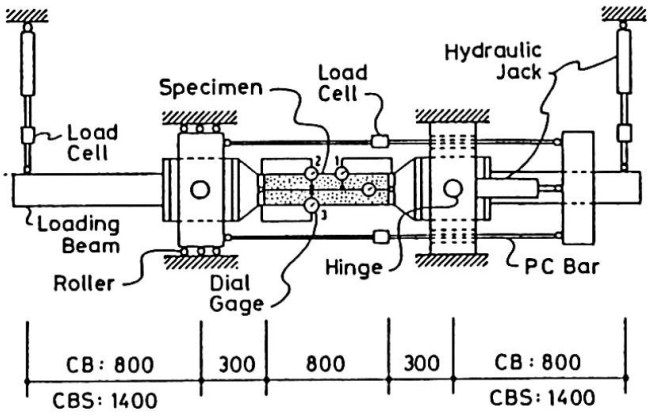

Fig 4. CB and CBS Test Setup

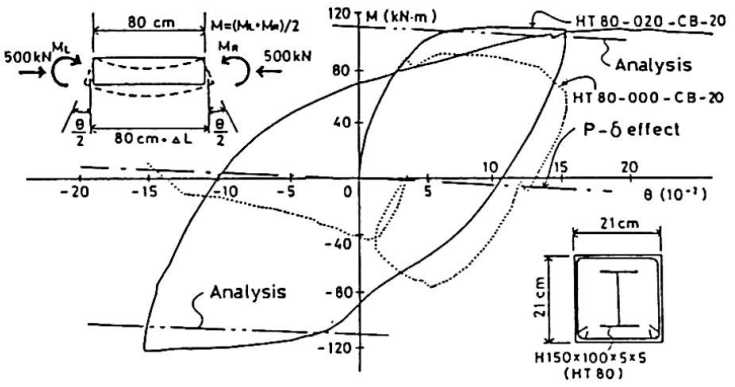

Fig 5. Moment - Rotation Angle Relations of CB Specimens

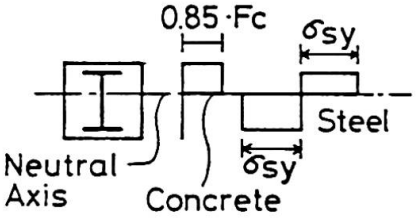

Fig 7. Assumed Stress Distribution

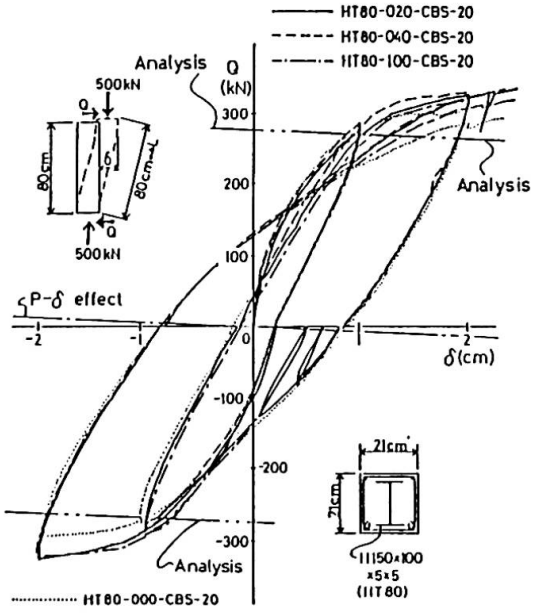

(a) Cyclic loops –

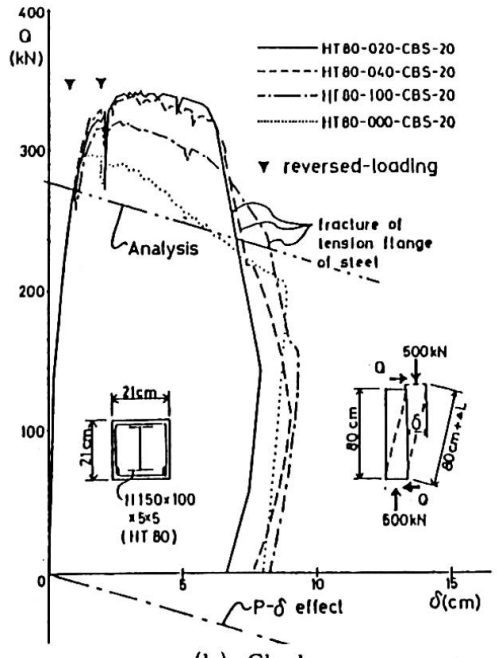

(b) Skeleton curves

Fig 6. Shear Force - Deflection Relations of CBS Specimens

the shell concrete spalled almost completely, the core concrete did not spall. The strength of the unhooped specimen was 73% of that of the hooped specimen. The concrete started to crush and spall at theta=0.04 rad. Local buckling of the steel flange was observed at theta=0.10rad. At theta = -0.15rad, the moment resistance of the specimen was completely lost.

Test results of HT80-CBS series are plotted in Fig 6. The strength of the unhooped specimen was 84% of that of the 20mm-pitched specimen. The ductility was also affected by the hoop. Local buckling of steel and diagonal cracks of concrete were observed in the specimens without hoop, but not in the hooped specimens. The flexural cracks concentrated at the critical sections in all the specimens. Flexural shear crack was not observed.

The resistance of all the HT80-CBS series specimens degraded largely by the fracture of the tension flange of steel at delta=6cm to 8cm (deflection angle=1/13 rad). Such fracture was not observed in the specimens of normal strength steel.

The ultimate strength was calculated assuming the stress distribution shown in Fig 7 and was indicated in Figs 5 and 6. The calculated strength agreed roughly with the observed strengths.

4. RESTORING FORCE CHARACTERISTICS OF THE BEAM-COLUMN JOINT

Twelve specimens were tested. An example of test specimen is shown in Fig 8. The beams are bare H-shaped steel. The variables were,
(a) the type of the H-shaped steel (SS41 or HT80),

(b) the amount of the hoop reinforcement, and
(c) the amount of the axial force on the column (0% or 25% of the calculated compressive concentric strength of the column)

The H-shaped steel of the column was continued through the joint; the beams and the stiffners were welded to the column. The hoop reinforcement was assembled through the slender holes of the beam webs. The joint panel was designed as the weakest; the column was designed stronger than the joint panel but weaker than the beam. (In the design of the actual structures, the order of the strengths shall be the opposite.) The compressive strength of the concrete was from 22.3 MPa to 24.4 MPa.

Loading and measuring system is shown in Fig 9. Forces were applied to the joint panel as Fig 10. The joint panel distortional moment PM was defined by the following equation.

$$PM = (Q_B+Q_B') \quad [H\ (L+J_c) - J_c\ (H+J_b)] \ /\ (H+J_b) \quad .....(a)$$

The panel moment PM corresponds to the shear deformation angle of the panel, 'gamma', according to Takizawa [2].

Test results of the specimens with HT80 steel and 25% axial force are shown in Fig 11. The joint panel strengths were affected by hoop reinforcement but not much by axial force. The strengths of hooped specimens were 14% to 17% higher than those of unhooped specimens, irrespective to the amount of the axial force. The ductility, however, was not affected by hoop reinforcement. The situation of the specimens with normal strength steel was very similar to those with high strength steel.

Failure patterns of the specimens were affected by the hoop reinforcement, but not much by the tensile strength of the H-shaped steel, nor by the amount of axial force. In the unhooped specimens, the joint panel concrete outside the stiffners and flanges of the column spalled almost completely. Only the concrete enclosed within the stiffners and flanges remained in the joint panel. Spalling occured in the connecting columns as well. On the other hand, the concrete of hooped specimens were well confined. A lot of inclined narrow cracks were observed in the joint panel but they did not penetrate the column.

The strength of the joint panel was calculated by the addition theorem [1] assuming as Fig 12. The shear force was assumed to be carried by the web of the H-shaped steel, the concrete, and the hoop reinforcement. The cracks of concrete were assumed to occur along the direction of the diagonal compressive force. The concrete was assumed to carry the compressive stress of 0.85 times of the compressive strength. The steel was assumed to carry the tensile or compressive yield stress. Calculated and observed strengths are shown in Fig 13. The theory explained the observed fact that axial force did not affect the strength within the tested range. However, it did not explain the observed effect of hoop reinforcement on the joint shear strength well.

5. INTERACTION BETWEEN THE COLUMN AND THE BEAM-COLUMN JOINT

Four specimens were tested. An example of the specimens is shown in Fig 14. The specimens were named as 'HT80-C-30','HT80-C-20','HT80-B-30', and 'HT80-B-20'. The variables in the specimens were,
(a) the thickness of the steel web in the joint, (This parameter was indicated by the second part of the specimens' name, C or B. The H-shaped steel of the Column or that of the Beam was continued through the joint; the web thickness of the column steel, 5mm, was thinner than that of the beam steel, 8mm.) , and
(b) the amount of the axial force on the column. (This parameter was indicated by the third part of the specimens' name. The axial force was 20% or 30% of BDFc, where B=D=350mm and Fc=22MPa.)

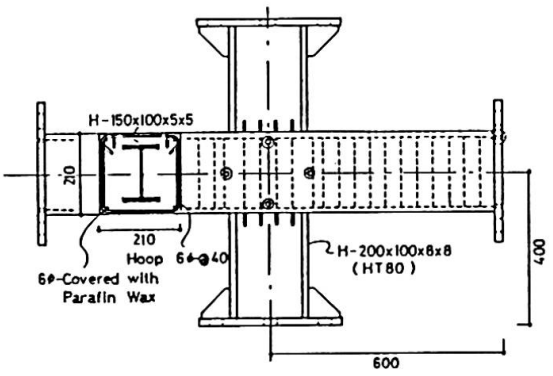

Fig 8. HT80-040-JPS-** Specimens

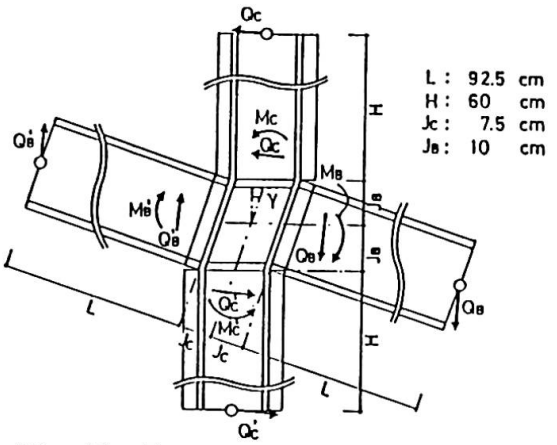

Fig 10. Forces around Joint Panel

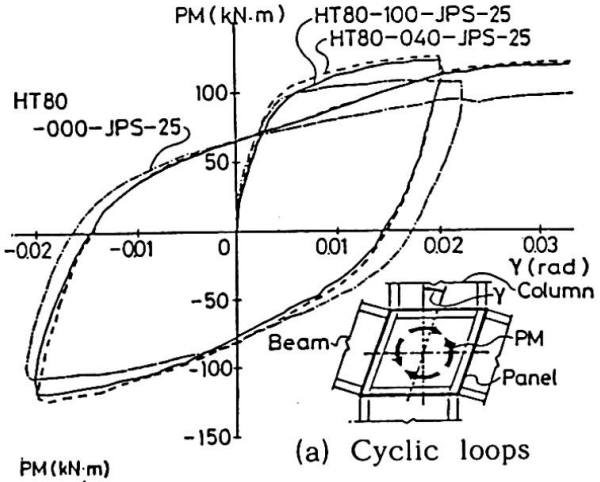

(a) Cyclic loops

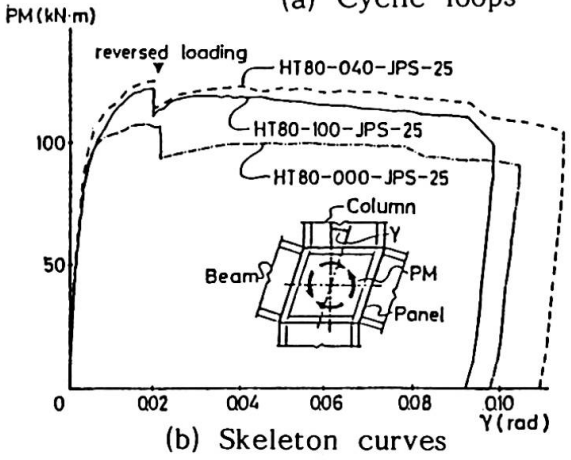

(b) Skeleton curves

Fig 11. Panel Moment-Shear Deformation Angle Relation of JPS Specimens

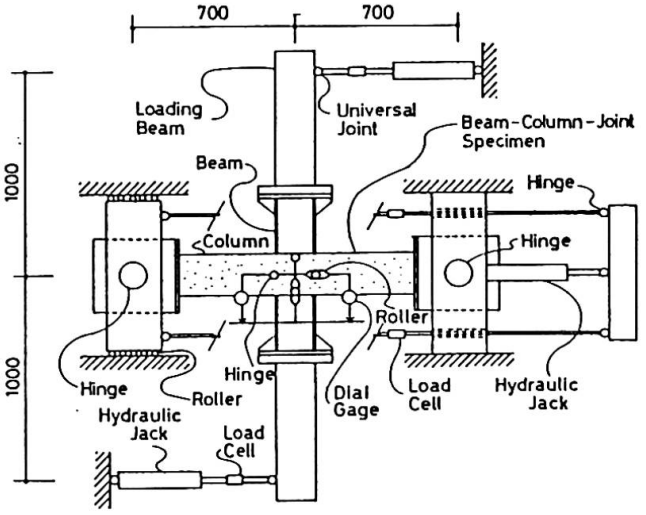

Fig 9. JPS Test Setup

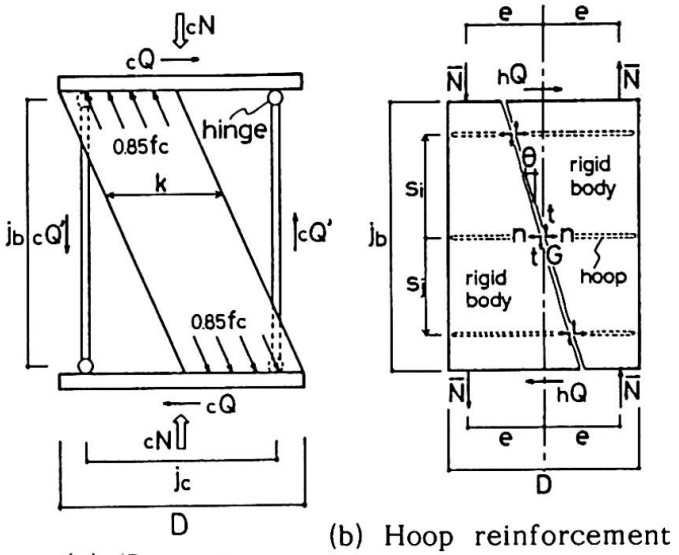

(a) Concrete (b) Hoop reinforcement

Fig 12. Assumed Shear Resistant Mechanism

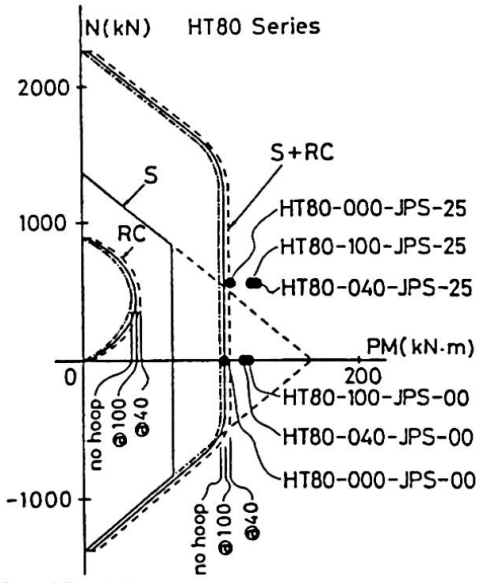

Fig 13. N-PM Interaction Curves

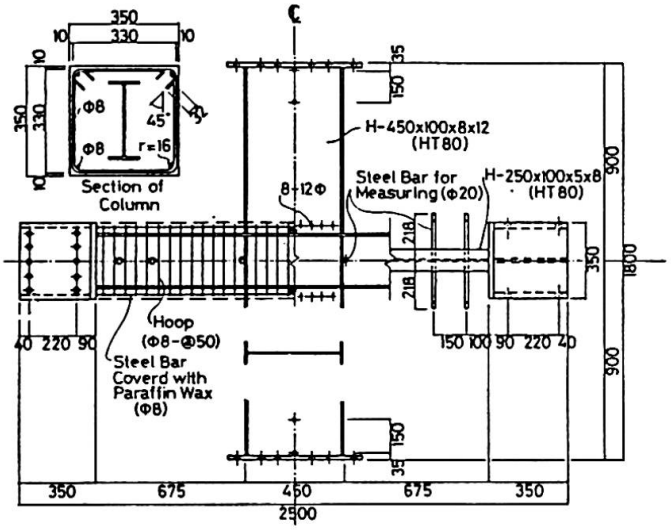

Fig 14. Dimensions of Interaction Specimens

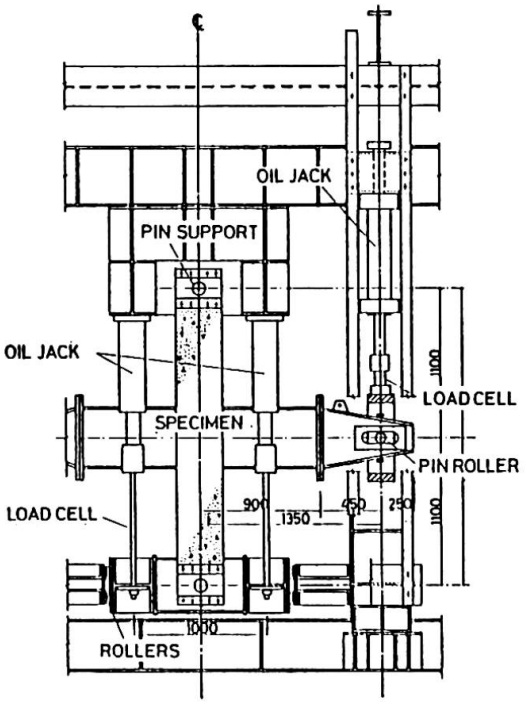

Fig 15. Interaction Test Setup

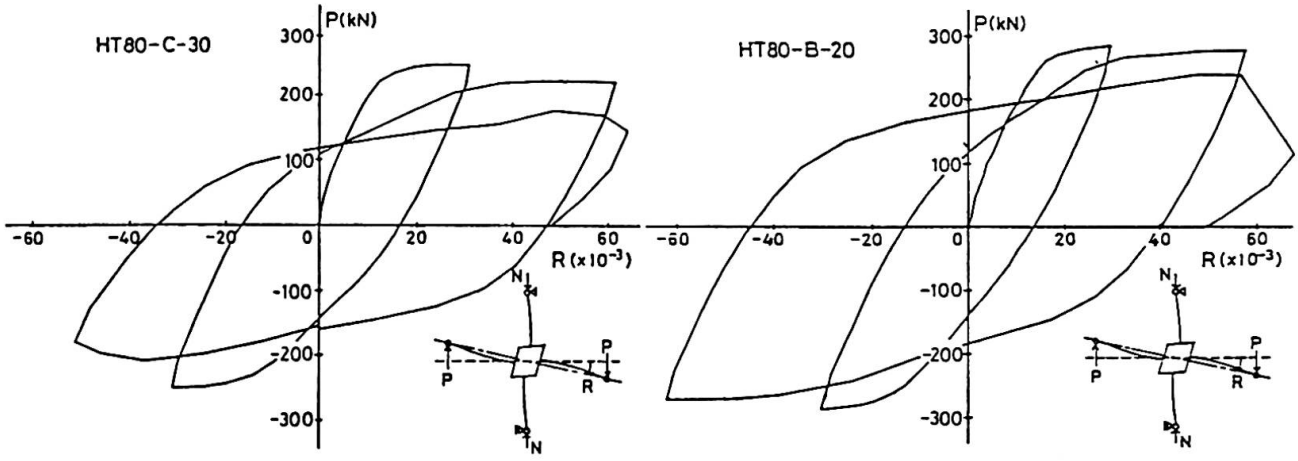

(a) HT80-C-30 (b) HT80-B-20

Fig 16. Beam End Force - Deflection Angle Relations

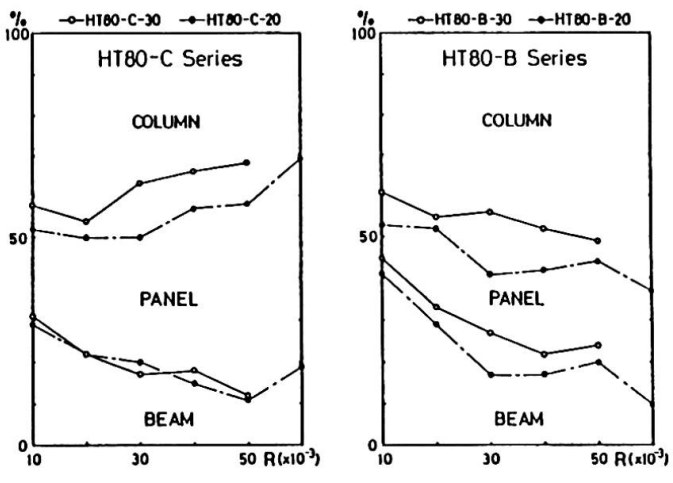

Fig 17. Component of Delection Angle

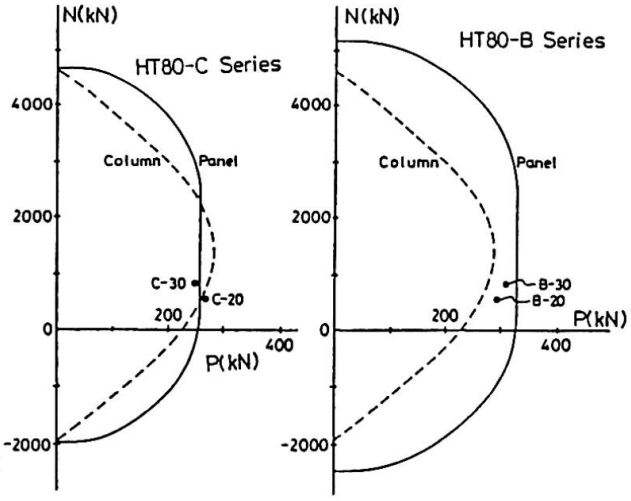

Fig 18. N-P Interaction Curves

The 'HT80' steel was used both in the column and in the beam. The web reinforcement ratio in the column and in the joint of all the specimen was uniformly 0.57%. The compressive strength of the concrete was from 25.5 to 26.8MPa. Loading and measuring system is shown in Fig 15.

Test results of the specimens HT80-C-30 and HT80-B-20 are shown in Fig 16. The P-R curves of all the specimens were spindle-shaped. The tensile fracture of the flange was observed at the critical section of the column of all the specimens at $R=50\text{-}60\times10^{-3}$rad of the final loading cycle. The column axial force N vs. the beam end force P interaction curves to be carried by the column or the joint were calculated by the addition theorem, and were shown in Fig 17, together with the observed strength. The observed strengths agreed with the calculated values. The contribution ratios to the beam-end deflection by the deformation of the columns, the joint panel, and the beams are shown in Fig 18. The HT80-C series and the HT80-B series specimens may be regarded as the joint collapse and the column collapse type, respectively. However, there existed an interaction between the collapse of the column and the joint; the yielding of the steel web and the hoop reinforcement was observed in the joint of all the specimens, including the HT80-B series.

6. CONCLUSIONS

(a) The proposed SRC system, [H-shaped high strength (784MPa or 80kgf/mm^2) steel] - [concrete] - [hoop reinforcement] composite has a large energy dissipating capacity as well as a large deformation capacity.
(b) Flexural cracks concentrate at the critical sections in the proposed SRC members subjected to bending-shear. Flexural-shear cracks do not occur. Concrete is liberated from the truss action in the proposed SRC.
(c) One defect of the proposed SRC member subjected to bending-shear is that the tensile fracture of the steel flange is more liable to occur than that of normal strength steel. This is attributable to the inelastic strain concentration, and shall be surmounted by some devices such as tapering of the steel flange.
(d) Hoop reinforcement improves the compressive behavior of concrete and protects the H-shaped steel from the local buckling.
(e) Hoop reinforcement contributes to the ductility as well as the strengths of the proposed SRC members and beam-column joint with high strength steel.
(f) The flexural strength of the column and the shear strength of the beam-column joint can be roughly estimated by the addition theorem.

ACKNOWLEDGEMENT

This study received the grant in aid for scientific research from the Ministry of Education, Science and Culture of Japan. The authors wish to thank the Ministry.

REFERENCES

1. NAKA, T., WAKABAYASHI, M., and TAKADA, S., Quake Resisting Design of Composite Structures in Japan. Proceeding of 2nd World Conference of Earthquake Engineering (TOKYO), 1960, Vol.III, pp.1811-1826.
2. UMEMURA, H. and TAKIZAWA, H., Dynamic Response of Reinforced Concrete Buildings. Structural Engineering Documents 2, IABSE, 1982, 64pp.
3. PARK, R., PRIESTLEY, M.J.N., and GILL, W.D., Ductility of Square Confined Reinforced Concrete Columns, Proceedings, ASCE, Vol.108, No.ST4, April, 1982, pp.929-950.
4. SUZUKI, T., TAKIGUCHI, K., ICHINOSE, T., and OKAMOTO, T., Effects of Hoop Reinforcement in Steel and Reinforced Concrete Composite. Proceedings of the Third South Pacific Regional Conference on Earthquake Engineering (WELLINGTON), 1983, pp.282-302.

Composite Timber and Concrete Components for Walls

Parois mixtes bois / béton

Verbundbauteile aus Beton und Holz für Wände

Ulf Arne GIRHAMMAR
Res. Prof.
RSFA
Märsta, Sweden

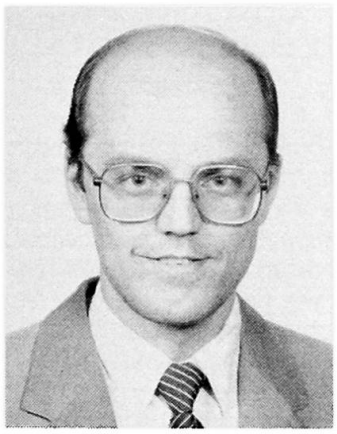

SUMMARY
Composite components often form technically and economically optimum structures. Composite concrete and timber components are often used in buildings and bridge construction. A composite concrete and timber component for walls has been developed. The component is a combined foundation and wall element and has nailplates as shear connectors. The component is mainly used in farm and industrial buildings. The behaviour and capacity of these components with incomplete interaction have been studied. The design and the way of erection of the component are described. Design procedures for service and ultimate loads are also presented.

RESUME
Les structures mixtes fournissent souvent d'excellentes solutions, en particulier celles composées de bois et de béton dans la construction de bâtiment et de ponts. C'est ainsi qu'une paroi mixte a été développée pour des bâtiments agricoles et industriels ainsi que pour leur fondation. Elle comprend des plaques de liaisons comme cloutage. Le projet et le montage sont décrits ainsi que les contrôles aux états limites.

ZUSAMMENFASSUNG
Eine Wandkonstruktion aus Beton und Holz wurde entwickelt. Der Bauteil besteht aus einem kombinierten Element, das Fundament und Wand umfasst. Die Schubverbindung erfolgt über Nagelplatten. Der Bauteil wird hauptsächlich bei Landwirtschafts- und Industriebauten verwendet. Das Verhalten und der Widerstand dieser Komponenten wurde untersucht. Die Montage der Wände wird beschrieben und Bemessungsverfahren für Gebrauchs- und Bruchzustand werden gegeben.

1. INTRODUCTION

Composite structural elements often form technically advanced and economically beneficial structures. Pre- and on-site fabricated composite timber-concrete elements have been successfully used in buildings as floors and walls, and in bridge construction [1,2] and [3,4]. Nails, bolts, glue or cutouts are usually used to develop shear connection in timber-concrete composites [5,6,7].

A new building element has been developed for application in industrial and agricultural builings [4]. The two important special features of the composite timber-concrete wall element are: (i) the element combines both the foundation and the wall elements; and (ii) the wall element is comprised of thin concrete plates attached to timber studs by means of nail-plate type shear connectors [8]. The structural details, the method of erection, and the design and behaviour of these elements are described in this paper.

2. DESCRIPTION OF THE COMPOSITE ELEMENT AND THE BUILDING SYSTEM

2.1 Details of the composite element

The composite wall element consists of concrete plates and two or more timber studs which are connected by nail-plates as shown in fig 1. The element is fabricated in five standard widths, the most commonly used width being 2400 mm. In addition to the standard widths, elements of any required non-standard width may also be manufactured. In agricultural buildings the concrete plate forms an impact resistant surface that can be easily cleaned. In addition to acting as a moisture barrier the concrete plate also serves to enhance the fire-resistance characteristics of the element. The timber studs form a bedding for the outer wall covering and reduce the risk of thermal bridges. The extention of the wall element to approximately 1.0 meters below ground surface level (the foundation part of the element) and the continuity of thermal insulation improve the stability and the thermal properties of the system. There are six holes at the bottom of the prefabricated wall element which permit the placement of reinforcement bars, allowing an in situ cast continuous footing. One of the timber studs extends above the element and the roof truss is anchored directly to the stud.

The placement of the composite element in a building is illustrated in fig. 2. The wall elements are attached to the floor slab by special anchors (reinforcement bars are placed in stirrups which are placed in the prefabricated elements prior to casting).

2.2 Erection of the composite elements

To erect the elements, the base layer of the concrete footing is first prepared, fig. 3. The elements are then lifted into position and adjacent elements are tied together by means of a nailed connection between the end studs of the units. A spacer block is used at the nailed connection to fill the gap between the end studs of adjacent units. The concrete is poured into the footing after the elements are in place, fig. 4. The footing thus obtained is integrated into the wall (fig. 2). After the concrete has cured and the soil is backfilled, the elements should be stable and the bracing is no longer needed. The roof trusses are attached to the wall elements after the concrete footing has set and after the special anchors have been fitted, the concrete floor slab is then poured at the desired elevation.

The erection procedure described above of an agricultural building designed to house 25 cows takes only two days to complete for three workers.

2.3 Special remarks

Even if water-tight concrete and jointing mastic are used in and between the wall elements, it is hard to prevent water from penetrating into the interior zone of the elment. For this reason the outer concrete plate just above the footing should be provided with ventilation holes in order to drain any possible penetrated water and ventilation channels should be arranged to aerate the elements below the ground level. This prevents the rotting of the timber studs and the loss of structural integrity of the element.

3. DESIGN PROCEDURES

3.1 General

The composite units are usually erected with the concrete plate exposed to the interior of the building, fig. 5. For the purpose of analysis the element is divided into two parts, the segment above the floor level (L) and the portion below the ground (ℓ). The segment above the slab is assumed to be fixed at the floor slab level and pin-connected to the roof trusses. The segment below the slab level is assumed to be fixed at the concrete footing and pin-connected to the concrete floor slab but subjected to a fixed end moment from the wall element above. If any window openings are placed in the upper part of the wall element, the bending stiffness of the wall can be assumed to be constant [9]. The axial compressive and tensile loads are assumed to act through the center of gravity of the concrete plate and the timber studs, respectively. (The shrinkage of the bottom chord of the roof truss and of the concrete plate will change the line of action of the axial loads).

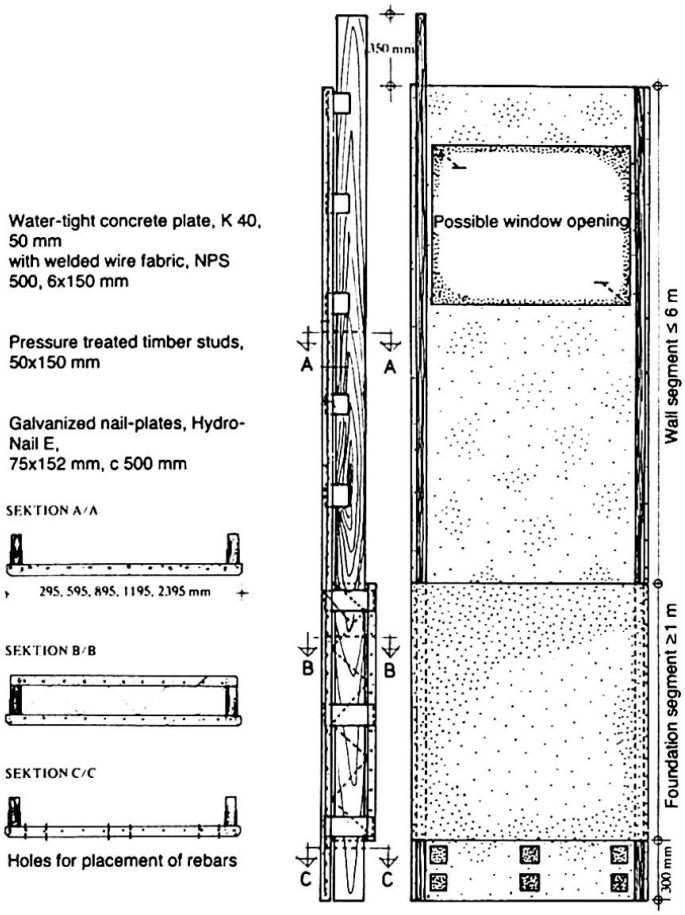

Fig. 1 *Details of the composite timber-concrete element with nail-plates*

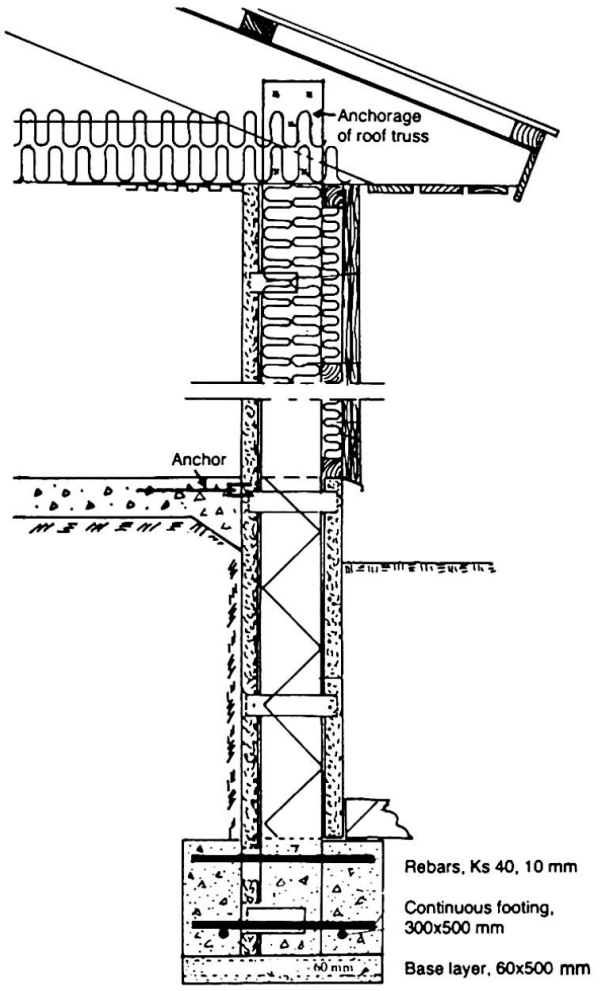

Fig. 2 *A wall section with the composite element*

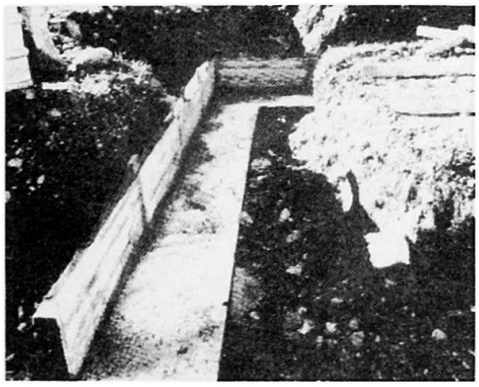

Fig. 3 *The base layer of the concrete footing*

Fig. 4 *The erected wall elements prior to casting of continuous footing*

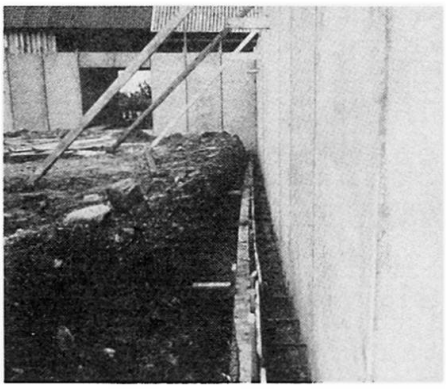

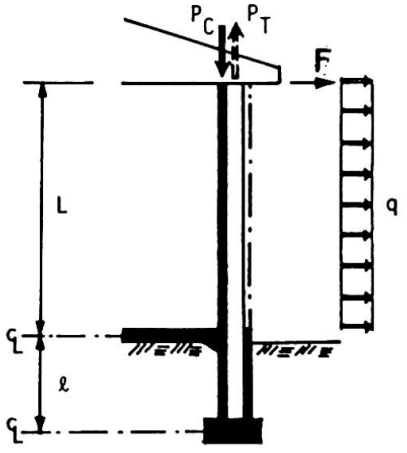

P_C = Axial compression (center of concrete plate)

P_T = Axial tension (center of timber stud)

F = Stay force (support force)

q = Wind load

L = Theoretical length of wall segment

ℓ = Theoretical length of foundation segment

Fig. 5 *Wall and cross section of the composite timber-concrete element*

3.2 Analytical model for the composite elements

The behaviour of the concrete plate influences the overall behaviour of the composite element and depends upon whether the plate is in compression or in tension (cf. fig. 6 for definition) and also upon the rigidity of the shear connectors(slip modulus K [N/m²]) [9]. In the case of highly flexible shear connectors, the behaviour of the element will be similar to the behviour of composite elements with no composite action ($K \rightarrow 0$) and the reinforced concrete plate will crack in tension due to bending tensile stresses in both cases of the concrete plate in compression and in tension. In the case of very rigid shear connectors, the behaviour of the element will be similar to the behaviour of composite elements with full composite action ($K \rightarrow \infty$) and the reinforced concrete plate will crack only in the case of the concrete plate in tension. The composite element described here belongs to the former group (the composite element could however easily be made more rigid in shear by increasing the number of nail-plates).

The analytical model is therefore based on the assumption of a cracked reinforced concrete plate in both loading cases, fig. 6. The exterior load gives rise to the cross section moment M, which in turn causes interior axial forces (N_t, N_c) and moments (M_t, M_c) in the timber studs and the concrete plate, and also interior slip forces (T_n [N/m]) at the interface between the two submaterials. Since the concrete plate is relatively thin, it is assumed to have no bending ($E_c I_c = 0$) but only axial stiffness ($E_c A_c$). For the sake of simplicity, the compressive stress (σ_c) is assumed to be evenly distributed over the cross section of the concrete plate and the tensile stress (σ_r) is assumed to be concentrated to the reinforcement, fig. 6. The true maximum compressive stress in the concrete would be twice this assumed uniform stress as approximately half the concrete thickness is in a cracked condition. The failure modes are then due to: (i) combined bending and axial tension/compression of the timber studs (f_t); (ii) shear or anchorage failure of the nail-plates (f_n);(iii) compression failure of the concrete plate (f_c); and (iv) tension failure of the steeel reinforcement (f_r). (In the case of rigid shear connectors, the only difference will be that the concrete plate in compression will be uncracked and thus have full axial and bending stiffnesses.)

3.3 Service load design

The composite elements are regarded as cantilevers subjected to five different kinds of loading as shown in fig. 7. The cantilevers represent the segment of the wall element above the floor slab level (with the length L) and the segment below (with the length ℓ), respectively, cf section 3.1. The real supporting and loading conditions at the upper end of the segments of the composite wall element can be represented by combining the different cases of loading. The first three and the last two cases refer to transversally and axially loaded elements, respectively. The force F is considered as positive when acting in the same direction as the evenly distributed load q and M_E is positive if it causes tension on the same side of the cantilever as that caused by the load q. By choosing the force $F = -3qL/8$ and by combining cases 1 and 2 a propped cantilever can be represented.

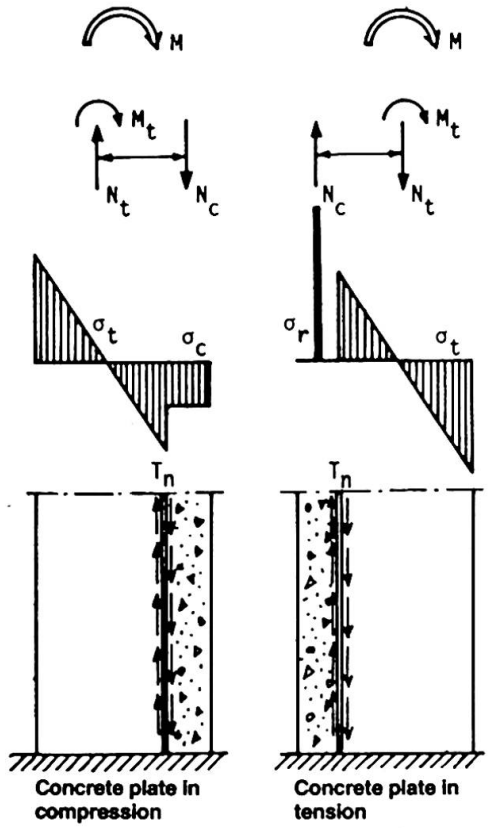

"Exterior" load (double arrows)

Interior axial forces and interior moments (single arrows), which act in the neutral axes of the submaterials

Distribution of normal stresses in the submaterials

Slip forces between the submaterials (shear forces at the interface between the timber and the concrete)

The subscripts t, c, r and n stand for timber,concrete, reinforcement and nail-plate, respectively. The distance between the centers of gravity of the wood and concrete parts is denoted by "r".

Fig. 6 *Definition of concrete plate in compression and concrete plate in tension. Analytical model for the composite element*

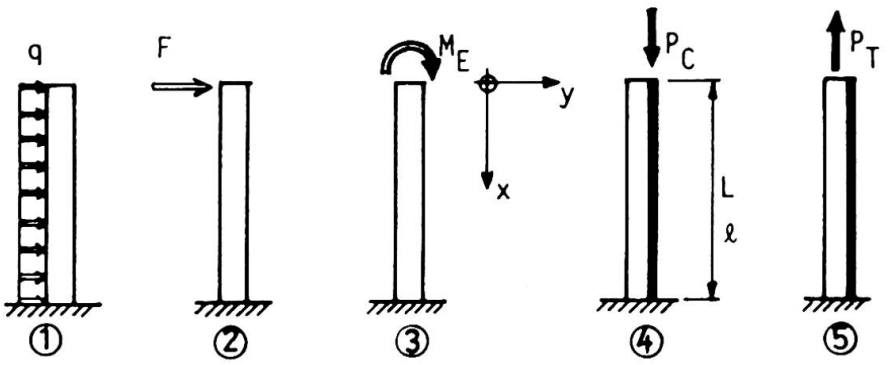

Fig.7 *Composite cantilevers subjected to three kinds of transversal loading and two kinds of axial loading*

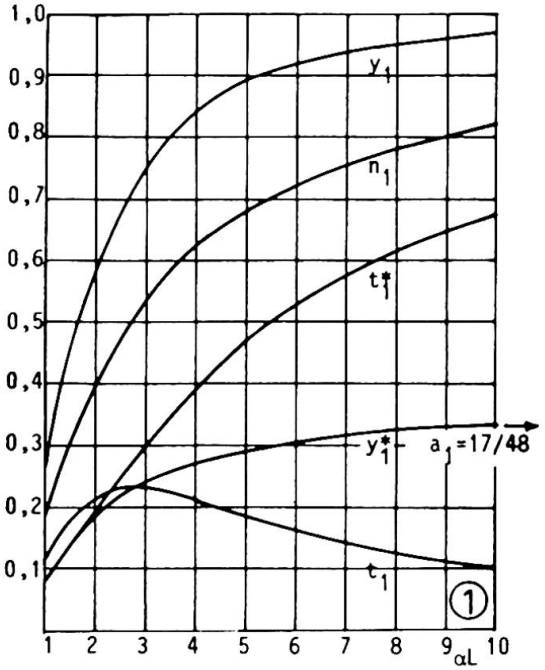

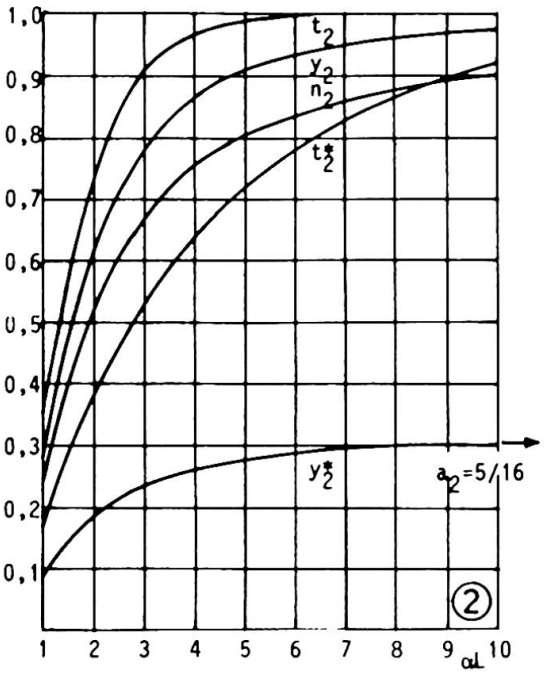

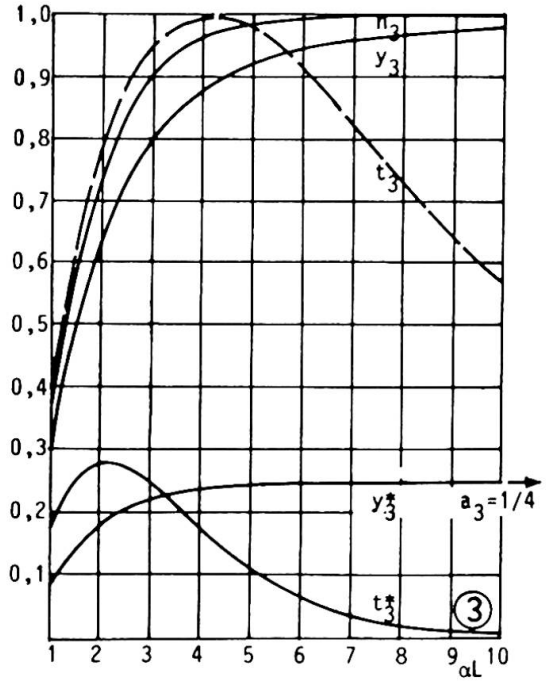

Axial loading

$$N_{x=L} = n_3(1-\gamma/\alpha^2)P$$
$$M_{t,x=L} = N_{x=L}r$$
$$T_{n,x=0} = t_3(1-\gamma/\alpha^2)P/L$$
$$T_{n,x=3L/4} = t_3^*(1-\gamma/\alpha^2)P/L \qquad (8)\ \&\ (9)$$
$$y_{x=0} = y_3(1-\gamma/\alpha^2)PrL^2/EI_0$$
$$y_{x=L/2} = y_3^*(1-\gamma/\alpha^2)PrL^2/2EI_0$$

4 Axial compression

$$P = P_C\ ;\ \gamma = \gamma_C\ ;\ N_{x=L} = N_{t,\,x=L} = P_C - N_{c,x=L} \qquad (8)$$

5 Axial tension

$$P = P_T\ ;\ \gamma = \gamma_T\ ;\ N_{x=L} = N_{c,x=L} = P_T - N_{t,x=L} \qquad (9)$$

Fig. 8 *Functions and equations for axial forces, slip forces and deflections for the five different loading cases*

The theory of composite structures with incomplete interaction or interlayer slip is well established, e.g. [10]. For cantilevers as shown in fig. 7, the boundary conditions are: (i) N=P at the free end (x=0) and Δu=0 at the fixed end (x=L). (Note that for the segment of the wall element above the floor level, the condition Δu=0 is not fully correct since the wall element is continuous at the concrete floor level.) For the loading cases in fig. 7, the interior axial forces (N_t,N_c), moments (M_t ,M_c), slip forces (T_n), slip (Δu) and deflections (y) are generally given by, cf. [11].

$$N = (\beta/\alpha^2)\{[(M_{x=0} + M''_{x=0}/\alpha^2 - \alpha^2 P_{x=0}/\beta)\sinh(\alpha L) - (M'_{x=L}/\alpha + M'''_{x=L}/\alpha^3)]\sinh(\alpha x)\cosh(\alpha L) - (M_{x=0} + M''_{x=0}/\alpha^2 - \alpha^2 P_{x=0}/\beta)\cosh(\alpha x) + M + M''/\alpha^2\} \quad (1)$$

$$M_t = (E_t I_t/EI_0)(M - Nr) \quad ; \quad M_c = (E_c I_c/EI_0)(M - Nr) \quad (2)$$

$$T_n = N' \quad ; \quad \Delta u = T_n/K \quad (3)$$

$$y = (1-\beta r/\alpha^2)y_0 + (N - N_{x=L})r/\alpha^2 EI_0 \quad ; \quad y_0 = \text{deflection for } K\to 0 \quad (4)$$

where

$$\alpha^2 = K(1/E_t A_t + 1/E_c A_c + r^2/EI_0) \quad ; \quad \beta = Kr/EI_0 \quad (5)$$

$$\gamma_C = K(1/E_t A_t + r^2/EI_0) \quad ; \quad \gamma_T = K(1/E_c A_c + r^2/EI_0) \quad (6)$$

$$EI_0 = E_t I_t + E_c I_c \; ; (K\to 0) \quad ; \quad EI_\infty = EI_0/(1-\beta r/\alpha^2 \; ; (K\to\infty) \quad (7)$$

where prime denotes differentiation with respect to x, and EA, EI and K denote the axial, bending and shear connector stiffnesses, respectively. See also figs. 6 and 7. In the three cases of transversally loaded cantilevers we have (i)N_t=N_c=N and $P_{x=0}$=0; for the case of axial compression (ii) N_c=N, N_t=P_C−N, M→P_C and β→γ_C in eq. (1), and M→P_Cr and βr→γ_C in eqs. (2) and (4); and in the case of axial tension (iii) N_t=N, N_c=P_T−N, M→P_T and β→γ_T in eq. (1) and M→P_Tr and βr→γ_T in eqs (2) and (4). The maximum interior axial forces and moments always occur at x=L (except in the case of axial compression and tension). The maximum slip forces and deflections occur at locations which are dependant on the type of loading, the element properties and the end support conditions. For practical cases the slip forces and deflections should be evaluated at x=0, x≈L/2 and x≈3L/4. The maximum interior forces and moments, and deflections for the three types of transversal loading can then be written [9]:

$$N_{x=L} = n_i(\beta/\alpha^2)M_{x=L} \quad ; \quad M_{t,x=L} = [1 - n_i(\beta r/\alpha^2)]M_{x=L}$$
$$T_{n,x=0} = t_i(\beta/\alpha^2)M'_{x=L} \quad ; \quad T_{n,x=3L/4} = t_i^*(\beta/\alpha^2)M'_{x=L} \quad (8)$$
$$y_{x=0} = [1 - y_i(\beta r/\alpha^2)]y_{0,max} \quad ; \quad y_{x=L/2} = [a_i - y_i^*(\beta r/\alpha^2)]y_{0,max}$$

where the functions n_i,t_i, t_i^*, y_i, y_i^* and a_i for the three cases of transversal loading (i=1,2,3) are given in fig. 8 [12].Note that for the case of end moment (i=3) we must choose, $M'_{x=L}$=M_E/L. The one-dimensional engineered beam theory f composite structures used here will not always render correct slip forces at the boundaries as pointed out in [9] and [13]. To remedy this deficiency, a two-dimensional theory of elasticity has to be applied, cf. [14]. In the case where i=3 we have $T_{n,x=0}\to\infty$ for K→∞ according to the theory, which obviously is not correct.t_3, therefore, has been evaluated at a selected distance from the free end of the cantilever (x≈L/4) according to fig. 8. The maximum interior forces and moments and deflections for the two kinds of axial loading are given in eqs. (9) and (10) in fig. 8.

In combined loading cases, the sign conventions for moments, axial forces, slip forces and deflections are shown in fig. 9.

The normal stresses, slip forces and deflections are then given by

$$\sigma_t = N_t/A_t + M_t/W_t \le f_t^a \quad (11)$$

$$T_n \le f_n^a \quad (12)$$

$$\sigma_c = 2N_c/A_c \le f_c^a \quad ; \quad \text{Concrete plate in compression} \quad (13)$$

$$\sigma_r = N_c/A_r \le f_r^a \quad ; \quad \text{Concrete plate in tension} \quad (14)$$

$$y \le y_{llmit} \text{ (e.g. L/90)} \quad ; \quad \text{Serviceablilty limit deflection} \quad (15)$$

where f^a denotes the allowable stress or force. In the case of combined bending and compression of the element, the internal moments (M_t) and deflections (y) should be multiplied by the following amplication factor [9]

$$v \simeq 1/(1\text{-}sP_C/P_{cr}) \quad (16)$$

where s=1,5-1,8 is the safety factor and where the critical load, P_{cr}, along with the buckling coefficients, λ, are given as

$$P_{cr} = P_{cr,\infty}/[1+(\beta r/\alpha^2)/(1-\beta r/\alpha^2)(1+\alpha^2/\lambda^2)] \quad (17)$$

$$\lambda = \begin{cases} \pi/2{,}1L \\ \pi/0{,}8L \end{cases} \quad ; \quad \begin{matrix} \text{Cantilever case} \\ \text{Propped cantilever case} \end{matrix} \quad (18)$$

3.4 Ultimate load design

The idealized load-slip curve for the nail-plates as shear connectors are given by fig. 10 [8]. As shown there are two stages of behaviour for the shear connectors:the elastic and the strain-hardening stages. Since the shear connectors control the overall response of the composite element, the element behaviour can be assumed to be similar to that of the shear connectors if the composite member components behave elastically. The transition from one stage to another starts at the most strained section and then spreads along the wall element. Using the safe assumption that when the most strained section reaches the strain-hardening stage, the whole element is said to have reached this stage, the formulae given in section 3.3 are still valid, the slip modulus $K=K_e \rightarrow K_{sh}$ being the only difference. Thus, the law of piecewise superposition can be applied. (No consideration is given here to repetative loading and deflection stability. Further, no load factor of safety is discussed). At ultimate load, the normal stresses, slip forces and deflections are then given by

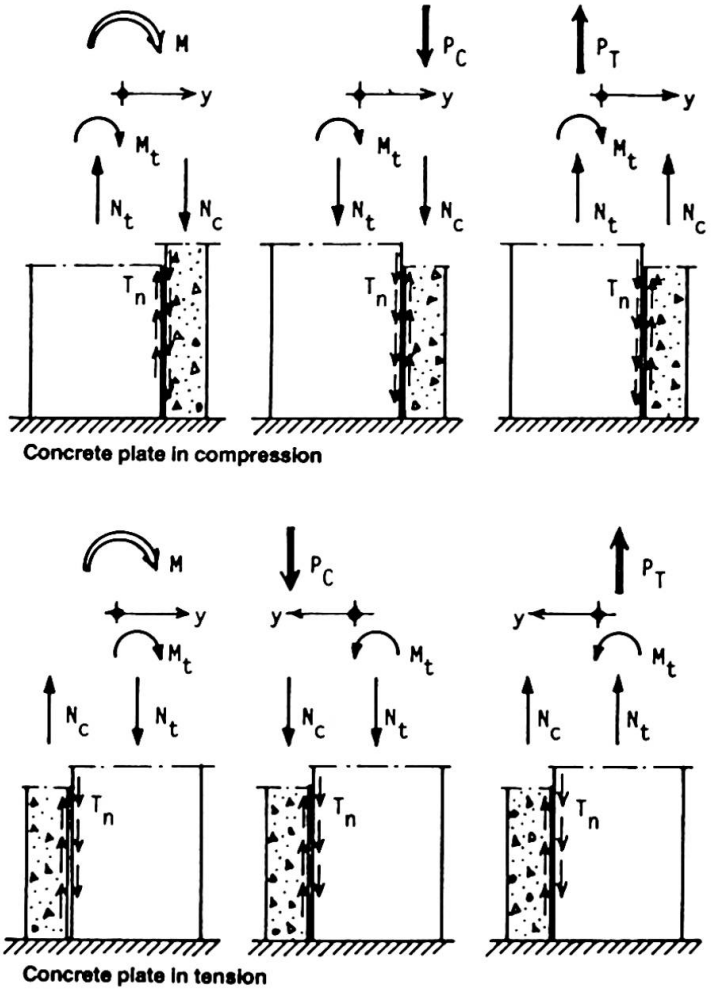

Fig. 9 *Sign conventions for axial forces, moments, slip forces and deflections in the composite elements*

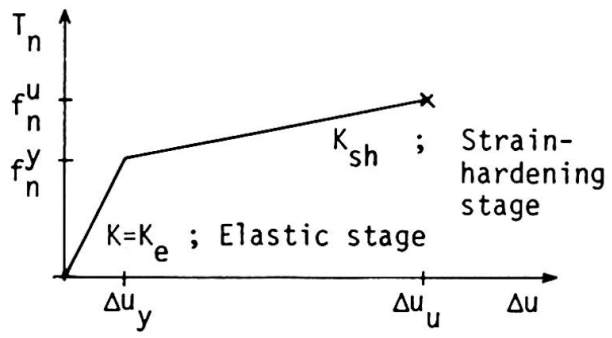

Fig. 10 *Idealized load-slipcurve for the nail-plates*

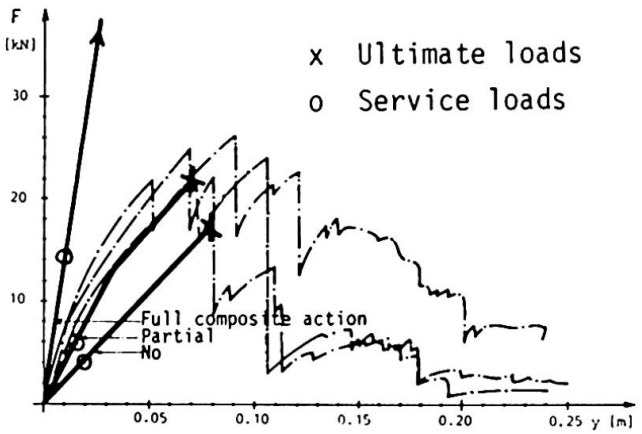

Fig. 11 *Test results for simply supported composite elements with concrete plate in compression compared to the proposed analytical model*

$$\sigma_t = N_t^e(Q_y) + [N_t^{sh}(Q-Q_y)]/A_t + [M_t^e(Q_y) + M_t^{sh}(Q-Q_y)]/W_t \leq f_t^u \quad (19)$$

$$T_n = T_n^e(Q_y) + T_n^{sh}(Q-Q_y) \leq f_n^u \quad (20)$$

$$\sigma_c = 2[N_c^e(Q_y) + N_c^{sh}(Q-Q_y)]/A_c \leq f_c^u \quad ; \quad \text{Concrete plate in compression} \quad (21)$$

$$\sigma_r = [N_c^e(Q_y) + N_c^{sh}(Q-Q_y)]/A_r \leq f_r^u \quad ; \quad \text{Concrete plate in tension} \quad (22)$$

$$y = y^e(Q_y) + y^{sh}(Q-Q_y) \leq y_u \quad ; \quad \text{Ultimate limit deflection} \quad (23)$$

where f^u denotes the ultimate stress or force, where $Q > Q_y$ is an arbitrary load and Q_y denotes the value of the load when the strain-hardening range is reached, i.e.

$$T_n(Q_y) = f_n^y \quad (24)$$

In a corresponding way the critical load in the strain-hardening range can be written (cf. Shanley's tangent modulus theory)

$$P_{cr} = P_{cr}^{sh} \quad (25)$$

3.5 Experimental verification

In order to verify the analytical method discribed above some tests on simply supported composite elements loaded at midspan were carried out [9] and one of the results is shown in fig. 11. The calculated values for service loads (eqs. 11-15) and for ultimate loads (eqs. 19-23) in the cases of full, partial and no composite action are also given in the figure. In all cases the determining failure mode was in the bending of the timber studs. It is evident from the figure that agreement is good.

REFERENCES

1. COOK, J.P.: *Composite Construction Methods.* John Wiley & Sons, 330 pp, New York 1977
2. SABNIS, G.M.: *Handbook of Composite Construction Engineering.* Van Nostrand Reinhold Company, 380 pp, New York 1979
3. PETERZÉN, S.: *EW Element - Concrete and Timber in Composite Action (in Swedish).* Swedish Journal of Building Art, No 1, pp 31-32, 1979
4. GIRHAMMAR, U.A.: *Rabo Foundation and Wall Element (in Swedish).* University of Luleå, Div of Struct Eng, Report 78:12, 16 pp, Luleå 1978
5. UNNIKRISHNA PILLAI, S. et. al.: *Nail Shear Connectors in Timber-Concrete Composites.* Journal Inst Eng (India) Civ Eng Div, Vol 58, No 1, pp 34-39, July 1977
6. PINCUS, G.: *Bonded Wood-Concrete T-Beams.* Proc ASCE, Journal Struct Div, Vol 95, No ST 10, pp 2265-2279, Oct 1969
7. DEGERMAN, T.: *Building Element Composed of Concrete and Timber - An Investigation of Different Types of Connections (in Swedish).* Lund Institute of Technology, Div of Struct Eng, Report TVBK-3012, 104 pp, Lund 1981
8. GIRHAMMAR, U.A.: *Nail-Plates as Shear Coonnectors in Composite Timber and Concrete Structures.* IABSE 12th Coongress, Vancouver, Final Report, Sept 1984
9. GIRHAMMAR, U.A.: *Rabo Wall Element - A Theoretical and Experimental Study of a Composite Element of Timber and Concrete (in Swedish).* University of Luleå, Div of Struct Eng, Research Report TULEA 1980:30, 286 pp, Luleå 1980
10. GOODMAN, J.R.: *Layered Wood Systems with Interlayer Slip.* University of California, Dept of Civ Eng, Doctoral Dissertation, 192 pp, Berkeley 1967
11. GIRHAMMAR, U.A.: *Composite Structures in Wood (in Swedish).* University of Luleå, Div of Struct Eng, Research Report TULEA 1983:43, 38 pp, Luleå 1983
12. GIRHAMMAR, U.A.: *Rabo Wall Element - Design Instructions and Documents of Standard Approval (in Swedish).* University of Luleå, Div of Struct Eng, Report 1980:11, 65 pp, Luleå 1980
13. SZALAI, J.: *Ermittlung der Verformung einseitig furnierter Platten infolge Feuchteänderung mit den Methoden der Festigkeitslehre.* Holztechnologie 21(1980)4, S. 221-226
14. CHEN, D. and CHENG, S.: *An Analysis of Adhesive-Bonded Single-Lap Joints.* ASME, Journal of Applied Mechanics, Vol 50, pp 109-115, March 1983

Pont à haubans de Coatzacoalcos II

Die Schrägseilbrücke Coatzacoalcos II

Coatzacoalcos II Cable-Stayed Bridge

Adolpho SANCHEZ-SANCHEZ
Ing. Civil,
Dir. S.T.C.
Mexico, Mexique

avec la participation de Messieurs
Carlos KING REVELLO
Dir. Ponts

Juan-Manuel GARCIA CHAVEZ
Resp. Constr.

Ladislas PAULIK
Ing. en Chef,
Dir. SOGELBERG RH
Lyon, France

avec la participation de Messieurs
Jacques MATHIVAT
Ing.-cons. SECOA, Prof. ENPC

Jacques COMBAULT
Ing. en chef Campenon Bernard

RESUME

Le pont à haubans de Coatzacoalcos II au Sud du Golfe du Mexique, sera le plus grand pont mexicain et figurera dans les dix grands ponts de ce type dans le monde, aura une longueur de 1170 m, répartie en 472 m pour le viaduc d'accès et 698 m pour le pont béton haubanné dont la travée centrale fait 288 m avec des pylônes en Y renversé de 100 m de hauteur. Cet ouvrage a été calculé sous des sollicitations exceptionelles de vents et séisme et à fait l'objet d'études spécifiques tant au niveau des structures (efforts et déformées) que de la technologie du haubanage avec des tests uniques au monde.

ZUSAMMENFASSUNG

Die Schrägseilbrücke Coatzacoalcos II im Süden des Golfes von Mexico wird die grösste Brücke Mexikos sein und zu den zehn grössten Brücken dieser Art auf der Welt zählen. Sie wird eine Gesamtlänge von 1170 m haben und besteht aus einem Anschlussviadukt von 472 m Länge und der abgespannten Brücke mit einer Länge von 698 m und einer Mittelspannweite von 288 m. Der Pylon hat die Form eines kopfstehenden Y und eine Höhe von 100 m. Das Bauwerk ist für ausserordentliche Windkräfte und Erdbeben bemessen und hat spezielle Studien auf Seite der Bemessung wie auch in der Abspanntechnik erfordert. Weltweit einmalige Grossversuche wurden durchgeführt.

SUMMARY

The Coatzacoalcos II cable-stayed bridge, situated at the south of the Mexico Gulf, will be the longest Mexican bridge and will be among the ten longest bridges of its kind in the world. Its total length will be 1170 m, with a 472 m long access viaduct and a 698 m long cable-stayed bridge with a central span of 288 m. Pylons will be 100 m high and of an upside down Y shape. This structure has been designed to resist high winds and earthquakes. It has been tested using sophisticated structural design procedures and through new technology in cable staying.

1 – HISTORIQUE

La liaison avec le SUD-EST du Mexique croise obligatoirement le fleuve navigable de COATZACOALCOS près de la ville du même nom au Sud du Golfe.

Avant l'inauguration en 1962 du premier pont COATZACOALCOS I (longueur 966 m,2 voies routières, 1 voie ferroviaire) la traversée du fleuve s'effectuait grâce à un bac transbordeur. Le trafic, à l'époque, était de 1 300 véh/j avec coupure totale lors du passage d'un bateau, puisque l'ouvrage comporte une travée centrale levante jusqu'à 66 m de hauteur.

En 1972, le pont fut endommagé par un choc d'un bateau ce qui entraîna une coupure totale du transit de plus d'un mois pour réparation et créa une perte considérable à l'économie régionale. Cet accident et l'augmentation importante du trafic avec l'expansion du pays (17 000 véh/j en 1980) ont conduit les autorités à s'engager dans la construction d'un nouveau pont, objet de la présente communication.

Figure 1 : Vue générale du site depuis la pile 2 vers Minatitlan

Le pont de COATZACOALCOS II se situe dans une courbe très prononcée du fleuve, site qui présentait les meilleures caractéristiques géologiques pour les fondations et topographiques pour la longueur de l'ouvrage.

Il s'intègre dans le projet de déviation de la ville industrielle de COATZACOALCOS, port important du Golfe du Mexique.

L'ambiance agressive de l'environnement (mer, hygrométrie, raffinerie) et la fréquence de vents violents nous ont poussés à choisir un pont en béton plutôt que métallique pour sa meilleure stabilité aéroélastique et son meilleur comportement aux agents agressifs.

De plus, le site est situé en zone sismique.

3 – LES CONTRAINTES ET DONNEES DE BASE

Le Rio étant navigable, le gabarit minimum à respecter était de 150 m de largeur sur 35 m de hauteur.

L'ouvrage doit livrer le passage à deux sens de circulation de deux voies avec les charges AASTHO HS 20 44 (MS 18) conformes au nouveau règlement du Ministère des Communications.

Situé en région de cyclones, l'ouvrage devra supporter des vents allant jusqu'à 200 km/h, exerçant une pression maximum de 320 kg/m².

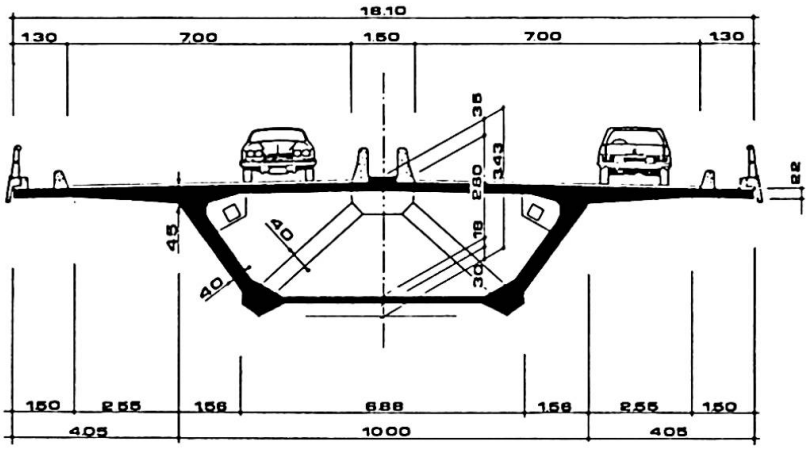

Figure 2 : Coupe transversale

S'agissant d'une région sismique, il est nécessaire de prendre en compte un séisme suivant deux spectres différents dans les trois dimensions avec des combinaisons du type : $\pm 0{,}3\ S_x \quad \pm 0{,}3\ S_y \quad \pm 0{,}3\ S_z$.

Enfin les différentes températures à considérer ont été :
± 6° C de variation uniforme,
10° C de différence de température entre haubans et tablier,
6° C de différence de température entre fibres supérieure et inférieure du tablier.

4 – LES CARACTERISTIQUES TECHNIQUES

Les choix respectifs des paramètres fondamentaux de l'ouvrage ont été faits en prenant comme critères :
– le meilleur comportement statique et dynamique des structures,
– les facilités d'exécution tenant compte de l'évolution technologique souhaitée,
– l'aspect architectural de l'œuvre.

Cet ouvrage, qui sera le plus grand du pays, figurera dans la série des dix plus grands du Monde de ce type, aura une longueur totale de 1 170 m répartie en 472 m pour le viaduc d'accès comportant des travées de 60 m, et 698 m pour l'ouvrage principal haubané, objet de la présente communication, dont les travées sont respectivement de 30 - 49 - 112 - 288 - 112 - 60 et 46 m (environ). (Figure 3 : Coupe longitudinale).

Le mode de suspension axial est longitudinalement du type semi-éventail, comportant 17 haubans (de 37 à 61 torons de 150 mm^2 de section sous gaine métallique injectée de 205 mm de diamètre) ancrés dans le tablier tous les 7,20 m et passant dans le mât en déviation.

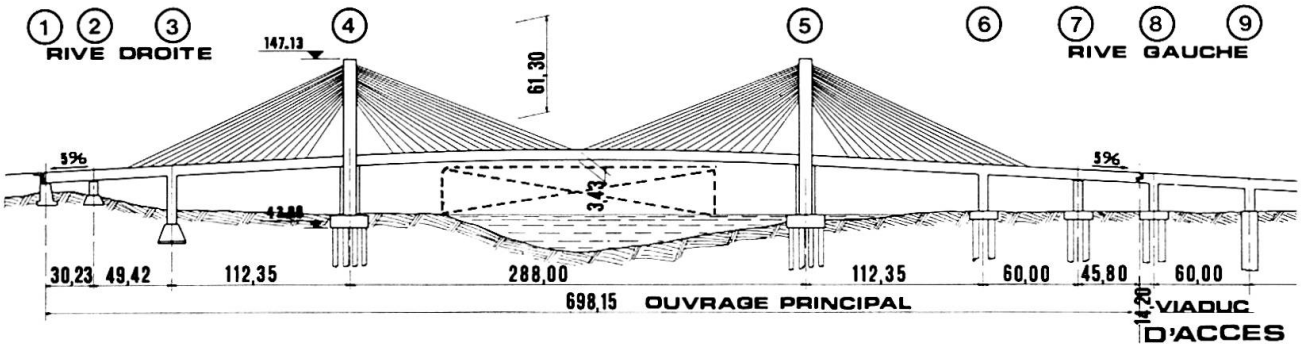

Figure 3 : Coupe longitudinale

En raison des sollicitations importantes dans le sens transversal (vent et séisme), le pylône choisi a été du type Y renversé, ce qui ne conduit à aucun élargissement du tablier.

Les appuis 2 - 3 - 6 et 7 sont de type classique, de section rectangulaire évidée, armée et précontrainte pour les plus sollicitées. Les appuis 4 et 5 ont une hauteur de 97 m, le tablier passant à 35 m au-dessus du niveau du fleuve, et ont fait l'objet d'études tant structurelles qu'architecturales.

Les piles principales et adjacentes sont encastrées dans le tablier, les autres étant équipées d'appuis glissants longitudinalement et comportant des butées en béton pour la transmission des efforts sismiques transversaux.

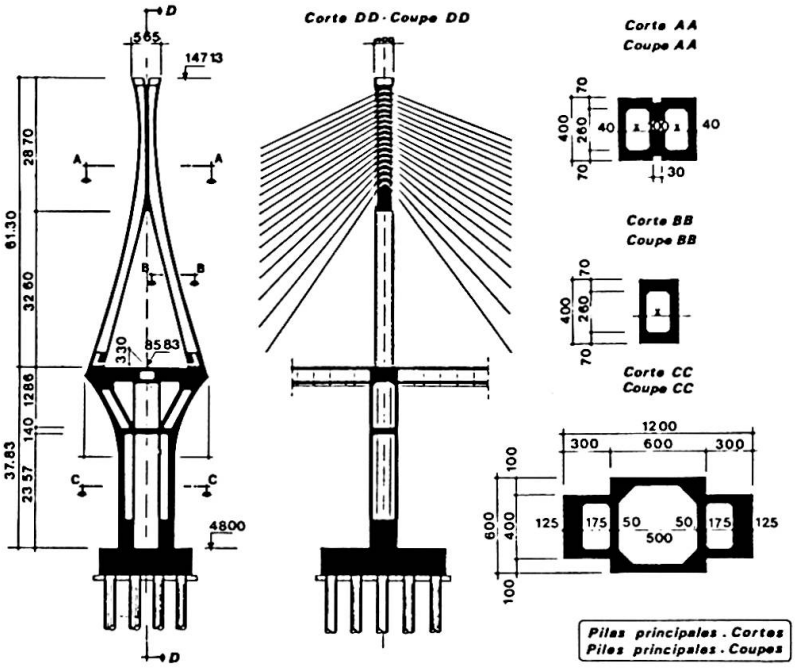

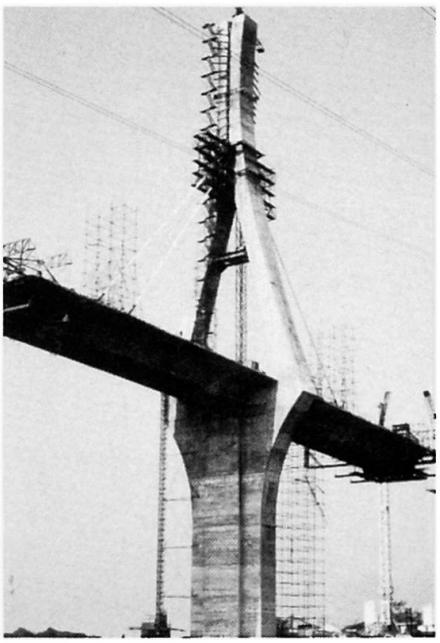

Figure 4 : Piles principales – Coupes

Les fondations sont du type profond, sur pieux de 2,50 m de diamètre et de 30 m de profondeur, avec élargissement en base de 3,50 m. Les piles principales comportent 18 pieux reliés par une semelle en béton armé de 6 m d'épaisseur, réalisée à l'abri d'un batardeau circulaire de 30 m de diamètre.

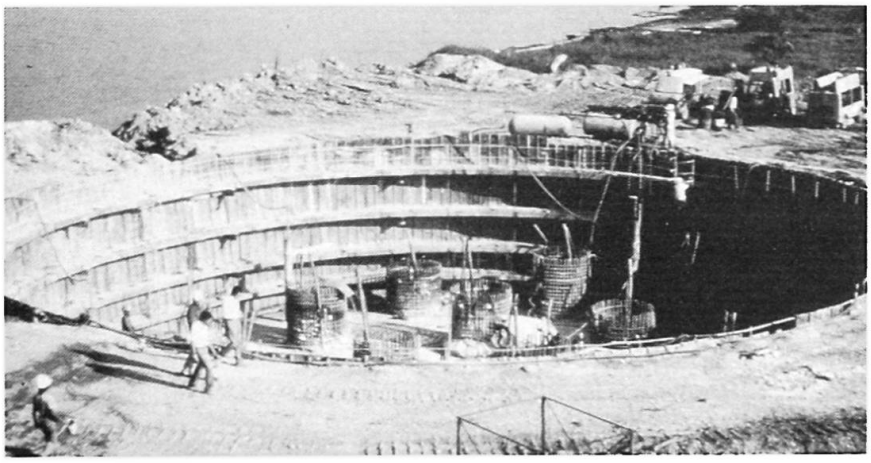

Figure 5 : Fondations des piles principales

Le tablier est constitué d'un caisson de 3 m de hauteur avec des âmes inclinées. La largeur du hourdis supérieur est de 18 m, avec deux chaussées de 7 m, un terre plein central de 1,50 m où s'ancrent les haubans, et deux trottoirs latéraux de passage de 1,30 m.

Le mode de construction est du type classique par encorbellements successifs réalisés à l'aide d'un équipage mobile permettant l'édification de voussoirs complets de 3,53 m de longueur. Chaque voussoir présente des butons préfabriqués avec uniquement au droit des ancrages une précontrainte extérieure 2 x 12 K 13 dans une gaine métallique injectée.

L'ouvrage présente une précontrainte longitudinale réalisée pour la première fois au Mexique, en 12 et 19 K 15, ancrée dans des bossages préfabriqués et une précontrainte transversale du type 12 Ø 7 tous les 44 cm.

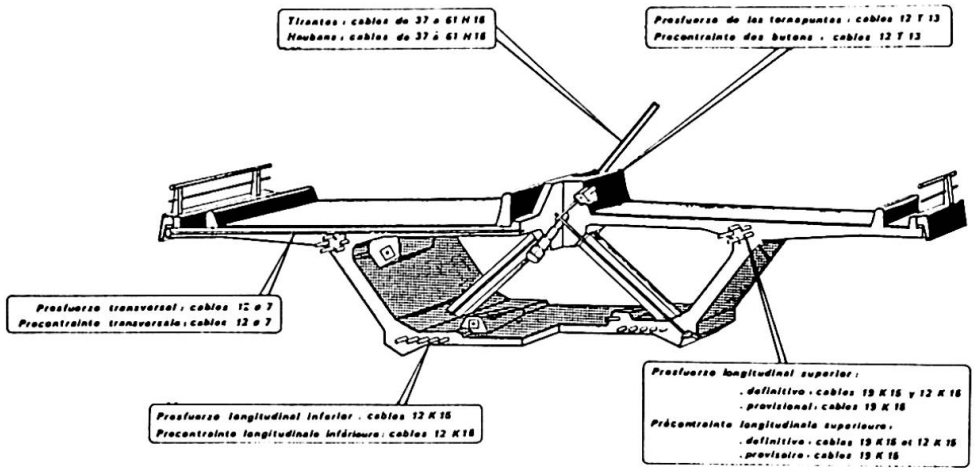

Figure 6 : Principe de précontrainte du tablier

Les séquences de réalisation ont été :
- exécution des fléaux sur piles 2 - 3 - 6 et 7 en encorbellement classique,
- exécution de la partie restante sur pile 1 avec échaffaudage au sol, et sur pile 7 par haubanage provisoire des quatre derniers voussoirs avant l'articulation, et ce après avoir procédé aux clavages des travées adjacentes,
- exécution des fléaux sur piles 4 et 5 en encorbellement classique jusqu'au 10ème voussoir,
- mise en place des deux premiers haubans et exécution de la partie restante haubanée avec trois voussoirs en encorbellement (équipage en position de coulage du quatrième) par rapport au dernier hauban tendu. Le cycle normal d'exécution est de 1 hauban par quinzaine, soit 14,50 m de tablier.

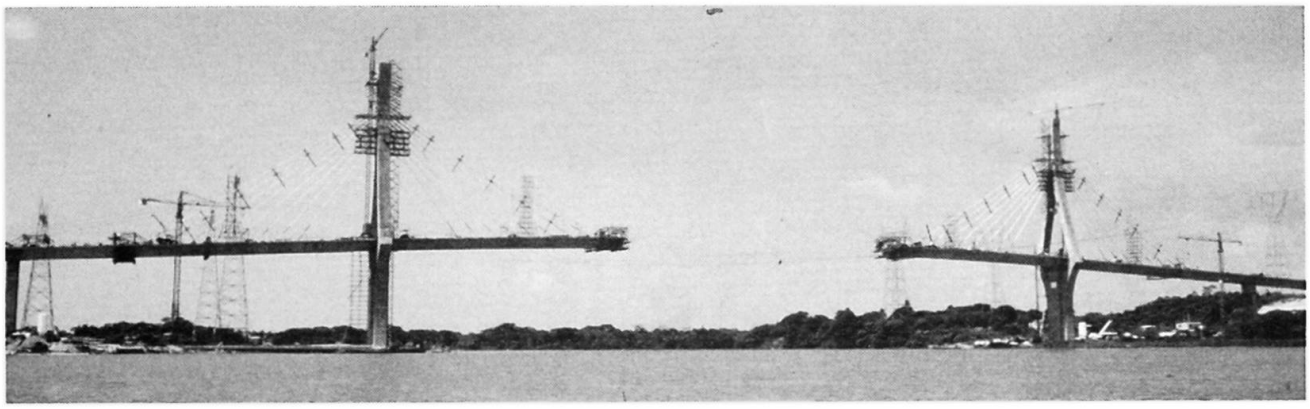

Figure 7 : Vue générale du chantier après clavage latéral

A l'exception des deux premiers haubans, qui sont montés à l'aide d'une tour provisoire, tous les haubans sont hissés grâce à un appareil dénommé " bicyclette " qui roule et prend appui sur le dernier hauban tendu et est stabilisé transversalement par des jambes butant sur les deux haubans antérieurs. Ces appareils sont munis de galets sur lesquels roulent les gaines métalliques, après soudure en partie basse par éléments de 12 m. A partir des plates-formes mobiles du mât sont introduits les torons un par un, par l'intermédiaire d'une fenêtre entre le tube de transition et la gaine courante, à travers des grilles de classification (fig. 9).

Figure 9 : Enfilage de torons.

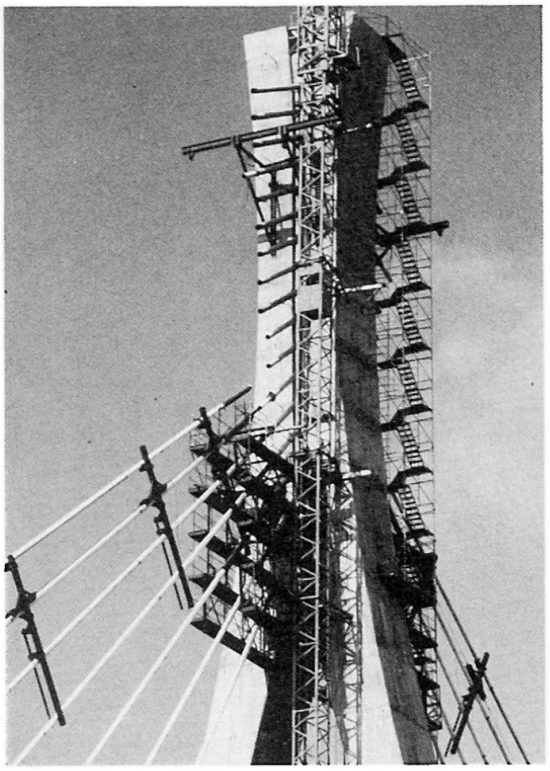

Figure 8 : Plate-forme supérieure et "bicyclette "

Après blocage par vissage du tube de transition inférieur sur l'ancrage, on tend à la tension initiale du calcul. On mesure et les déplacements du mât et du tablier, et la température, afin de comparer ces valeurs à celles calculées (profil pratique et théorique), pour calculer des corrections éventuelles et ainsi assurer une parfaite géométrie finale.

Avec un décalage de trois haubans on procède alors à l'injection selon le procédé original suivant :

- Surtension du hauban à injecter, à la valeur maximum de sa vie, simultanément de part et d'autre du mât. Ce processus nous a permis dans une phase connue du calcul de peser les réactions du hauban et d'effectuer une comparaison fiable avec le calcul prévisionnel. Les différences constatées ont été inférieures à 1 %, montrant la fiabilité du module de calcul. Outre cette vérification, la surtension a pour objet d'assurer par la suite, à la détension, une compression du coulis d'injection, augmentant ainsi la sécurité quant à une éventuelle fissuration du coulis par traction.
- Blocage du tube courant avec le tube de transition, par injection à la résine de l'espace entre tube coupleur et ces derniers.
- Injection de huit des haubans, simultanément de part et d'autre de la pile, à partir du tablier vers les mâts, à l'aide d'un coulis de ciment refroidi, jusqu'au réservoir d'exudation en partie supérieure du mât.
- Détension du hauban après prise du coulis.

Toutes ces opérations ont fait évidemment l'objet d'un contrôle très strict, ce qui a permis de claver la travée centrale avec seulement un décalage entre fléaux de 4 mm.

5 – LES ETUDES PARTICULIERES

Cet ouvrage a fait l'objet d'études spéciales et originales, qu'il est intéressant de faire connaître et qui seront développées :

1 - Etude de répartition des travées latérales de 60 m ou 112 m. La travée la plus longue a été finalement choisie pour des raisons essentiellement esthétiques, le surcoût n'étant pas significatif.

2 - Une étude des fondations profondes des appuis principaux a été réalisée, tout d'abord suivant la technique des caissons havés, méthode très utilisée au Mexique.

3 - Et plus tard avec utilisation de gros pieux coulés en place, méthode toute nouvelle dans le pays, à l'époque. Un essai " in situ " a été réalisé sur un pieu de 0,90 m de diamètre et de 25 m de profondeur avec un chargement cyclique de 80 à 520 t, ce qui détermina la capacité portante finale.

4 - L'étude des effets du séisme (les premières études de stabilité générale ayant mis en évidence l'effet prépondérant du séisme dans le dimensionnement) a été faite par superposition de différents modes de vibration avec deux types de spectres mexicains. L'analyse réalisée dans les trois directions avec combinaison aSx + bSy + cSz a donné comme résultat un déplacement de 38 cm sous séisme vertical et un déplacement de 18 cm en haut du mât sous séisme transversal. De plus, l'Institut d'Ingénierie Mexicain a étudié l'influence d'une réponse sismique suivant les différentes phases de mouvement des appuis.

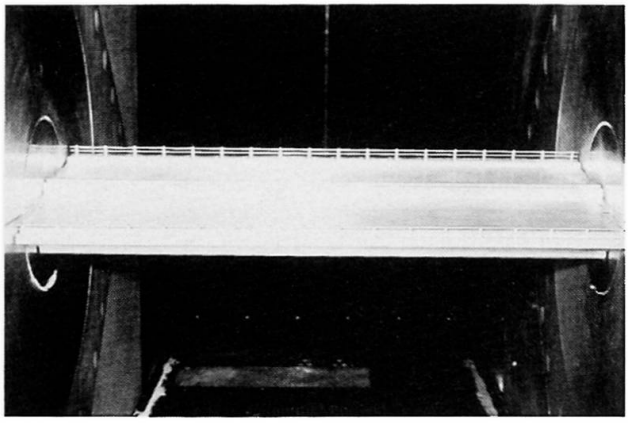

Figure 10 : Essais de l'O.N.E.R.A.

5 - Etude des effets du vent réalisée à l'ONERA sur modèle réduit en soufflerie, pour appréhender le phénomène de " flottement " à deux degrés de liberté flexion-torsion du tablier, et le phénomène d'échappement tourbillonnaire et les vibrations induites. Avec un coefficient d'amortissement de 5.10^{-3}, le déplacement vertical en bout de console, dans l'axe de la grande travée de 288 m, pourra atteindre une valeur de l'ordre de 16 cm correspondant à un angle de torsion de 1 degré.

6 - Etude aux éléments finis (calcul spatial) de la répartition des efforts à différents voiles de la partie supérieure des piles principales (liaison entre le tablier, les bras du pylône et le cœur de la pile).

7- Etude aux éléments finis (modèle spatial) de la répartition des efforts dans le tablier entre hourdis inférieur, supérieur, butons et ancrages.

8 - Les haubans étant des éléments essentiels pour la stabilité de la structure, le choix de leurs composants à fait l'objet d'études spécifiques et pour certaines inédites.

a) Calcul pour chaque hauban des variations de tension résultant à la fois des différents chargements et des variations angulaires (vent, charges d'exploitation, fluage, gradient de température) et de l'existence du tube de transition.

b) Différentes recherches pour le passage des haubans dans le mât (tube déviateur, ancrages doubles croisés à une ou deux nappes). Le système de déviation a été retenu pour son économie et son esthétique (alignement de la nappe des haubans).

c) Enfin des tests uniques au monde ont été réalisés pour cet ouvrage à l'EMPA (Suisse) :

1 - Test dynamique comparatif des ancrages de deux fournisseurs, sur des ancrages de 37 torons injectés avec une charge maximum de 0,45 R_G. Trois séries de 2×10^6 cycles ont été faites successivement, avec une amplitude croissante correspondant à 16 - 22 et 26 kg/mm ^{2}, avec, entre chaque série, un test statique allant à 0,70 R_G (la puissance de l'installation ne pouvant aller au-delà sans démontage ; il s'agit de test en traction pure à 4,2 Hz).

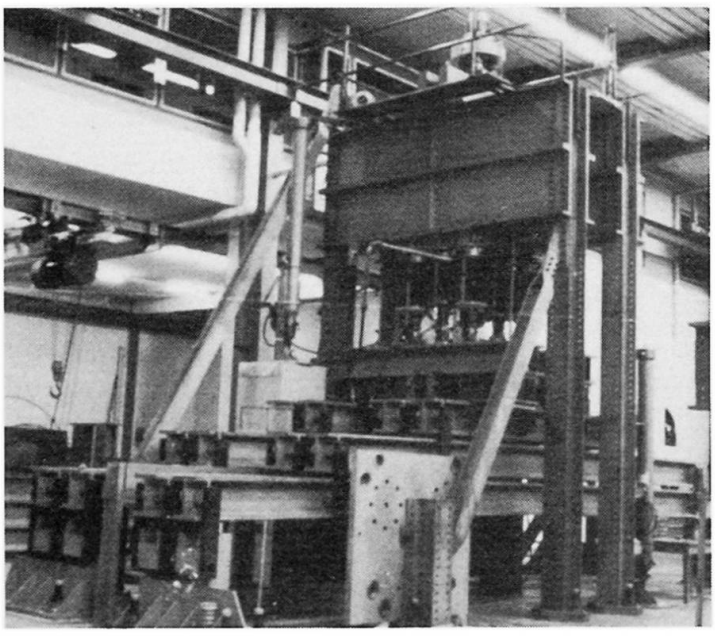

Figure 11 : Test de la résistance à la fatigue d'ancrages 37 T 15.

2 - Test dynamique à la fatigue sur un système de déviation dans le mât, avec un hauban de 12 T 15 injecté, muni de sa gaine métallique et des tubes de transition en sortie du bloc bas simulant le tablier et dans le bloc haut simulant le mât, avec un rayon de courbure de 2,50 m conduisant à des pressions de contact équivalentes à celle de l'ouvrage réel. La tension du hauban varie entre 600 et 750 MPA, avec une variation angulaire de 3.10^{-3} radian. Il est à noter que le test est beaucoup plus représentatif de la réalité que les tests classiques, puisque s'ajoutent aux variations de tension axiale les surtensions dues au mouvement angulaire des câbles. La fréquence trop rapide de 4,2 Hz a contribué à une perte d'adhérence du tube coupleur, mais le système a tenu $2,1.10^6$ cycles.

3 - Test dynamique de $2\text{-}10^6$ cycles sur toron, à 0,8 Rg et avec une amplitude de 20 kg/mm^2

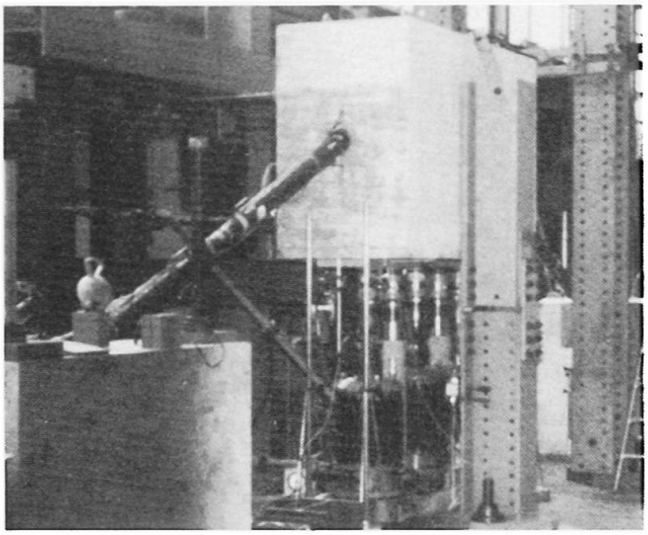

Figure 12 : Test de résistance à la fatigue sur un câble 12 T 15 dévié.

6 – QUANTITES ET DATES

L'ouvrage représente 25 000 m^3 de béton, 3500 t d'acier de béton armé, 670 t d'acier de précontrainte dont 100 pour la précontrainte transversale, 170 t pour la précontrainte longitudinale définitive, 400 t pour les haubans. Le projet comporte 480 plans.

Les études de faisabilité ont démarré en 1979, les travaux de fondations ont débuté à la mi avril 1980, le clavage central a été réalisé le 8 mars 1984, les épreuves ont eu lieu en juillet 1984. Il faut de plus ne pas perdre de vue que le rythme du chantier a été très affecté à la fin de 1982 par la crise économique.

7 – CONCLUSIONS

Cette réalisation, fruit d'une coopération technique Franco-Mexicaine en tout point de vue remarquable, sera un symbole manifeste de l'expansion du Mexique, qui se hisse ainsi au niveau technique des pays les plus avancés en matière de construction de pont.

BIBLIOGRAPHIE

1. Projet et construction des ponts à haubans de COATZACOALCOS II et TAMPICO. Communication de A. SANCHEZ-SANCHEZ – L. PAULIK - Congrès F.I.P. Stockholm. Juin 1982.

2. Revue I.A.B.S.E. STRUCTURES C-28/83 - Constructions récentes-Part II 15 pages 94-95, Pont de COATZACOALCOS II (Mexique) L. PAULIK - P. SAINTIER.

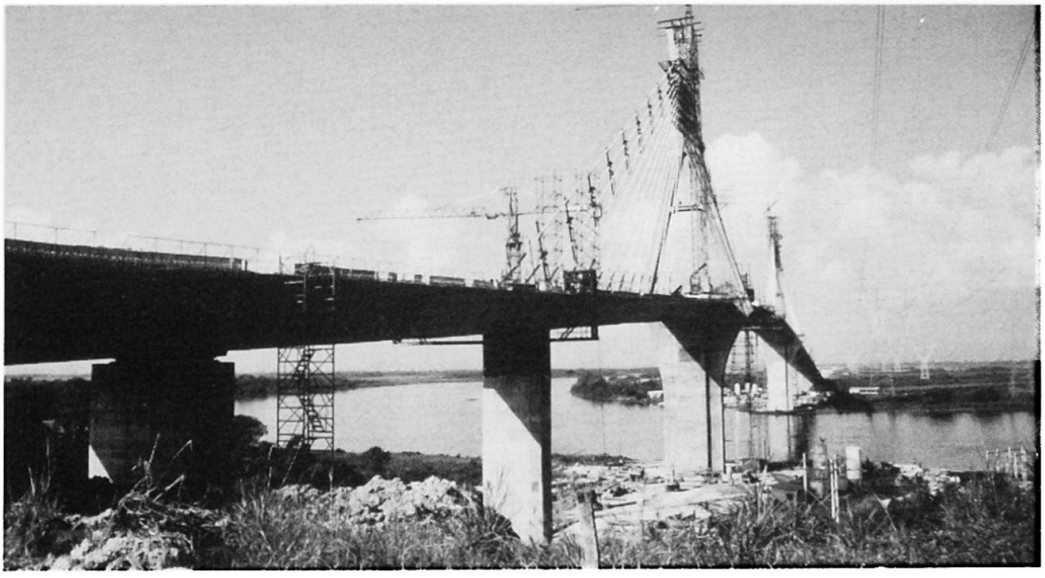

Figure 13 : Vue générale du pont.

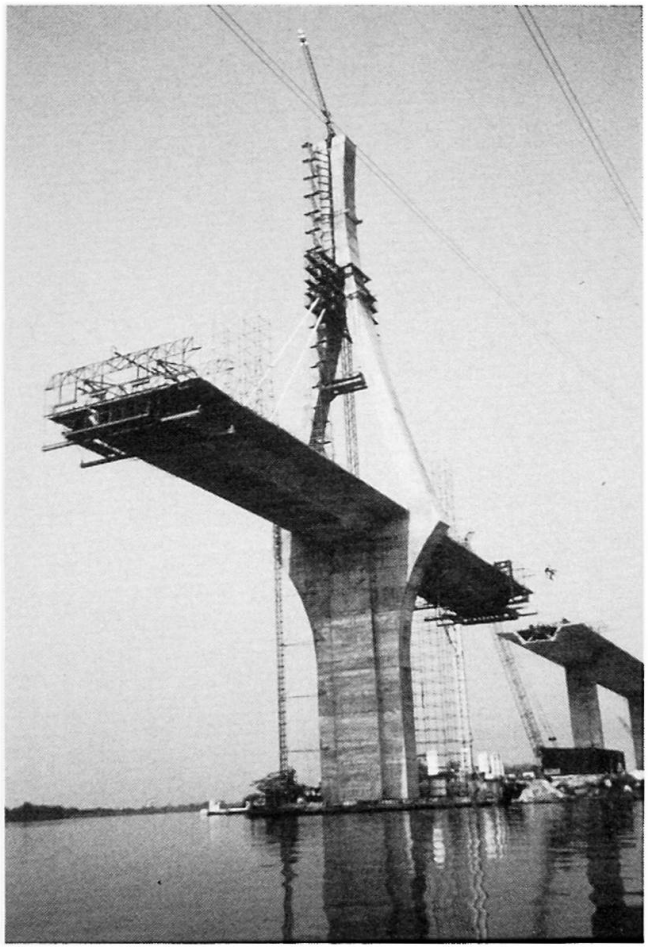

Figure 14 : Un grand fléau en cours de construction

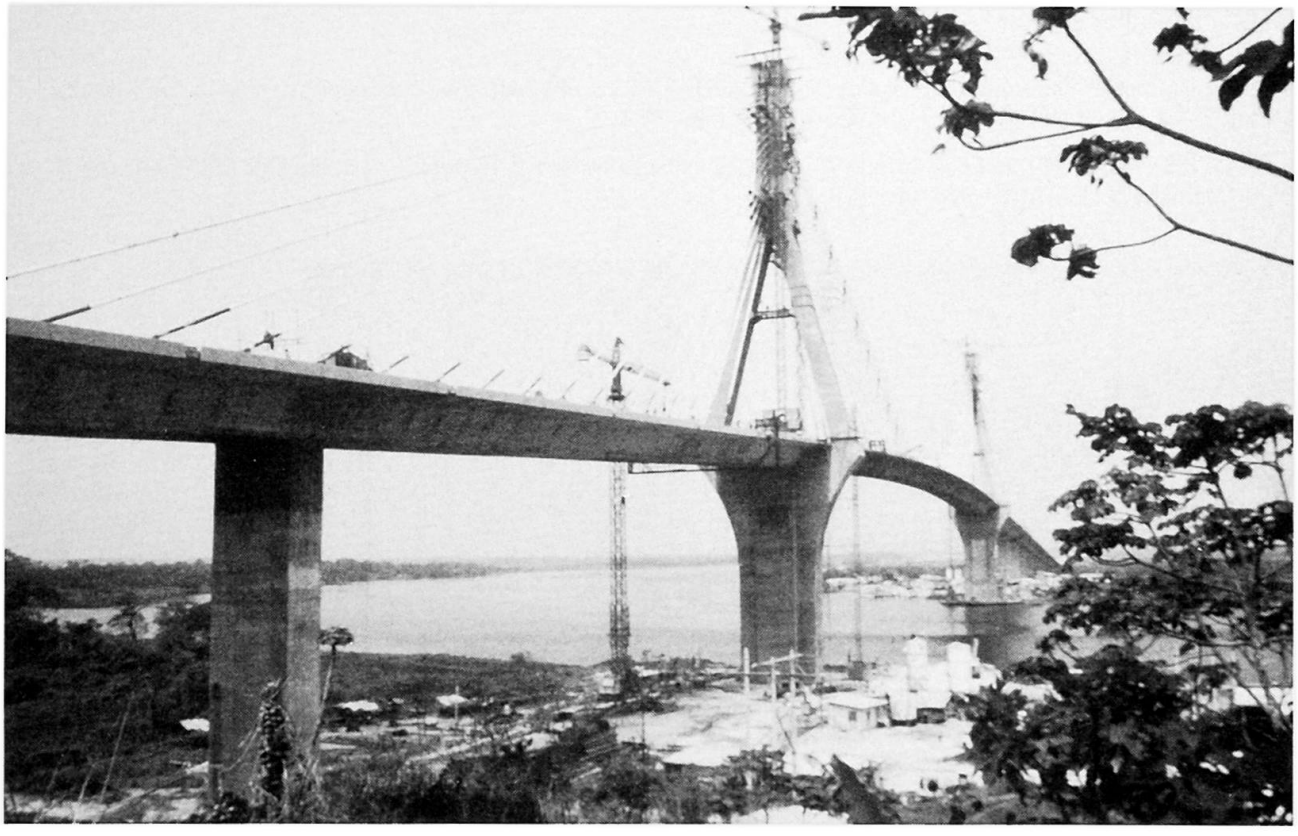

Figure 15 : Le pont achevé

Composite Slab Bridges Using Deformed Flange T-shapes

Ponts-dalles mixtes utilisant des profilés en T à membrure déformée

Verbundplattenbrücken aus T-Trägern mit Formflansch

Tokuya YAMASAKI
Technical Adviser
Kawasaki Steel Corp.
Chiba, Japan

Tadao KANEKO
Manager
Kawasaki Steel Corp.
Chiba, Japan

Masakatsu SATO
Senior Researcher
Kawasaki Steel Corp.
Chiba, Japan

Tokuya Yamasaki, born 1922, got his Dr. degree in 1962, engaged as Prof. of structural engineering at Kyushu University, 1962–1971. From 1971 to 1982 he was General Manager and is now Technical Adviser at R&D Center of Kawasaki Steel Corp.

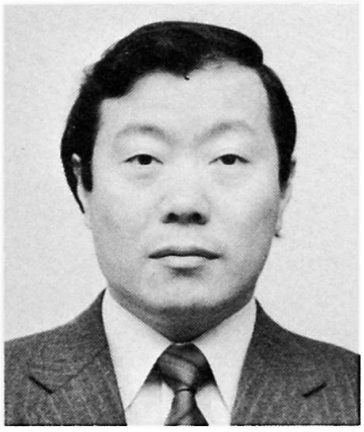

Tadao Kaneko, born 1943, got his Dr. degree in civil engineering at Kyushu University. Since 1972, he has studied the strength analysis of steel structures and is now senior researcher at R&D Center of Kawasaki Steel Corp.

Masakatsu Sato, born 1942, got his Dr. degree in analysis of composite girders at Tokyo University. For ten years he has been conducting research on composite and mixed structures at R&D Center of Kawasaki Steel Corp.

SUMMARY

Composite slab bridges made by filling up deformed flange T-shapes with concrete have been used for road bridges since 1982 in Japan. The structural characteristics of this bridge type have been investigated by conducting a high cycle fatigue test and a static bending rupture test. A design method is proposed.

RESUME

Les ponts-dalles mixtes — fabriqués en remplissant de béton des profilés en T à membrure déformée — sont utilisés au Japon depuis 1982, en tant que ponts routiers. Les caractéristiques structurales de ce type de pont ont été contrôlées au moyen d'essais de fatigue et d'essais statiques de rupture à la flexion. Une méthode de calcul est proposée.

ZUSAMMENFASSUNG

Verbundplattenbrücken, bestehend aus mit Beton gefüllten T-Profilen mit Formflansch, kommen seit 1982 in Japan als Strassenbrücken zur Anwendung. Das charakteristische Tragverhalten dieser Brücken konnte mit einem Ermüdungsversuch und einem statischen Biegebruchversuch bestätigt werden. Ein Bemessungsverfahren wird vorgestellt.

1. INTRODUCTION

Today, steel-concrete composite structures are widely used as materials for civil engineering and building because of a rational combination of the advantageous characteristics on steel and concrete; steel's tensile strength and toughness, concrete's compressive strength and stiffness, and composite structure's noise and vibration absorption and high corrosion resistance properties.

It is of primary importance that the steel-concrete composite structure be provided with an effective stress transmission mechanism in its steel-concrete interface. The bond strength between steel and concrete may be increased through either mechanical shear connectors, as used in composite girders, or surface projections as of deformed bar[1]. The latter has a great advantage in executive efficiency and material saving, and therefore, any substantial improvement in steel-concrete bond must be derived from the optimum selection of steel surface projections. In 1977, Kawasaki Steel corp. developed deformed flange H-shapes with lateral projections on the outside surface of both flanges, as shown in Fig. 1 for composite structures. The encased T girder in which the above-mentioned H-shapes were covered with expansive concrete and SRC piers in which these H-shapes were used instead of deformed bars were put to practical use in 1978 and 1979, respectively[2].

Recently, the authors have developed a new-type composite slab bridge made by filling up deformed flange T-shapes (cutting in half the new H-shapes) with expansive concrete. In this slab bridge, projections on the upper flange play the roll of shear connector to permit the concrete covering to make thinner. Therefore, the depth of this bridge can be made lower than that of coventional bridges. Further, the bottom plates can be utilized as permanent forms, thereby making it possible to achieve higher execution accuracy and reduce construction time.

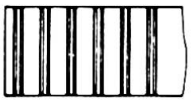

In this paper, the bond strength of deformed flange H-shapes to concrete are made clear. Then, the mechanical properties of this slab in the elastic range as well as the characteristics of constructional co-operation of steel girder and slab concrete at the failure stage are confirmed by conducting a high-cycle fatigue test and static bending rupture test on the approximately full-sized slab specimens. Finally, a design method is proposed for road bridges.

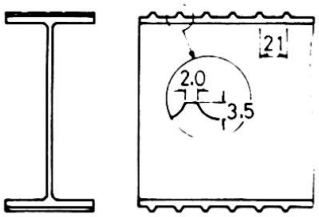

Fig. 1 Profile of deformed flange H

2. SELECTION OF PROJECTION SHAPES

2.1 Pull-out Tests for Flat and Lugged Steel Plates

The bond characteristics of lugged plates are considerably affected by such factors as height h, spacing d and setting angle θ of projection, and it has been empirically confirmed that the influence of θ is negligible when it is not less than 50°. In the present pullout tests where θ was set at 60° with h and d adopted as parameters, 17 sets of steel plates with lateral projections, including deformed flange plates of H-shapes, all of which are shown in Table 1, were used. The maximum size of aggregate coarse was 25 mm, and the

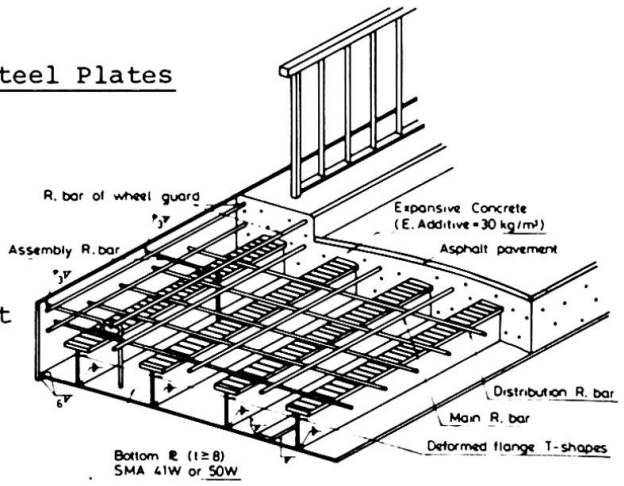

Fig. 2 Schema of composite slab bridges using deformed flange T-shapes

design strength of concrete was 29.4 MPa. Following four weeks of air curing, pull-out tests were performed to determine the relationship between bond stress τ_b and slip δ_f at the free end of test specimens.

2.2 Effect of Projections on Bond Stress

The relationship between τ_b and δ_f in pull-out tests is shown in Fig. 3 Bond strength of flat steel plate depends on inherent adhesion on the steel-concrete interface, such as agglutination and friction. Much of it is on the latter. Consequently, as the steel plate begins to slip, the amount of slip rises sharply to reach the maximum bond stress τ_{bmax}. On the other hand, lugged steel plates are designed to reinforce mechanical resistance to slip by means of projections. δ_f increases in proportion to pull-out load after relative slip is generated. Therefore, τ_b is more important factor rather than τ_{bmax} in pull-out test for lugged steel plate. It can be recognized from Fig.4 that τ_b is roughly in proportion to h and inverse proportion to d.

However, there are limiting factors in manufacturing of projection on flanges such as pressing capacity and temperature control during rolling process. On the basis of the test results and investigations, 3.5 mm and 19 mm have been adopted as lateral projection height and space on surface of deformed flange H-shapes, respectively.

Sign of specimen	Projection h (mm)	Projection d (mm)	Bond stress τ_b(MPa) δ_f=0.05 mm	Bond stress τ_b(MPa) δ_f=1.00 mm	Remark
A 0			2.2	2.4	Flat plate
A-1.5-a	1.5	7.5	10.1	14.5	Lateral lug
b	,,	15.0	8.6	15.5	,,
c	,,	22.5	6.0	13.8	,,
d	,,	30.0	5.0	10.9	,,
A-3.0-a	3.0	15.0	11.6	18.1	,,
b	,,	30.0	7.1	17.1	,,
c	,,	45.0	5.1	13.7	,,
d	,,	60.0	4.7	11.1	,,
A-4.5-a	4.5	22.5	10.3	18.2	,,
b	,,	45.0	7.5	16.3	,,
c	,,	67.5	7.2	16.2	,,
d	,,	90.0	6.8	13.4	,,
A-6.0-a	6.0	30.0	11.0	20.6	,,
b	,,	60.0	7.5	16.9	,,
c	,,	90.0	7.0	15.6	,,
DFH	3.5	20	11.5	20.5	Deformed flange
D51	3.5	15	8.4	15.5	Deformed bar

Table 1 Results on pull-out test

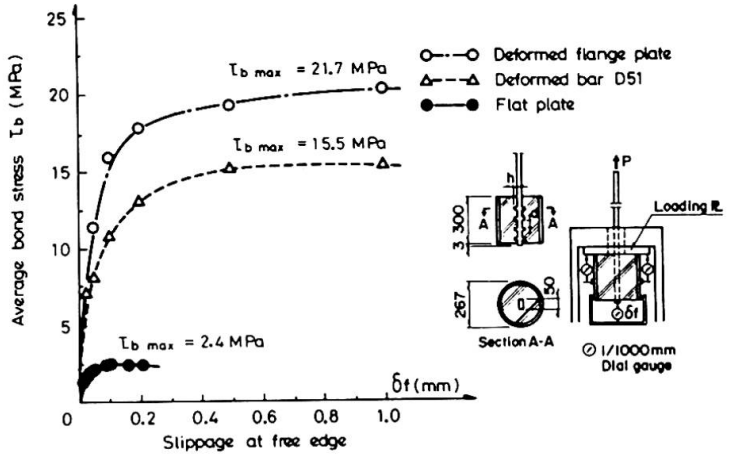

Fig. 3 Average bond stress and slip curves

3. CALCULATION OF WORKING STRESS AND ULTIMATE STRENGTH

3.1 Calculation of Neutral Axis and Shearing Stress

When concrete is sufficiently bonded to steel girder and they form the unit construction, it is an usual practice to neglect the tensile stress of concrete and obtain the stress of the composite materials on the basis of the converted sectional area method in which the compressive concrete is transposed to that of steel by using the elastic modulus ratio.

The distance X from the upper extreme edge of concrete to the

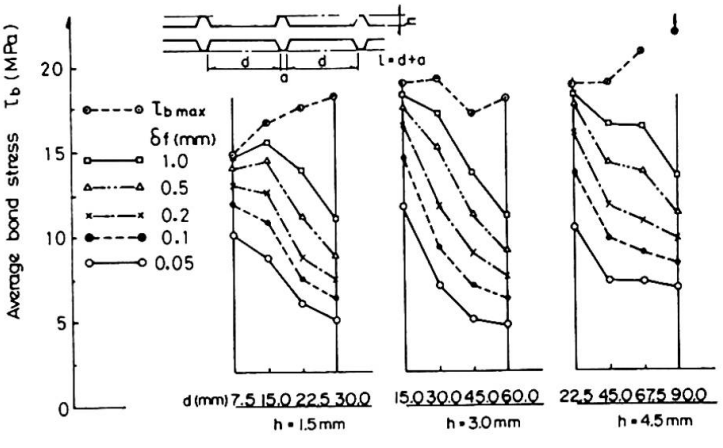

Fig. 4 Relation between average bond stress and projection height & space

neutral axis is obtained by

$$X = \frac{n \cdot A_s}{B}\left(-1+\sqrt{1+\frac{2 \cdot B \cdot g_s}{n \cdot A_s}}\right) \quad (1)$$

where B: Lateral distance between deformed flange T-shapes (cm)
A_s: Sectional area of steel girder (cm^2)
g_s: Distance from upper extreme edge of concrete to the center of gravity of steel grider (cm)
n: The elastic modulus ratio of steel to concrete

Next, the moment of inertia of the composite section I_v is obtained by

$$I_v = \frac{B \cdot X^2}{3n} + I_s + A_s(g_s - X)^2 \quad (2)$$

where I_s: The moment of inertia of steel girder (cm^4).

Assuming that horizontal shearing force is transmitted by projection on the upper flange, shearing stress τ_d is given by

$$\tau_d = \frac{Q_c \cdot S_d}{I_v \cdot b_f} \quad (3)$$

where Qc: Statical moment of area converted into steel on the compression side of concrete (cm^3)
b_f: Width of upper flange (cm)
S_d: Shearing force (N)

3.2 Calculation Formulas of Ultimate Strength

3.2.1 Assumptions

(1) Ultimate stress distribution of steel and concrete section is assumed to be rectangular shape.
(2) Tensile stress of concrete is neglected.
(3) The sectional area of steel is not subtracted from that of concrete.
(4) Ultimate strengths of concrete and steel are definited as 85% of design strength of concrete and nominal yield point of steel, respectively.

3.2.2 Calculation Formulas for X_p, M_u and τ_u

The distance X_p from the upper extreme edge of concrete to the neutral axis at the failure stage is obtained from the following equilibrium equation,

$$\Sigma A_i \cdot \sigma_i = 0 \quad (4)$$

The ultimate resisting moment M_u is calculated as follows,

$$M_u = \Sigma A_i \cdot \sigma_i \cdot X_i \quad (5)$$

where X_i: the distance from the neutral axis to the center of gravity of the divided sectional area A_i of steel girder, reinforcement and concrete.

The ultimate shearing stress τ_u on the upper flange projection is derived from the equilibrium equation at the failure stage and expressed as

$$\tau_u = \frac{0.85\sigma_{ck} \cdot B \cdot X_p \cdot S_u}{M_u \cdot b_f} \quad (6)$$

where S_u: The ultimate shearing force (N)
σ_{ck}: The design strength of concrete

4. EXPERIMENT OF COMPOSITE SLAB BRIDGE

4.1 The Purpose of Experiment

Static bending rupture test was conducted on the composite slab bridge with the aim of verifying the characteristics in the elastic range and the unification of the steel girder and slab concrete at the failure stage. High-cycle fatigue test was conducted on the other slab specimen with the aim of investigating the fatigue characteristics of composite slab under repeated loading.

4.2 The Dimensions of Specimen

The dimensions of composite slab specimen for static test are shown in Fig. 5. T-248 x 199 x 9 x 14 with projections were welded on the 12 mm thick bottom plate at a pitch of 40 cm in the longitudinal direction, D13 bars were arranged in the middle of the upper flange, and the slab depth was made 31 cm. In the specimen for fatigue test, the slab depth was made 21 cm and the bottom plate thickness was 8 mm, as shown in Fig. 6, in order to make the slab depth thinner than the lower limit of "Specification for Highway Bridges" in Japan and achieve economical cost performance. In both specimens, the maximum size of coarse aggregate was 25 mm, and the water cement ratio was 47%. Two kinds of ready mixed concrete having the design strength of 29.4 and 34.3 MPa were used for static and fatigue test specimen, respectively. An expansive admixture in a dose of 30 kg/m^3 was used to prevent cracking of concrete due to dry shrinkage.

4.3 Discussion

4.3.1 Static Bending Rupture Test

Fig. 7 shows the lateral distribution of bending stress at mid-span section when concentrated load 235 kN is applied to the center of the slab bridge. The experimental value is measured from the right-angle strain gauge, and the calculated value are obtained by the converted sectional area method in which the bending moment is obtained on the basis of the isotropical slab theory. The experimental value is nearly equal to the calculated value and rationally distributed over the entire width. Thus, the validity of the calculation method of working stress by using the isotropical slab theory and converted sectional area method has been verified.

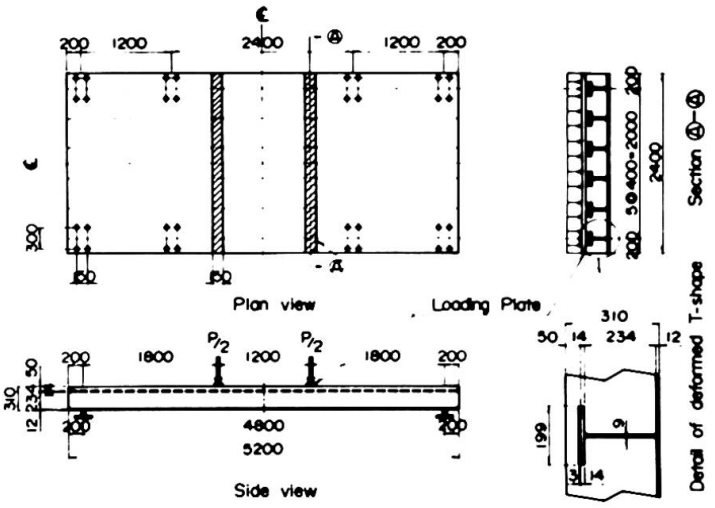

Fig. 5 Dimensions of specimen for static test

Fig. 8 shows the relation between bending moment and strain at the cross section of the mid-span when 2-point concentrated line loads are applied. This figure has verified that (i) the experimental values are approximately equal to the calculated ones up to the loading stage P_{ds} where the calculated stress of the bottom plate

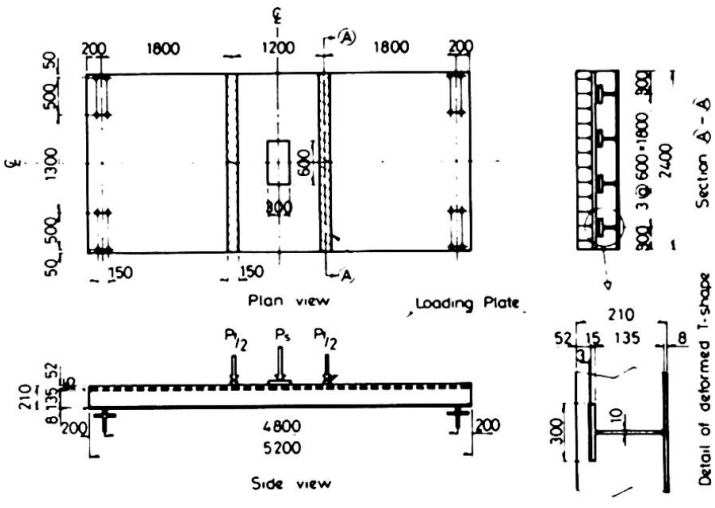

Fig.6 Dimensions of specimen for fatigue test

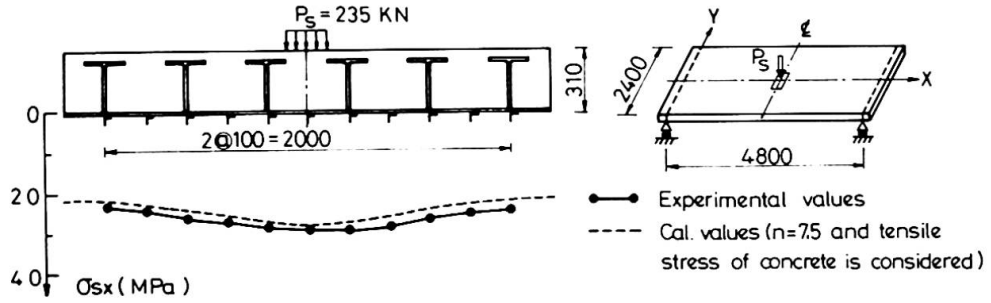

Fig. 7 Lateral distribution of tensile stress at mid-span section

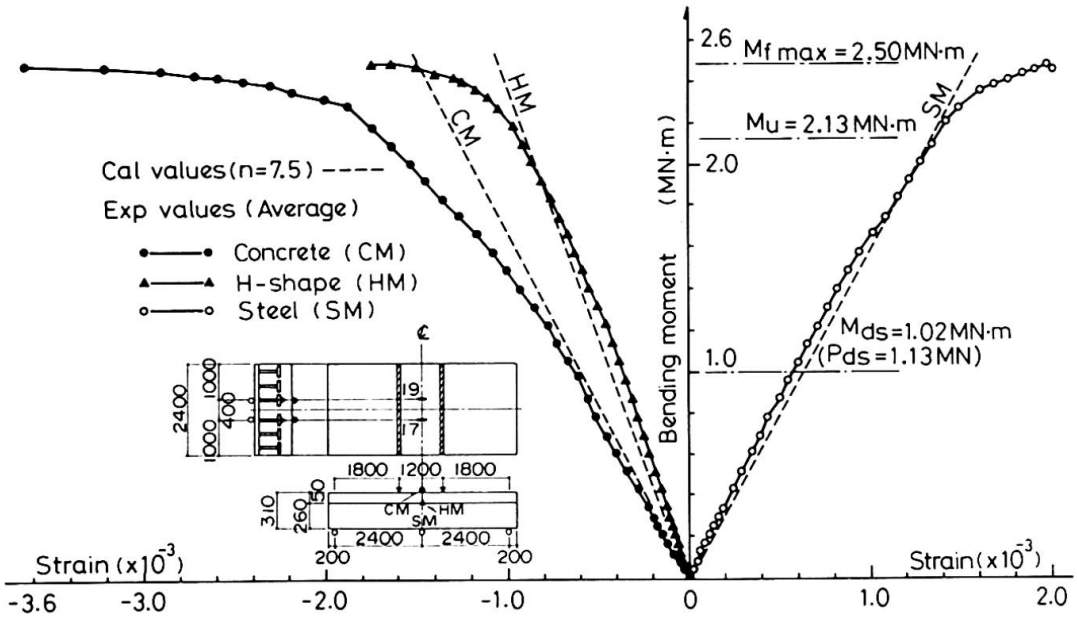

Fig. 8 Relation between bending moment and strain at mid-span section

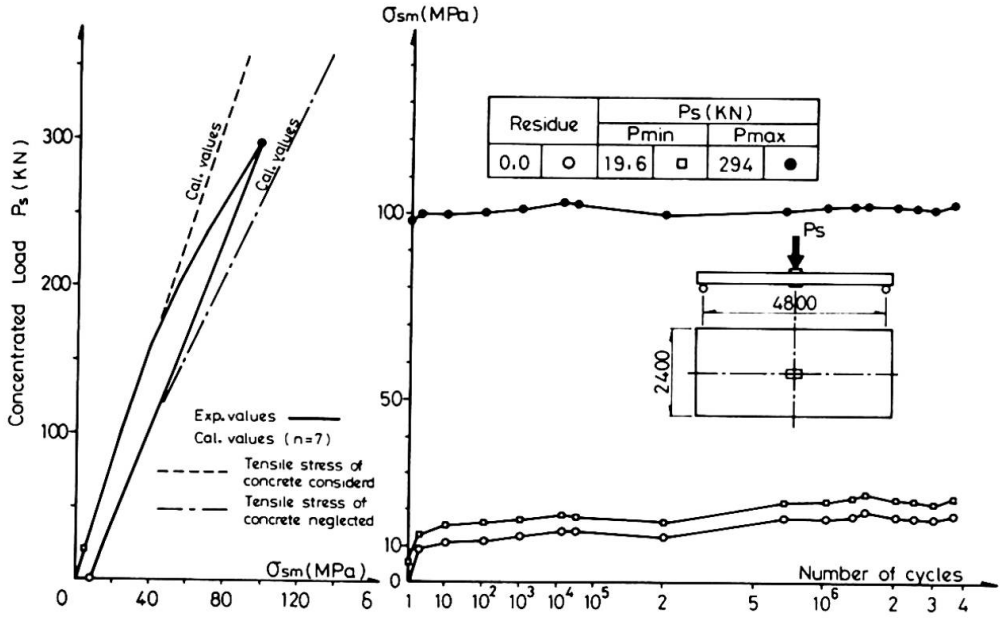

Fig. 9 Relation between number of cycles and tensile stress at mid-span section on fatigue test

corresponds to the allowable tensile stress, (ii) the ultimate bending compressive strain of concrete is 3.6×10^{-3} which is larger than that of conventional reinforced concrete, (iii) the ultimate bending moment is 2.50 MN·m which is about 1.2 tomes the calculated ultimate moment of 2.13 MN·m obtained from the Eq. (5) and (iv) the steel girder and slab concrete remain in the unit construction at the failure stage.

4.3.2 Fatigue Test

Fig. 9 shows the relation between the stress of the bottom plateand the number of cycles of repetition when a concentrated load is applied to the center of the slab bridge. Up to the load of 157 KN in the initial loading, the experimental value was nearly equal to the calculated one which has been obtained by considering the tensile stress of concrete, but thereafter, the experimental value became asymptotically to the calculated value in which the tensile stress of concrete was neglected. Under repeated load range from 19.6 to 294 KN, residual stress after the initial loading slightly increased, but no increase in the amplitude of stress range was observed, and the residual stress remained at a nearly constant level during 3.6 million cycles of repetition.

5. THE DESIGN

5.1 Design in General

Load: Calculation of sectional force by live load shall conform to "Specification for Highway Bridges" (called Spec.), III, 6.4. Namely, the design bending moment at the mid-span due to live load can be calculated by assuming that the total load (a uniform load of 3.43 KPa is applied to the whole width of the sidewalk and the principal L load is applied to the whole width of the roadway) will be uniformly borne by main girders.

Impact coefficient: The formulas applicable to reinforced concrete bridges given in Spec. Table 2.1.7 shall be applied.

Main materials: Atmospheric corrosion resisting steel (SMA 41W and SMA 50W) shall be used for the bottom plates, and SM50Y for the deformed flange T-shapes. For the slab concrete, the design strength shall be 26.5 MPa or above, and expansive concrete with the unit admixture quantity of 30 kg/m shall be used.

Determination of cross section: Sectional stress can be calculated according to Spec., II, Chapter 9 "Composite Girders". Namely. calculation shall be made on the assumption that the dead load of steel girder and slab concrete will be borne only by steel girder, and the dead load after placing concrete and the live load will be borne by the complete composite section. Stress variation due to creep and dry shrinkage of the slab concrete can be calculated by Spec., II, 9.2.6 and 9.2.8, respectively.

Shearing stress: Shearing stress at the projection on the upper flange can be calculated by Eq. (3). The allowable shearing stress shall be the same as that of deformed bar.

Limit of deflection: The maximum deflection due to live load shall be the value of 1/600 or below.

5.2 Standard Design

Road bridges having a span of 10 to 24 m were designed for three cases, the 2nd class bridge having the roadway width of 6 m, the 1st class bridge having the roadway width of 7 m and the 1st class bridge having the roadway width of 6.5 m and the sidewalk width of 2 m. The span/depth ratios of these standard design bridges are more than 33 as shown in Fig. 10.

6. CONCLUSION

As the result of experimental and analytical investigations on the composite slab bridge using deformed flange T-shapes, following concepts were obtained.

(1) Working stress can be obtain by the calculation method based on the isotropical slab theory and converted sectional area method.
(2) The steel girder and slab concrete retain a co-operative behavior even at the failure stage owing to the effect of projections on the upper flange.
(3) The composite slab can satisfactorily endure untill 3.6 million cycles of 294 KN repeated loading, which corresponds to three times as large as the design wheel load.
(4) The depth of the composite slab bridge can be greatly lower compared with the depth of steel plate girders and prestressed concrete bridges.

Since the commencement of sales for this slab bridge in the fall of 1982, more than fifty bridges have already been designed and five bridges have been completed, including four Bridges (see Figs.11 & 12) as a result of river improvement and another composite slab bridge used as the top slab of a tunnel (see Fig. 13).

In the future, the guide of the design and construction for curved bridges will be established and hollow type composite slab bridge will be developed for longer span.

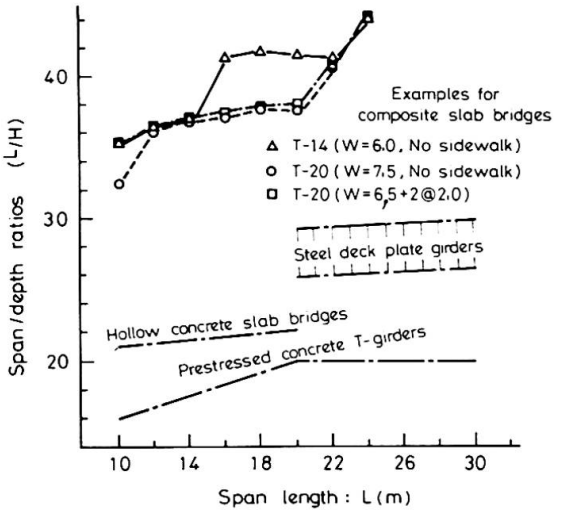

Fig. 10 The span/depth ratios for road bridges in Japan

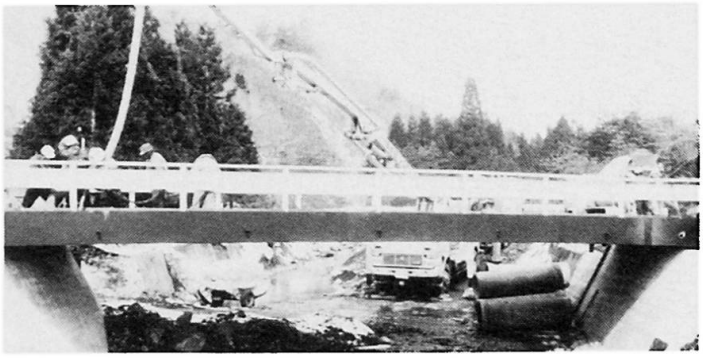

Fig. 11 Yachi-nakagawa bridge (L/H=42)

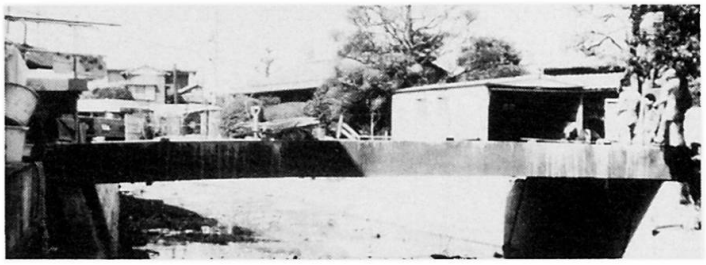

Fig. 12 Sengen-uemachi bridge (L/H=33)

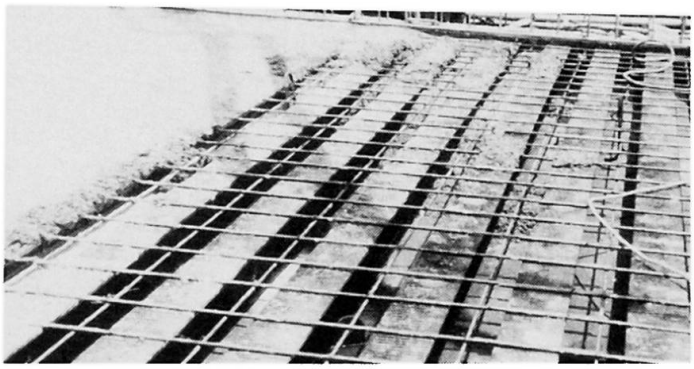

Fig. 13 The top slab of a tunnel (L/H=23)

REFERENCES

1. YAMASAKI T. et al., Studies on Fatigue Characteristics of Large Diameter Deformed Bar D51 in Axial Loads and Reinforced Concrete Beams. Trans. of JSCE, Vol. 10, pp.301 ∿ 302, 1978

2. SATO M. et al., Introducing Composite Structures using Newly Developed Checkered Steel Pipe and Deformed Flange H-shapes, KAWASAKI STEEL TECHNICAL REPORT No. 5, pp.94 ∿ 104, May 1982

Fire Resistance of Concrete-Stiffened Steel Structures

Résistance à l'incendie des structures en acier renforcées de béton

Feuerwiderstand betonversteifter Stahlbauten

Tohiro SUZUKI
Prof. Dr.
Tokyo Inst. of Technol.
Tokyo, Japan

Mamoru KIMURA
Chief Res. Eng.
Takenaka Techn. Res. Lab.
Tokyo, Japan

Akio KODAIRA
Res. Eng.
Takenaka Techn. Res. Lab.
Tokyo, Japan

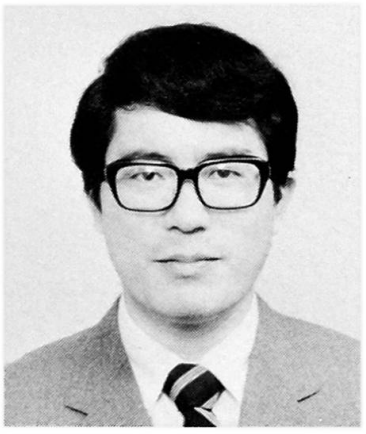

Toshiro Suzuki, born in 1936, received his doctor of engineering degree from the University of Tokyo. His major research activities include buckling, ultimate strength and plastic behaviour of steel structures. He was awarded the Prize from the A.I.J. for his study in 1981.

Mamoru Kimura, born in 1944, received his masters degree in engineering from Nagoya Institute of Technology. Since then he has been engaged in researches on the inelastic behaviour of steel structures, especially torsional problems. In recent years he has also been involved in composite structures.

Akio Kodaira, born in 1945, received his masters degree in engineering from Chiba University. His research is mainly concerned with structural fire safety, particularly with respect to analytical evaluation of fire resistance, water filled steel columns, fire-proofing materials.

SUMMARY

This report is concerned with the development of concrete-filled square steel pipe structures, particularly the fire resistance of such columns. When fire resistance is evaluated for the collapse of the member, load transfer to filled concrete can be expected to cope with the lowering of steel pipe strength at high-temperatures. This report clarifies mainly the basic behavior for this case.

RESUME

Ce rapport traite du développement des structures en tubes d'acier à section carrée remplis de béton, en particulier quant à leur résistance à l'incendie. Lorsque la résistance à l'incendie est évaluée par la rupture d'un élément, le transfert de la charge sur le béton de remplissage doit pouvoir compenser la diminution de résistance du tube en acier provoquée par le chauffage à haute température dans l'incendie. Ce rapport éclaircit principalement le comportement fondamental dans ce cas.

ZUSAMMENFASSUNG

Diese Arbeit befasst sich mit der Entwicklung von betongefüllten Vierkant-Stahlrohren für Bauwerke, insbesondere mit dem Feuerwiderstand solcher Stützen. Es ist zu erwarten, dass das Abnehmen der Festigkeit des Stahlrohrs im Laufe der Erhitzung durch das Feuer durch Übertragung der Last auf die Betonfüllung ausreichend ausgeglichen wird, wobei der Feuerwiderstand auf den Kollaps des Bauteils bezogen wird. Die Arbeit untersucht im wesentlichen den Grundmechanismus dieser Lastübertragung.

1. INTRODUCTION

Steel structures have many advantages, but also have the following drawbacks in addition to corrosion: 1) Liability to buckle, 2) lower elastic rigidity and 3) liability to be deteriorated by high-temperature heating. One of the effective measures to improve these drawbacks is the concrete-stiffening of steel structural members. This report has investigated the development of the concrete-filled square steel pipe structures for this purpose, particularly the fire resistance of such columns.

Filled concrete is effective in achieving excellent fire resistance in the following two points: (1) When fire resistance is evaluated by the steel-pipe temperature, the heat capacity of filled concrete contributes to the suppression of a temperature rise of the steel pipe [1] [2] and (2) when fire resistance is evaluated by the collapse of the member, load burden transfer to filled concrete can be expected to cope with the lowering of steel pipe strength due to high-temperature heating in fire [3]. This report clarifies mainly the basic behavior of concrete-filled steel pipe for the latter case.

2. HEATING EXPERIMENT FOR CONCRETE-STIFFENED STEEL COLUMNS UNDER A CONSTANT AXIAL FORCE

2.1 Parameters in the Experiment and Specimens

With the selection of sectional dimensions, axial force, heating time, and the presence or absence of

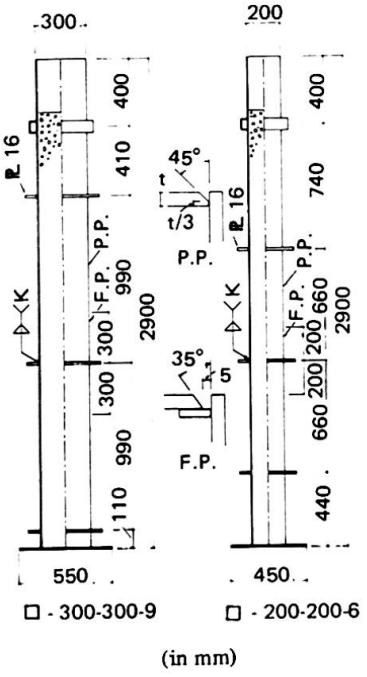

Fig. 1 Specimen

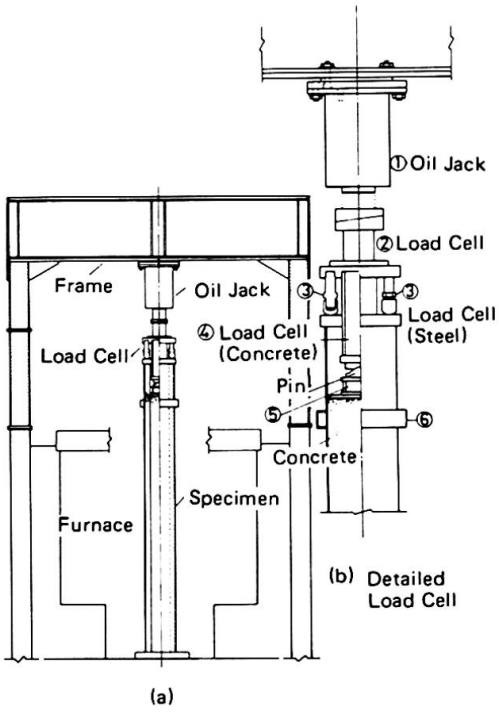

Fig. 2 Experimental Equipment

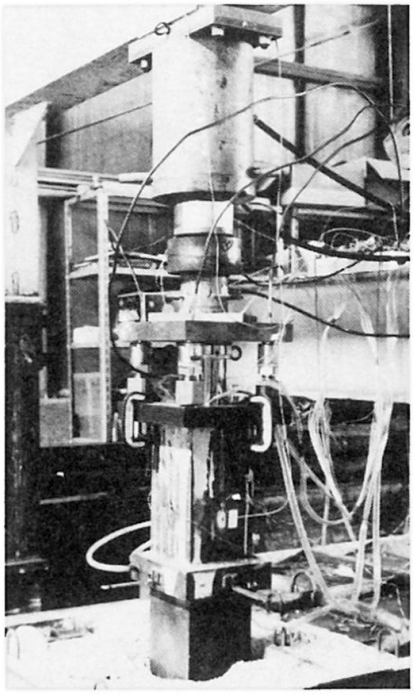

Photo 1 Loading System

Specimen No.	Heating Time (min.)	Pipe Width (mm)	Fire-Proofing Thickness (mm)	Axial Load (sPy*)
1	60	200	0	0.2
2	60	200	30	0.4
3	60	300	0	0.4
4	60	300	30	0.2
5	120	200	0	0.2
6	120	200	30	0.4
7	120	300	0	0.4
8	120	300	30	0.2

* sPy = A·F (A: Sectional Area of the Steel Pipe, F = 235 N/mm²)

Table 1 Parameters of Experiments

Steel Pipe Thickness (mm)	Yield Stress (N/mm²)	Tensile Strength (N/mm²)	Elangation (%)
6	351	468	25.9
9	333	455	25.7

Filled-Concrete	Comp. Strength (N/mm²)	Tensile Strength (N/mm²)	Young's Modulus (KN/mm²)
Wax Curing	27.4	1.99	28.9

Table 2 Mechanical Properties at Normal Temperature

fire proofing as parameters affecting the properties of members of a concrete-stiffened steel structure when it encounters fire and after it is cooled by fire extinguishing, eight specimens were made as shown in Table 1. Figure 1 shows shapes and dimensions of concrete-filled square steel column models whose sizes were 1/2.5 to 1/3 of actual members. Table 2 shows mechanical properties of materials used in the experiment.

2.2 Experimental Equipment and a Method of the Experiment

Figure 2 and Photo 1 outline the experimental equipment. A specimen was to be laid in the center of the heating furnace installed in Takenaka Technical Research Laboratory. The column top of the specimen was protruded above the furnace cover and compression by the reaction frame joined to the heating furnace was applied to the top of the specimen through the oil jack with a constant loading facility and the load cells. Figure 2(b) shows the load cell in detail. The load applying system, including load cells, was provided with much higher rigidity than that of the specimen. The transfer of axial force from the steel pipe to the filled concrete was closely detected by the set of load cells so equipped. The axial force to the filled concrete was introduced through the cylindrical load cell ④. at the center and the axial force to the steel pipe was introduced through four bolt-type load cells ③. Allotment of initial axial force was carried out by means of screw adjustment of ③ and ④. In addition, load cells were water proofed and provided with heat resisting property.

Heating in the experiment was carried out in compliance with the standard temperature-time curve specified in JIS-A-1304 (ISO-834) which assumes fire. A predetermined axial force was introduced primarily in the steel pipe before heating was started and the entire load had been kept constant until heating was completed.

3. BASIC BEHAVIOR

3.1 Temperature Property

Temperature measurement was carried out using C.A. thermocouples. Figure 3 shows the heating temperature in the furnace. It approximately satisfied the standard temperature-time curve.

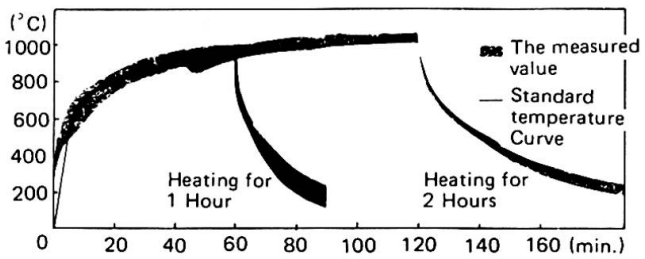

Fig. 3 Temperature inside the Furnace

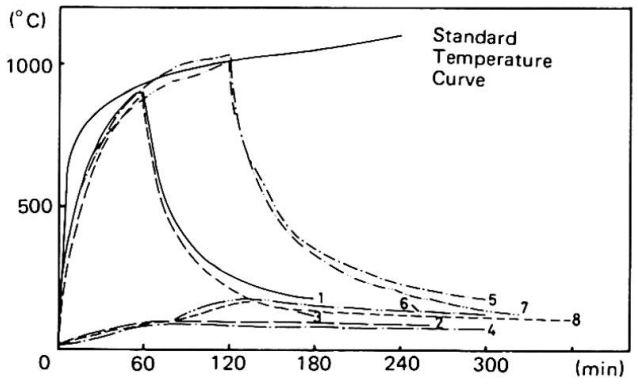

Fig. 4 Average Temperature on the Surface of Steel Pipe

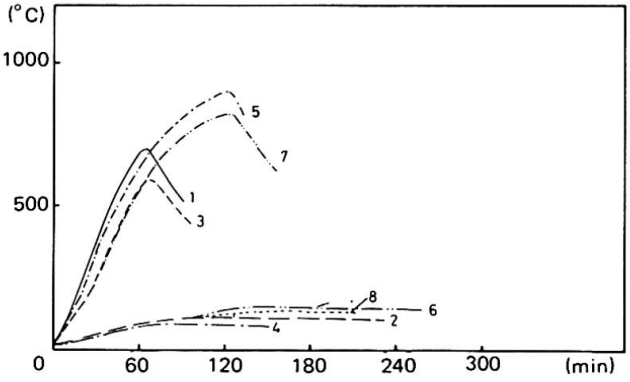

Fig. 5 Average Temperature at the Corner of Concrete

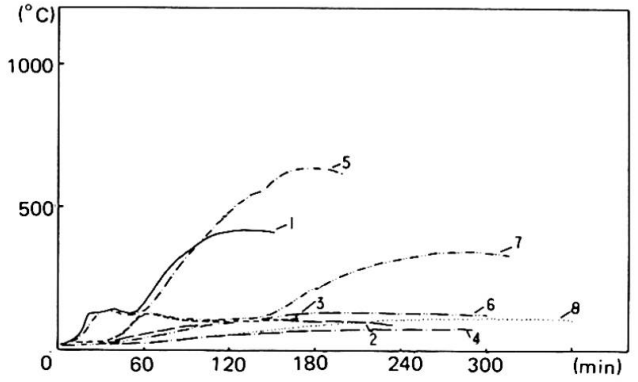

Fig. 6 Average Temperature in the Central Part of Concrete

Figure 4 shows the average temperature on the surface of the steel pipe of each specimen. The fire-proofed specimen presented the maximum temperature of 100°C after 60 minute heating and the maximum temperature of 180°C after 120 minute heating, which is extremely low. The temperature of the specimen without fire proofing rose somewhat later than the temperature rise inside the furnace, but approximately in parallel with the latter.

Figure 5 shows the average value of the observed temperature at a point in the corner of the square section of the concrete and 25 mm distant from the inner surface of the steel pipe, and Figure 6 shows the temperature at the center of the concrete. It proves that the temperature rise at the center of the concrete stopped rising once in the neighborhood of 150°C, and after that it restarted. This stagnation is considered to be due to the influence of free water contained in the concrete. The time duration of the stagnation was greatly different with the column size. The maximum reachable temperature at the point in the corner in the section of the concrete and that at the center of the concrete were both greatly different with the heating time and the column size. On the other hand, the temperature rise of the fire-proofed specimen was extremely moderate and the maximum reachable temperature of the specimen was lower.

3.2 Mechanical Properties

3.2.1 Axial Deformation of the Steel Pipe

Figure 7 shows the change in the length of the steel pipe with time. The deformation is the relative displacement between points which are located on the top of the specimen outside the furnace and on the top of a silica tube with a negligibly small thermal expansion elected on the pedestal base for the specimen inside the furnace and was observed by the water- and fire-proof displacement gages. The specimen without fire proofing presented an abrupt deformation due to heating expansion of the steel pipe after heating was applied, and the elongation of the steel pipe reached its maximum at 18 to 20 minutes after heating was started. The temperature of the steel pipe rose to 600°C then. After this, local buckling of the steel pipe caused an abrupt contractive deformation, but its degree was gradually reduced. After heating was terminated the steel pipe presented contractive deformation for long due to lowering of the temperature of the specimen. The steel pipe with fire-proofing was found to have a slight elongation due to the temperature rise of the steel pipe.

3.2.2 Axial Load Sharing of the Steel Pipe and the Filled Concrete

Figure 8 shows the change with time in load sharing ratio of the entire axial force to the axial force of the filled concrete. The specimen without fire proofing mostly maintained the sharing ratio of the beginning of heating. However, at 20 minutes after heating was applied when local buckling occurred in the steel pipe the load bearing capability of the steel pipe was greatly reduced and the load sharing of the filled concrete abruptly increased. After a predetermined time of heating was terminated, the contraction of the steel pipe took place due to sudden drop in the temperature inside the furnace, and the burden of the allotment of the axial force to the filled concrete further increased. However, specimen No. 7 as a whole lost its load bearing capacity at 106 minutes after heating was started. The fire-proofed specimen presented less temperature rise in its body and the initial load sharing ratio was maintained.

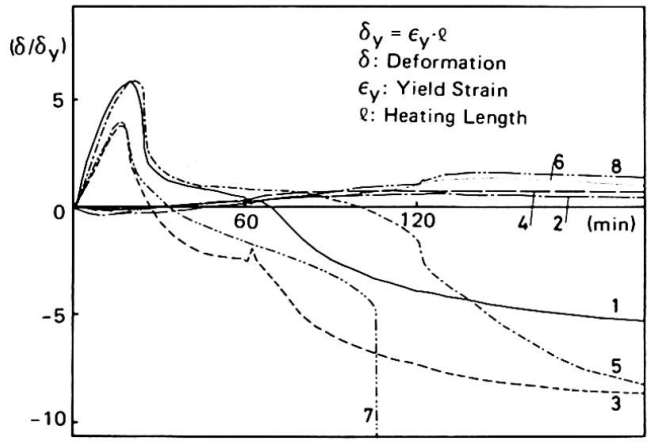

Fig. 7 Change in Length of Steel Pipe Columns

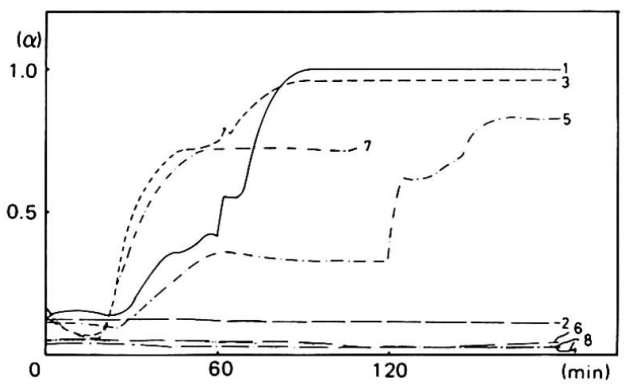

Fig. 8 Load Shearing Ratio of the Filled Concrete (α)

4. INVESTIGATION OF THE LOCAL BUCKLING

4.1 Specimens and Experimental Method

Three specimens were used in the experiment; one having a variable ratio of its width to thickness and the two others being stiffened with stud bolts. Tables 3, 4 and 5 shows these specimens. The stiffening stud bolts were designed assuming that the axial yield force of the steel pipe or the half of the axial yield force can transfer from the steel pipe to the filled concrete between story height. Therefore, the lower part of the specimen stiffened by stud bolts was fire-proofed in order to heat the ordinary story height. The method of applying compression, method of heating, and the method of measuring were the same as the preceding methods.

4.2 Influence of the Width-to-Thickness Ratio and of the Stud Bolt Stiffening

Figure 9 shows the change in length of the steel pipe in connection with the experimental result of the Specimen No. 1 (width-to-thickness ratio of 33.3) obtained in the preceding section. They are values converted into the magnitude of deformation for the ordinary story height. There is only a slight difference in the behavior between Specimen No. 9 (a width-to-thickness ratio of 44.4) and No. 1, and it was considered that the influence of the reduction in yield stress and that in Young's modulus accompanied by the temperature rise of the steel pipe were much greater than the influence of the width-to-thickness ratio. The effect of stud bolt stiffening could be seen to some extent of unification of concrete and steel pipe, and it was moderate in elongation and contractive deformation when compared with the unstiffened specimen, but no considerable difference in buckling behavior was observed between them. Photo 2 shows the behavior of the local buckling deformation of the steel pipe obtained after heating was applied. Specimen No. 11 having a stud bolt pitch of the half of the width of the steel pipe presented considerable constraint effect against local buckling deformation.

5. PRACTICAL FLOW OF THE EXTERNAL FORCE APPLIED TO THE SPECIMEN

5.1 Specimens and Experimental Method

Considering the practical flow of the external force to the column, the investigation was made for

Specimen No.	Heating Time (min.)	Width-to-Thickness Ratio	Stud Bolt Pitch	Axial Load (sPy)
9	60	44.4	–	0.2
10	60	33.3	B*	0.2
11	60	33.3	B/2	0.2

* B: Pipe Width (= 200 mm)

Table 3 Specimens without Fire-Proofing

Steel Pipe Thickness (mm)	Yield Stress (N/mm²)	Tensile Strength (N/mm²)	Elongation (%)
4.5	287	451	36.6
6	319	452	27.4

Table 4 Mechanical Properties of Steel Pipe at Normal Temperature

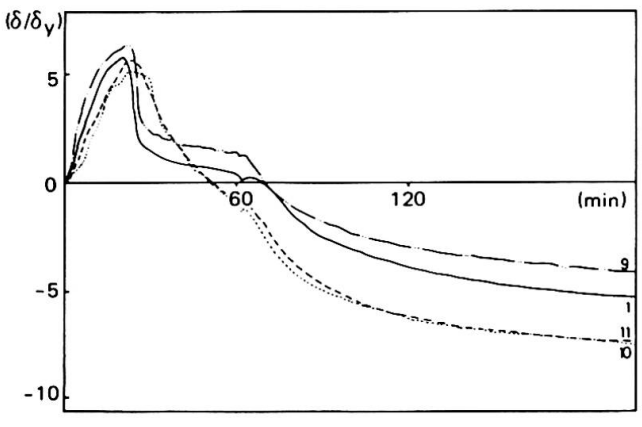

Fig. 9 Influence of the Width-to- Thickness Ratio and of Stud Bolt Stiffening

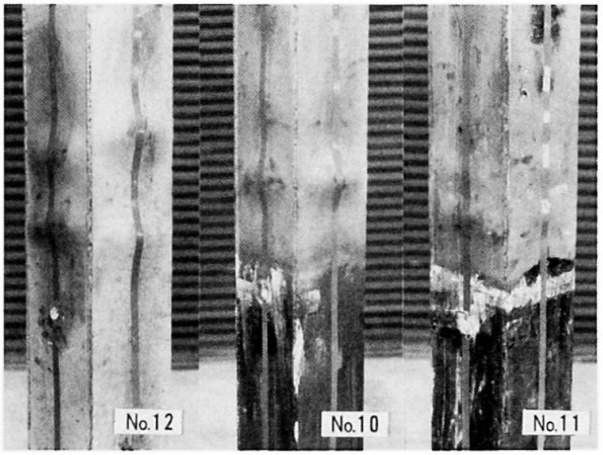

Photo 2 Local Buckling Deformation

the mechanical behavior of the specimen appearing when load was applied from the beam-to-column connection (external diaphragm type) to the column, and when the column was heated. With further consideration for the influence of the upper story of the column which was not heated, the column was extended upward by one more story height. Figure 10 and Tables 4, 5 and 6 show an outline of the specimen. Moreover, the external diaphragm connection aiming at force applying device was fire-proofed. Force was applied by four oil jacks to which the bolt-type load cell was mounted, which was used in the preceding section. When introducing only the axial force, the concentric compression by which the bottom of the specimen loaded was pressed flat was used and when loading the axial force and the constant bending moment, the eccentric compression was used which could be realized by inserting a pin bearing at the bottom.

Photos 3 and 4 show schematic views of the experimental equipment.

5.2 Comparison of the Behavior for Different Loading Conditions

Figure 11 shows the deformation characteristics of the external diaphragm type specimen in conjunction with the Specimen No. 1 which used flat holding. The difference between the external diaphragm type Specimen No. 12 and No. 1 could be observed to some extent in the neighborhood of the maximum elongation where they showed fairly good correspondence. The external diaphragm type specimen was measured for the relative displacement between the steel pipe and the filled concrete at the top of the specimen which corresponded to the column top of the upper story and no slippage was observed between the steel pipe and the filled concrete. Although a considerable amount of water was observed to rise between the steel pipe and the filled concrete, they behaved as a body. As a result the flat holding pressure type specimen was considered to enable evaluation of the practical loading of axial force.

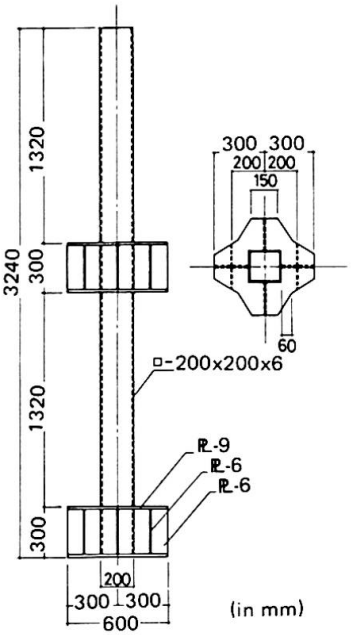

Fig. 10 External Diaphragm Connection Type Specimen

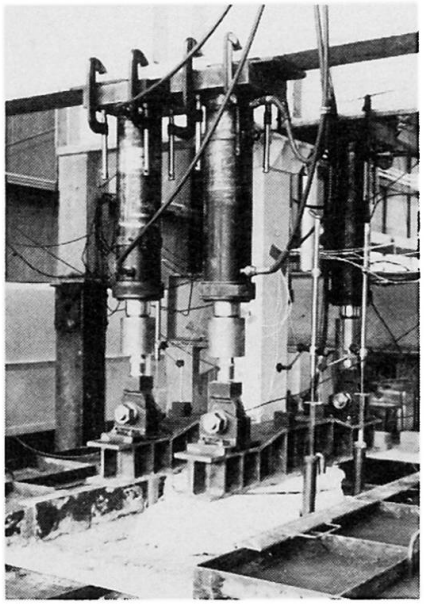

Photo 3 Loading Equipment

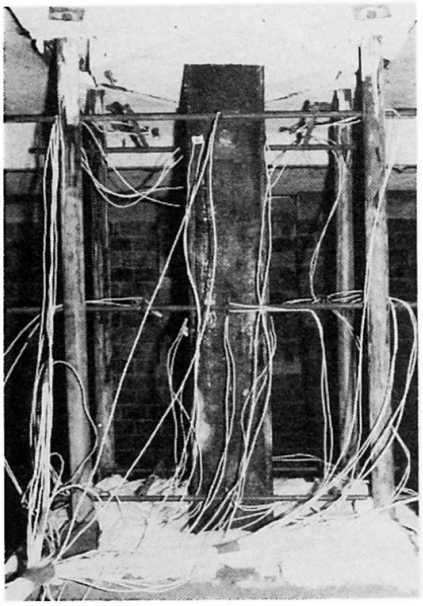

Photo 4 Internal View of the Furnace

Specimen No.	Heating Time (min.)	Pipe Width (mm)	Bending Moment (sMy*)	Axial Load (sPy)
12	60	200	0	0.2
13	120	200	0	0.4
14	60	200	1/3	0.2
15	60	200	1/6	0.2

* sMy = Z·F (Z: Sectional Modulus)

Table 5 External Diaphragm Type Specimen without Fire-Proofing

Filled-Concrete	Comp. Stress (N/mm^2)	Tensile Strength (N/mm^2)	Young's Modulus (KN/mm^2)
Wax Curing	28.2	2.33	28.7

Table 6 Mechanical Properties of Filled-Concrete at Normal Temperature

5.3 Introduction of Bending Moment

A constant bending moment was introduced, whose strength is 1/6 or 1/3 of the yield bending moment of the steel pipe. The specimen under 1/6 yield bending moment lost its load bearing capacity at 40 minutes after heating was started, while the one under 1/3 yield bending moment, 30 minutes (Fig. 11). Figure 12 shows the change in the rotation of the specimen in the external diaphragm connection, with time. The rotation was non-dimensionalized by an elastic rotation of θp corresponding to the plastic moment of the steel pipe at the normal temperature. When 20 minutes passed after heating was started, it caused local buckling in the steel plate element on the compression side and the rotation increased, but eventually the steel plate exhibited deformability until the rotation reached to 5 θp. Considering the framed structure at the occurrence of fire, it would possibly be expected that due to the sufficient rotational capability of the connection the movement to the pin bearing condition is possible and the amount of bending moment introduced into the column can be reduced.

5.4 Fire Resistance

Fire resistance of the concrete-filled steel pipe column without fire-proofing can be evaluated as the capability that the load which acts in fire transfers to the filled concrete. Therefore, it can be considered that the greater the ratio of load bearing capacity of the filled concrete to the steel pipe is, the more it is advantageous. A steel pipe having a width-to-thickness ratio of 33.3 falls within the range having a sufficient plastic rotational capacity at normal temperature and it is safer than a thin steel pipe, considering the load in terms of the ratio of axial yield force of the steel pipe. As a result of the experiment for Specimen No. 13 shown in Figure 11 and that for Specimens No. 5 and No. 7 shown in Figure 7, it was found that the steel pipe had sufficient fire resistance of longer than 2 hours for 20% of the axial yield force of the steel pipe and longer than 1 hour for 40% of the axial yield force.

It was also found that the temperature of the column immediately above the external diaphragm connection was nearly equal to normal temperature and that the influence of heat transmission on the upper story of the column was very small.

6. BENDING CAPACITY OF THE COLUMN AFTER COOLING

6.1 Test Member and Experimental Method

Investigation was made for the bending capability of the column in order to evaluate the earthquake resistance of the column after suffering fire. Specimens were taken from those used in the experiments described in Chap. 2. Mechanical properties of steel material used are as shown in Table 8 and tension coupons were cut out of the specimens without fire-proofing. A simple-beam was loaded with central concentrated type load and the bending span was set to the assumed ordinary story height.

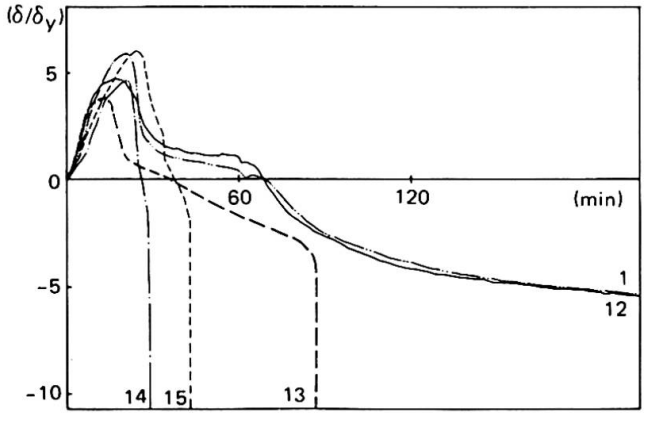

Fig. 11 Influence of Loading Conditions and Bending Moment

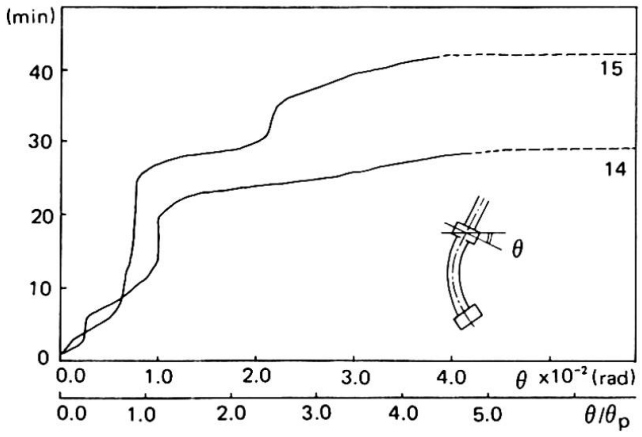

Fig. 12 Rotation Capacity

Specimen No.	Steel Pipe Width (mm)	Bending Span (mm)
1, 2, 5, 6	200	1320
3, 4, 7, 8	300	1980

Table 7 Specimens for Bending Test

Steel Pipe Thickness (mm)	Yield Stress (N/mm^2)	Tensile Strength (N/mm^2)	Elongation (%)	Heating Time (min.)
6	228	375	26.9	60
6	202	386	22.8	120
9	268	399	35.7	60
9	201	396	34.4	120

Table 8 Mechanical Properties of Steel Materials after Cooling

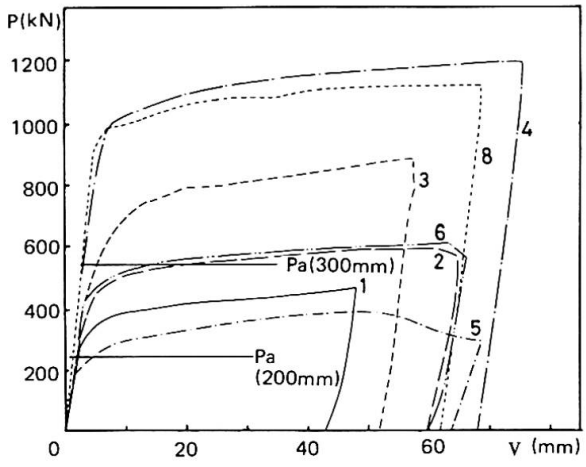

Fig. 13 Load-Deformation Relationship

6.2 Flexural Behavior

Figure 13 shows the results of the experiments. If the fire-proofed specimen was evaluated to have characteristic of the specimen obtained before heating, the yield strength of the specimen without fire-proofing was reduced down to 60% to 70% when the central deflection presented 6 v_p, where, v_p is the elastic deformation corresponding to the plastic moment of the steel pipe at normal temperature. In Figure 13, design load, P_a, is shown which corresponds to the seismic load.

7. CONCLUSION

This paper has introduced the investigation carried out experimentally for temperature characteristics of the concrete-filled square steel pipe column in fire, its mechanical characteristics, and flexural characteristics after cooling, and clarified the following items.

(1) If the square steel pipe column is fire-proofed equivalent to that applied to a steel structure, the pipe column is sufficed redundant characteristics.

(2) If the square steel pipe column is without fire-proofing, when about 20 minutes passed after heating starts, local buckling occurs in the steel pipe and presents abrupt contraction. However, if the compression is 20% of the axial yield force of the steel pipe, the column maintains fire resistance over two hours, and if the ratio is 40%, it maintains fire resistance over longer than one hour.

(3) The presence of the upper story of the column makes it possible to transmit the load introduced from the beam sufficiently to the filled concrete.

(4) Sufficient rotational capacity of the column top would be able to reduce the bending moment from the beams.

(5) Although the bending characteristics of the column without fire-proofing is reduced by about 60% to 70%, the column strength still sufficiently exceeds the design load corresponding to the seismic load.

REFERENCES

1. SAITO H. and UESUGI H., Heating Test of the Concrete-Filled Square Steel Columns. Transaction, Annual Meeting of A.I.J. Sept. 1977 (in Japanese)
2. UESUGI H., Fire Resistance of the Concrete-Filled Steel Pipe Columns (Effects of the Filled Concrete). Transaction, Annual Meeting of A.I.J. Oct. 1978 (in Japanese)
3. GRANDJEAN G., GLIMAULT L. and PETIT L., Détermination de la durée au feu des profils creux remplis de beton. EUR Rep. Comm. Eur. Commun. No. EUR-7171, 1981

Strengthening of Brinsworth Road Bridge, Rotherham

Renforcement du pont de Brinsworth Road à Rotherham

Verstärkung der Brinsworth Road Bridge in Rotherham

Bryan L. DAVIES
Chief Engineer
South Yorkshire County Council
Barnsley, U.K.

Bryan Davies, a graduate of Imperial College, London, has spent the major part of his professional career in the design and maintenance of highway bridge structures and for the past ten years has been in charge of the Bridges and Structures Division of the South Yorkshire highway authority.

John POWELL
Principal Engineer
British Waterways Board
Leeds, U.K.

John Powell received his engineering training at Liverpool College of Building. After early experience in the design and construction of both industrial buildings and bridge works he joined the South Yorkshire County Council in 1974 as Assistant Chief Bridge Engineer. In 1983 Mr. Powell was appointed Principal Bridge Engineer of the British Waterways Board.

SUMMARY
The paper describes the strengthening of a precast, prestressed hollow-box beam skew bridge deck by means of steel plates bonded transversely to the soffit. During the passage of a 456 tons load deflection and strain measurements were undertaken and the transverse profiles compared with those obtained by theory.

RESUME
La contribution décrit le renforcement d'un pont biais précontraint et préfabriqué à l'aide de poutres à caisson, effectué à l'aide de plaques d'acier collées transversalement. Lors du passage d'une charge de 456 to, les mesures ont été comparées avec les valeurs calculées.

ZUSAMMENFASSUNG
Der Beitrag beschreibt die Verstärkung der Fahrbahnplatte einer vorfabrizierten, vorgespannten schiefen Hohlkastenbrücke mit quer zur Brückenaxe aufgebrachten Stahlplatten. Durchbiegungs- und Dehnungsmessungen wurden während des Verschiebens einer Last von 456 Tonnen vorgenommen und mit den theoretischen Werten verglichen.

1. DESCRIPTION OF BRIDGE

Brinsworth Road Bridge was constructed in 1965 to carry the M1 London - Leeds Motorway over a side road. The existing road alignment dictated a 45° skew crossing with a clear span between abutment faces of 16.3m.

The deck supporting each carriageway was formed from 17 no. 965mm. wide x 1117mm. deep hollow prestressed concrete box beams placed at close centres. Following concreting of the interbeam gap transverse post-tensioning was applied on the line of internal diaphragms in the boxes. An external fascia beam was placed to carry the parapets. A plan on the bridge deck is shown in figure 1.

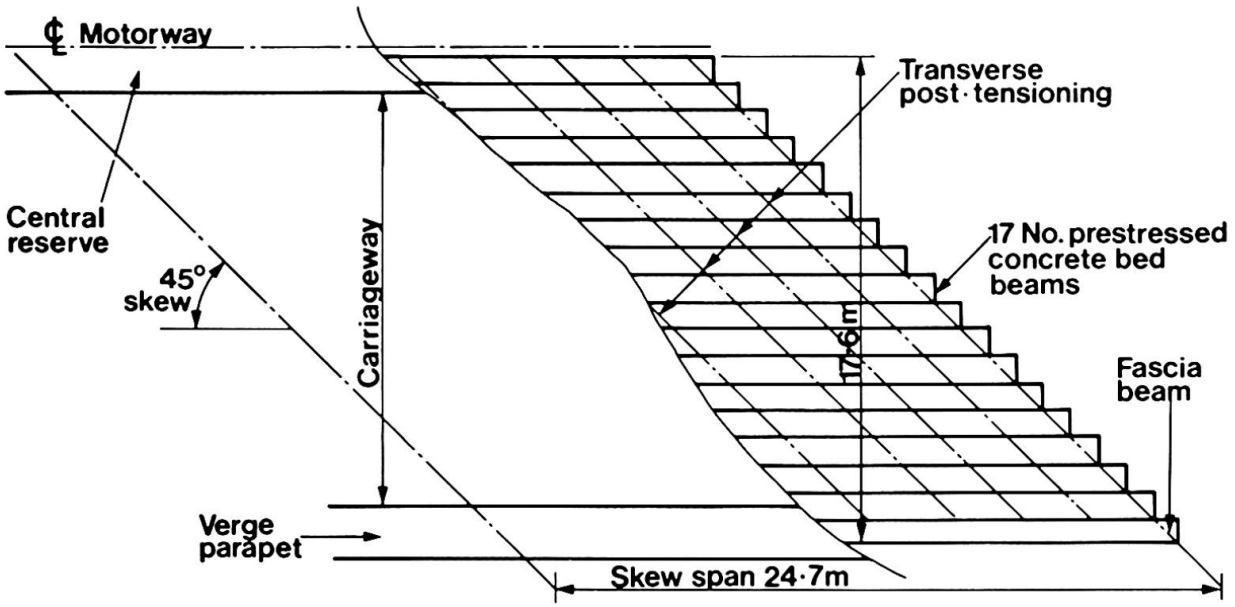

Fig. 1 Plan on Bridge Deck

2. INITIAL DESIGN AND SUBSEQUENT CHECK

The bridge was designed for the Ministry of Transport standard loading of HA and 45 units of HB, all as given in the British Standard[1]. In designing the main beams use was made of the reduction factors allowed in the Standard for HB loading, the transverse stressing being proportioned using the rules suggested by the Prestressed Concrete Development Group[2] cross referencing the recommendations of Gifford[3]. Subsequent to completion of the bridge it was felt that the above rules might not be applicable to a deck of such a high skew and an analysis was made using computer grillage techniques. This demonstrated that, in order to achieve the lateral distribution assumed in the design, a much higher level of transverse strength would be required than that provided by the post-tensioning. The bridge was limited to a maximum vehicle loading of 100 tonnes.

3. PRELIMINARY STRENGTHENING CONSIDERATIONS

Alternative systems for strengthening included:-

(a) Additional overlay reinforced concrete slab. Discounted due to additional dead weight and need to undertake considerable road works to preserve a satisfactory highway alignment.

(b) Enhancing strength of box beams by addition of longitudinal plates to soffits. Whilst increasing the bending strength this did little to enhance the deficient shear capacity.

4. ADOPTED SOLUTION

The strengthening technique finally adopted consisted of bonding, 400 x 100mm steel plates to the soffit of the deck in a direction parallel to the abutments using a 2 pack epoxy resin. Primary strengthening was provided in line with the transverse diaphragms, intermediate secondary plates being provided over the middle third of the spans.

Whilst the technique itself was not innovative two aspects called for further investigation.

(a) With a 2% cross fall on the deck and each box beam placed vertically a step of over 25mm. occurred at the junction of each beam. Little information was available on the behaviour of epoxy resin adhesives at this thickness.

(b) What restrictions, if any, should be placed on traffic using the deck during fixing of the plates and curing of the resin.

Swamy and Jones of Sheffield University were retained to undertake a testing programme and report. Their conclusions[4] [5] confirmed the soundness of the strengthening technique and that the above would have negligible deleterious effect on its effectiveness.

5. PRACTICAL CONSIDERATIONS

In detailing the proposals it was decided to limit plate lengths to 2.8m., bonding 1.75m. cover plates across the gaps. 20mm. diameter expanding anchor bolts were fixed into the interbeam insitu concrete which served the dual purpose of retaining the plates in position during curing of the resin and for safety in holding the plates should long term deterioration of the plate/ Resin/concrete interface occur. (Fig. 2.)

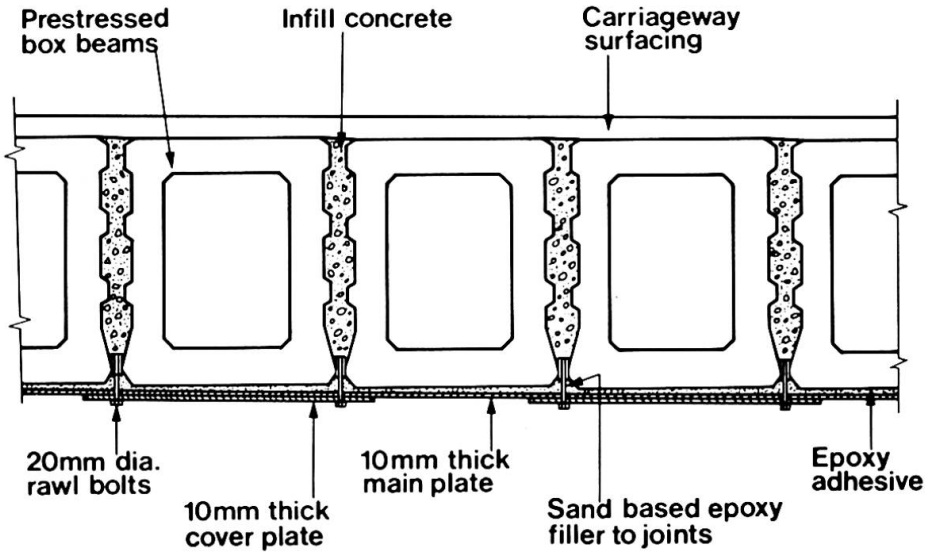

Fig. 2 Section on Deck

The specification required all plates to be cleaned and grit blasted and all dust removed by vacuum cleaner, the first coat primer being applied within a stated period. A similar treatment for cleaning and blasting was applied to the soffit concrete to remove all laitance and to expose the aggregate.

The resin adhesive for the concrete/steel interface was initially applied to both surfaces as a primer followed by the main filled resin, all to Formulated Resins specification XD 808. The specification for the steel/steel bond on the cover plates was Epoxy RS1 again as supplied by Formulated Resins Ltd.

Implementation of the strengthening was undertaken the County Engineer's Department. Whilst the staff and operatives within the Maintenance Division had had no previous experience of this or similar techniques, test procedures enabled a satisfactory method of working to be developed and a high level of output was maintained throughout. Figure 4 shows the use of extensions to the expanding bolts to provide a "table" for application of the resin. Spreader beams were used to support the plates during setting and curing of the resin to avoid localised distortion of the plate.

As the work was undertaken from October to December, artificial heating was employed to ensure satisfactory curing.

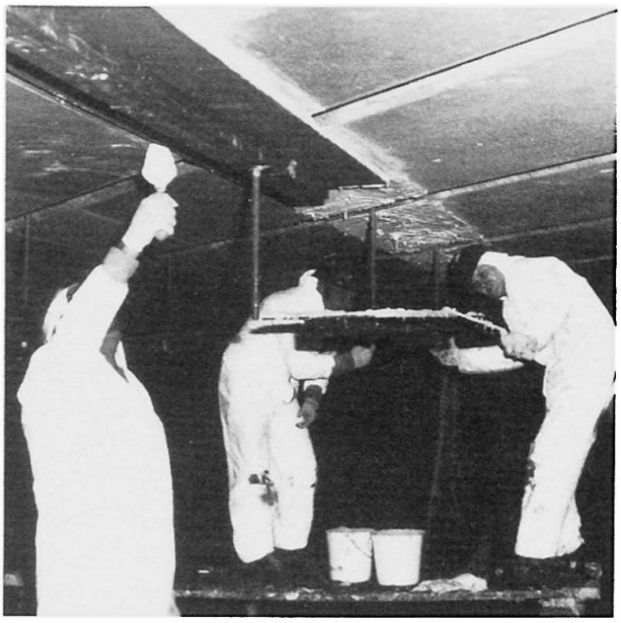

Fig. 3 Bonding of Steel Plates

On completion all external steel surfaces were given a four coat protective treatment of epoxy primer followed by Zinc Phosphate/M.I.O. Chlorinated Rubber under and finishing coats.

6. TEST LOADING OF STRUCTURE

The main incentive for undertaking the strengthening was the routing of a series of 456 tonne loads for which no suitable alternative route was available and it was decided to use the first of these loads to monitor the behaviour of the bridge deck with its strengthening.

The transporter, carrying a 334 tonne casting, was of 24 axles, axle spacing being a constant 1.6m. Equalisation of loading between the axles was achieved by spreader beams directly under the load and an interconnected hydraulic system to each axle. The vehicle, with load, is shown in Fig. 4

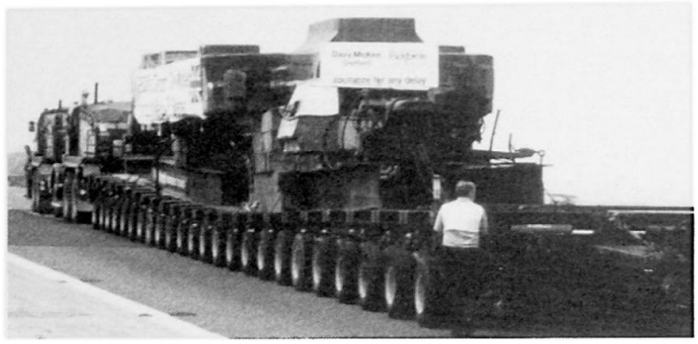

Fig. 4 Test Load Vehicle

The transporter was positioned on the longitudinal centre line of the bridge deck, all other traffic being diverted to the adjacent carriageway. With an overall wheelbase of 36.8m. only some 67% of the total gross load was carried by the bridge super-structure but this was equivalent to 46.4 units HB for bending 44.4 units HB for end shear.

Deflection readings were taken transversely across the mid span of the deck together with 50 Demec strain gauge points located to monitor the transverse bending effects at mid span, the distribution of moments across the deck, localised strains over the precast beam interface and strains in the web adjacent to the central reserve. The strain gauge readings were supplemented by 6 low voltage linear transducers fitted to detected strains in parts of the deck which were inaccessible during the test.

7. TEST RESULTS

The deflection profile on the skew centre line of the deck is as shown in Fig. 5. It is of interest to note that during the 100 mins. the load remained on the bridge a uniform increase of deflection of 0.4mm. occurred across the deck. The test took place in the late afternoon with a falling air temperature and a differential temperature of $1^{o}C$ across the deck would result in a 0.6mm. deflection.

Unfortunately the correlation between sets of Demec and L.V.D.T. readings was not particularly good but, in general, the strains recorded confirmed the low values of the deflection profile. It is also of interest to note, that strains measured across the beam joints under the load showed nearly double the value of strains in the adjacent steel plate.

Following the load test PUNDIT (Portable Ultrasonic Non-Destructive Digital Indicator Test) tests were undertaken on bridge beams to attempt to ascertain the elastic modulus for the concrete. Readings gave values between 32.3 and 50.4kN/mm^2 and a mean value of 41.3 has been taken.

8. PREDICTIVE ANALYSES

In conjunction with the independant checkers, two mathematical analyses were performed on the deck using a grillage idealisation and used to check the strengthening system for adequacy. In both cases full section properties were taken for the members modelling the main boxes and a transformed section assuming full tensile cracking of concrete section transversely.

The analyses were then performed using

(a) the assumption of no torsional rigidity in the grillage members,

and
(b) taking the full torsional properties on all members.

In addition the charts produced by Rüsch and Hergenröder[6] for an isotopic slab of aspect ratio of 1.0 and skew of 45° were used to make a comparison with the test load results.

Figs. 5, 6 and 7 show the results of the analyses for deflection, longitudinal and transverse moments on the skew deck centre line.

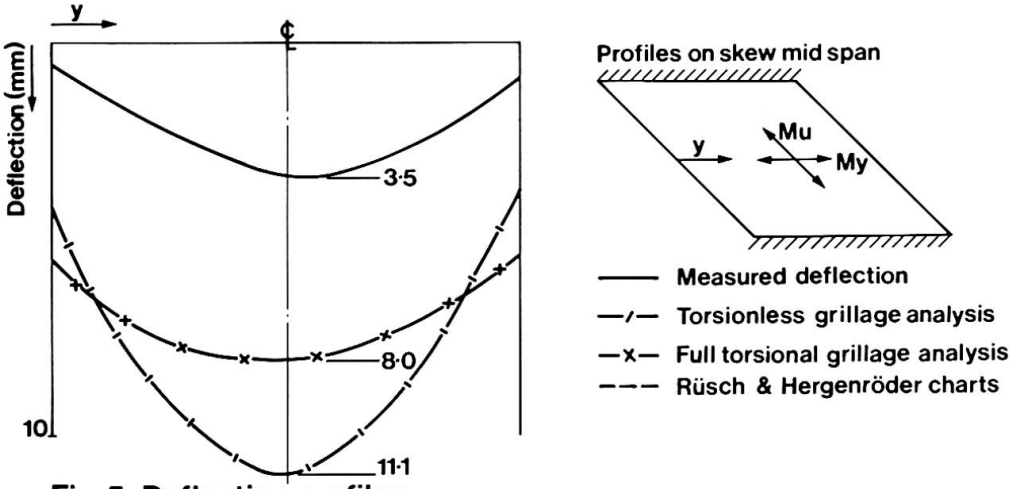

Fig.5 Deflection profiles

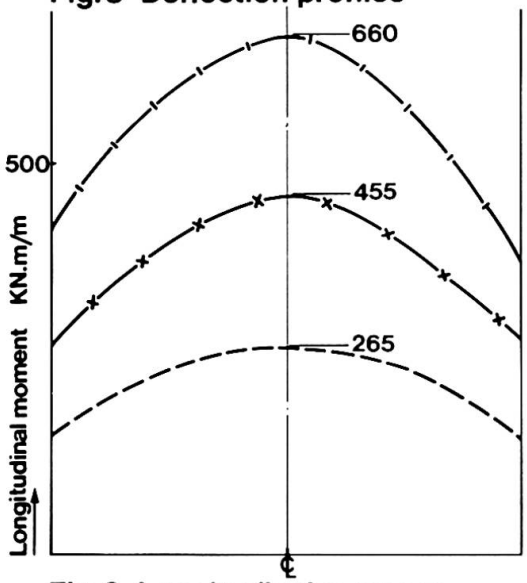

Fig.6 Longitudinal moment (Mu) profiles

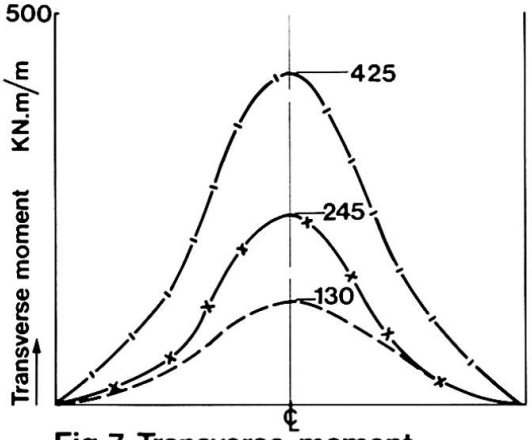

Fig.7 Transverse moment (My) profiles

Fig. 5, 6 and 7 Deflection and Moment Profiles

9. COMPARISON OF TEST RESULTS WITH THEORY

The first and obvious point of note is that the measured deflections were substantially less than those predicted by either of the grillage analyses. Whilst the participating effect of surfacing may be a contributory factor it is not considered that this is sufficient to account for the wide variation. On the basis of a mean measured deflection across the deck of 2.5mm. the equivalent effective span is of the order of 18.2m. and it would appear as if the deck is behaving in a much more "square" manner than the anlyses would indicate.

With this order of deflection the maximum moment in the boxes will have reduced to the order of 250kN/m which compares favourably with that obtained from the Rusch and Hergenroder approach.

Transversely the deflection measurements would indicate a moment My of the order of 150kN/m, a figure which again is comparable with the isotropic slab method.

10. CONCLUSIONS

Whilst there is no comparable load test data for the bridge deck in its original unstrengthened state it is highly probable that the equivalent effective span would have been much nearer that of the primary box beams. The strengthened deck has behaved in a far better manner than that predicted by grillage analyses and, for the particular vehicular loading position, approaches quite closely the characteristics of an isotropic slab.

Whilst, in retrospect, it may be felt that the bridge may have been over-strengthened, the comparative ease and economy with which this was done has more than justified the approach taken.

11. ACKNOWLEDGEMENTS

The work of evolving the strengthening proposals and their implementation was carried out by the South Yorkshire County Council as agents for the U.K. Department of Transport and thanks are expressed to the County Engineer, John F. Kirkham for his encouragement at all stages of the project and for permission to publish this paper.

REFERENCES

(1) British Standard 153; 1954 Part 3A - Loads.

(2) P.C.D.G. Standard beam sections for prestressed concrete bridges (2) Barsection beams for span from 40ft. to 85ft. Prestressed Concrete Development Group. November 1963.

(3) F.W. GIFFORD "Tests on a Prestressed Concrete Hollow-box Bridge Deck" Magazine of Concrete Research Vol. 13 No. 39. November 1961.

(4) R. JONES, R.N. SWAMY, J. BLOCHAM and A. BOUDERBALAH "Composite behaviour of concrete beams with epoxy bonded external reinforcement" The International Journal of Cement Composites Vol. 2 No. 2 May 1980.

(5) R.N. SWAMY and R. JONES "Technical Notes - Behaviour of plate reinforced - concrete beams subject to cyclic loading during the hardening". The International Journal of Cement Composites Vol. 2 No. 4. November 1980.

(6) H. RÜSCH and A. HERGENRÖDER "Einflussfelder der Momente schiefwinkliger Platten" English translation - Cement and Concrete Association 1962.

Leere Seite
Blank page
Page vide

Technischer Fortschritt im Metallbau in der UdSSR

Technical Progress in the Metal Construction

Progrès technique dans la construction métallique

N.N. STRELETZKI
Prof. Dr.
Melnikow-Institut
Moskau, UdSSR

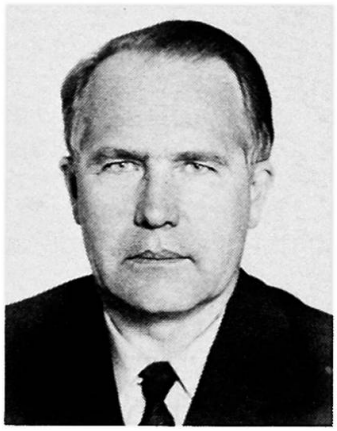

N.N. Streletzki wurde 1921 geboren. Nach dem Studium am Moskauer Bauinstitut war er als Projektierungsingenieur angestellt. 1948 fing er an, Lehr- und Forschungsarbeiten zu führen. Er hat Veröffentlichungen für Metallbrücken, Verbundkonstruktionen, Grenzzustände und ist der Autor vieler Bauwerke. Zur Zeit ist er der Abteilungsleiter für Ingenieurbauwerke.

ZUSAMMENFASSUNG

Die Verwendung von Stahl höherer Festigkeit, die Ausführung hybrider Trägersysteme, die Anwendung des Prinzips der Funktionsvereinigung, die Entwicklung von Rohrleitungsbrücken und die Vervollkommnung geschraubter Verbindungen werden unter dem Aspekt der Stahleinsparungen und der Arbeitsaufwandverminderung betrachtet. Der Wirkungsgrad dieser technischen Entwicklungen wird durch die Anwendung von Grenzzuständen für die Verformungen in der Bemessung von Tragwerken bedeutend erhöht.

SUMMARY

Steel strength improvement, using of hybrid beams, realization of the principle of structures functions combination, development of pipeline bridges, improvements of bolted connections are briefly described from the point of view of steel saving and reduction in labour consumption. Efficiency of the most part of these fields of technical progress is significantly increased by application of the limit state deformation criterion at the structural strength predictions.

RESUME

Dans l'optique de l'économie de l'acier et de la réduction de la quantité de travail, l'article passe en revue l'augmentation de la résistance de l'acier, l'utilisation des poutres bimétalliques, la réalisation du principe de la cumulation des fonctions, le développement des ponts-aqueducs, le perfectionnement des assemblages boulonnés. Le progrès technique augmente considérablement grâce à l'utilisation du critère déformatif de l'état limite dans les calculs de la résistance.

Die Besonderheit der Sowjetschule der Stahlkonstruktionen ist die Stahlökonomie und die Verringerung des Arbeitsaufwands bei der Sicherung der Betriebsanforderungen. Die Periode eines intensiven technischen Fortschritts im Metallbau der UdSSR dauert schon etwa 20 Jahre.

1. ERHÖHUNG DER FESTIGKEIT DER STÄHLE

Einer der wirksamen Wege der Metalleinsparung ist die Erhöhung der Festigkeitseigenschaften der Stähle, der Übergang von niedriggekohlten (Fliessgrenze von 23–24 kp/mm^2) zu niedriglegierten (Fliessgrenze von 29–40 kp/mm^2) und hochfesten (Fliessgrenze von 45–60 kp/mm^2 und höher) Stählen. In der UdSSR werden niedriggekohlte Stähle für Metallbrückentragwerke praktisch nicht mehr verwendet. Anstatt ihrer sind jetzt niedriglegierte Stähle in Gebrauch. Im Industrie- und Zivilbauwesen sind vorläufig niedriggekohlte Stähle vorherrschend, aber es gibt schon neue billige und effektive niedriglegierte und hochfeste Stahlsorten, besonders mit einer karbonitriden Verfestigung, die immer weitere Verwendung finden.

Die Effektivität hochfester Stähle kann sich bekanntlich in jenen Elementen verringern oder sogar völlig verschwinden, wo nicht die Festigkeitsberechnung sondern die Stabilitäts-, Ausdauer- oder Steifigkeitsberechnung bestimmend ist, oder wo die Festigkeitsreserven nicht völlig benutzt werden. Dementsprechend bilden eine wichtige Richtung des technischen Fortschritts Konstruktionen aus Stählen verschiedener Festigkeit, Gibridstahlkonstruktionen und insbesondere Gibridstahlträger. In der UdSSR werden Gibridstahlträger weit als Kranbalken und teilweise im Brückenbau verwendet.

Die Gibridstahlträger zeigen bei einem Fliessgrenzeunterschied verwendeter Stähle von 1,4–1,8 mal eine Metallaufwandverringerung von 12–18% und einen Kostenaufwand von 3–8% gegenüber den nichtgibriden Stahlträgern aus entsprechend weniger oder mehr festen Stählen.

2. PRINZIP DER FUNKTIONSVEREINIGUNG

Das Hauptprinzip des Entwerfens im Metallbau der UdSSR ist heute das Prinzip der Funktionsvereinigung der Konstruktionsteile. Diese Lösung kann manchmal eine grössere Stahleinsparung und Arbeitsaufwandverringerung geben, als das klassische Prinzip der Materialkonzentrierung.

Ein kennzeichnendes Beispiel erfolgreicher Realisierung des Prinzips der Funktionsvereinigung in Metallkonstruktionen der Industriegebäude sind Kranbahnunterzugbinder (Abb. 1), die Funktionen der Unterzugbinder und der Kranbalken bei einem Säulenabstand von 24–48 m effektiv vereinigen. Das Tragsystem wird durch kombinierte Gittergurte gebildet, mit einem starren Untergurt, der gut auf örtliche Biegung und Verdrehung beansprucht ist.

In modernen Metallbrückenkonstruktionen, die in der UdSSR entworfen und gebaut werden, dominiert das Prinzip der Funktionsvereinigung in mehrerem Masse als in Industriebaukonstruktionen. Im Brückenbau wird dieses Prinzip oftmals durch die Vereinigung

(oder die Mitwirkung) der Fahrbahn und der Hauptträger realisiert.

In getypten geschweissten und geschraubten Gittertragwerken der Eisenbahnbrücken mit nicht durchlaufender Brückenspannweite von 33 m bis 110 m und durchlaufender Brückenspannweite bis zu 176 m, wird eine effektive Mitwirkung der Fahrbahnlängsträger und der Hauptträgergurte, die in der Höhe der Fahrbahn liegen, gesichert. Das wird dank HV-Schrauben in allen Kreuzungspunkten der Längsverbanddiagonalen und der Längsträgergurte und zusätzlichen Spreizen 1 zwischen einigen dieser Knoten (Abb. 2) erreicht, was in der Fahrbahnhöhe nichtveränderliche horizontale Fachwerkdiaphragmen bildet. Dementsprechend geht ein Teil der Kräfte von Bindergurten in Längsträger über, die Gurtquerschnitte werden bedeutend erleichtert und die Längsträger erschweren sich nicht bedeutend. Die Stahleinsparung beträgt mindestens 5% von der Masse eines Brückentragwerks. Gleichzeitig werden sich die Sicherheit und Dauerhaftigkeit des Tragwerks erhöht. Das geschieht dank der Beseitigung einer intensiven Biegung der Querträger in der Horizontalebene und gleichzeitig der Gefahr ihres Ermüdungsbruchs. Das Fehlen von Bremsverbänden, längs-beweglichen Lagerungen in Längsträgern, längs-beweglicher Aufhängung der Verbände an Längsträger macht das Brückentragwerk nicht so kompliziert. Es ist ein Freivorbau vorgesehen, und die Mitwirkung der Längsträger erlaubt Deckelemente als Verfestigung der Bindergurte zu vermeiden.

Alle modernen metallischen Autobahnbrückentragwerkkonstruktionen (mit Verbundträgern, mit Stahlorthotropplatten, kastenförmige, in der UdSSR weit verwendete kombinierte Brückentragwerke mit Versteifungsträgern oder steifen Gurten in der Fahrbahnebene) sind praktisch auf dem Prinzip der Funktionsvereinigung der Hauptbinder, der Fahrbahn und der Verbände gegründet. Die Stahleinsparung beträgt hier dank dem Prinzip der Funktionsvereinigung 10-20%.

3. ROHRLEITUNGSBRÜCKEN

Im Zusammenhang mit Metallbrückenkonstruktionen sei eine neue Richtung des technischen Fortschritts - Rohrleitungsbrücken - als vollkommen neue Kategorie der Brückenkonstruktionen genannt. Die Rohrleitungsbrücken zur Übergabe von Erdgas, Erdöl, Erdölprodukten, Ammoniak und vielen anderen Produkten werden in der UdSSR immer breiter verwendet. Manchmal werden bei der Kreuzung von Wassersperren Überwasserkreuzungen als Rohrleitungsbrücken gebaut.

Eine wichtige Besonderheit der Rohrleitungsbrücken besteht in relativ geringen Nutzbelastungen. Das bestimmt die Wirksamkeit grosser Spannweiten und die Bevorzugung der Hänge- oder Schrägseilkonstruktionen. Die kleine Breite einer Rohrleitungsbrücke macht die Einrichtung spezieller vorgespannter Windträger oder Abspannungen notwendig, die sehr selten für Brücken anderer Zweckbestimmung verwendet sind.

Bei Spannweiten von weniger als 250 m werden Rohrleitungsbrücken mit Berücksichtigung örtlicher Verhältnisse als äusserlich schublose Seilträger- oder Hängekonstruktion mit vertikalen Aufhängungen verwendet. Bei Spannweiten von mehr als 250 m wird eine gewöhnliche Schubhängekonstruktion mit geneigten Aufhängungen,

die eine erhöhte aerodynamische Standsicherheit hat, gebraucht. Die sehr wirksamen Rohrleitungsbrücken als steife durchhängende Fäden finden wegen ihrer nicht völlig erlernter Sicherheit eine begrenzte Verwendung; für diese Fäden werden produktleitende Rohre genutzt. Produktleitende Rohre können als Versteifungsträger einer Hänge- oder Schrägseilkonstruktion genutzt werden. Die produktleitenden Rohre als Teil des Tragwerks einer Rohrleitungsbrücke werden in der UdSSR nur für Brücken mit nichtmagistralen Niederdruckrohrleitungen verwendet.

In der UdSSR ist eine effektive Bauform der Hängerohrleitungsbrücken ausgearbeitet. Sie besteht aus gespreizten Hängehauptbinder mit geneigten Aufhängungen, aus einem räumlichen gitterförmigen Versteifungsträger aus Rohrelementen und aus vorgespanntem Windsystem mit Seilwindgurten, die an der Ufer verankert und am Versteifungsträger in der Mittelspannweite befestigt werden (Abb. 3). Diese Bauart ist für Rohrleitungsbrücken über den Amudarja bei Kelif mit einer 660 m- Spannweite, über den Dnepr bei Saporoshje mit einer 720 m- Spannweite und (im Projektstadium) über den Amudarja bei Tschardshou mit einer 950 m- Spannweite verwendet. Diese Konstruktion ist nach dem Metallaufwand, dem hohen Montagetempo und der hohen aerodynamischen Standsicherheit sehr wirksam. Die letztere wird durch das Brückentragwerkschema und die Konstruktionsteile gesichert: rohrförmige Elementenquerschnitte, versteifungsblechlose Knoten, Fachwerkdeckplatten für Fussgängerbereiche, Verschiebung des Mittelpunkts der Rohrleitungsbiegung gegenüber des Mittelpunkts der Versteifungsträgerbiegung zwecks der Verbesserung der Schwingungsdämpfung.

4. VERVOLLKOMMNUNG DER MONTAGEVERBINDUNGEN

Der technische Fortschritt im Metallbau ist eng mit der Vervollkommnung der Montageverbindungen verbunden. Nach dem Verzicht auf Nietverbindungen werden jetzt in der UdSSR Reibungsverbindungen mit HV- Schrauben und im Industriebau - Schweissmontageverbindungen verwendet. In letzter Zeit finden eine breite Verwendung auch im Industriebau Schraubenverbindungen normaler und hoher Festigkeit. Wegen ihrer Massenverwendung brauchen Schraubenverbindungen eine Vervollkommnung und zwar, ihre Fertigungstechnologie und Rechnungsmethoden. Es sind auch neue Montageverbindungen mit HV - Schrauben interessant:

Klebestoffreibungsverbindungen - eine Art der HV- Schrauben - Reibungsverbindungen, die ermöglichen, einen hohen Reibungsbeiwert ohne aufwendige Bearbeitung der Kontaktflächen der Hauptblöcke montierender Konstruktion zu erhalten. Diese Kontaktflächen werden nur mit Stahlbürsten gereinigt. Eine spezielle Bearbeitung brauchen nur Kontaktflächen leichter Montagestosselemente - Stosslaschen und Knotenbleche. Die Kontaktflächen werden dabei sandstrahlgereinigt und mit einem Epoxidklebestoff bei dem Zusatz von Korundpulver beschichtet. Beide Operationen werden am stationären Arbeitsplatz durchgeführt.

Die HV- Tragschraubenverbindungen sind den Reibungsverbindungen gegenüber dadurch gekennzeichnet, dass sie nicht nur die Reibung, sondern auch das Quetschen und die Scherung benutzen. Die Schrauben werden so wie in Reibungsverbindungen auf kontrollierenden Zug beansprucht. Die durch die Schraube aufgenommene Zugkraft wird wegen der Quetsch- und Scherfestigkeit bei dem Scherverschi-

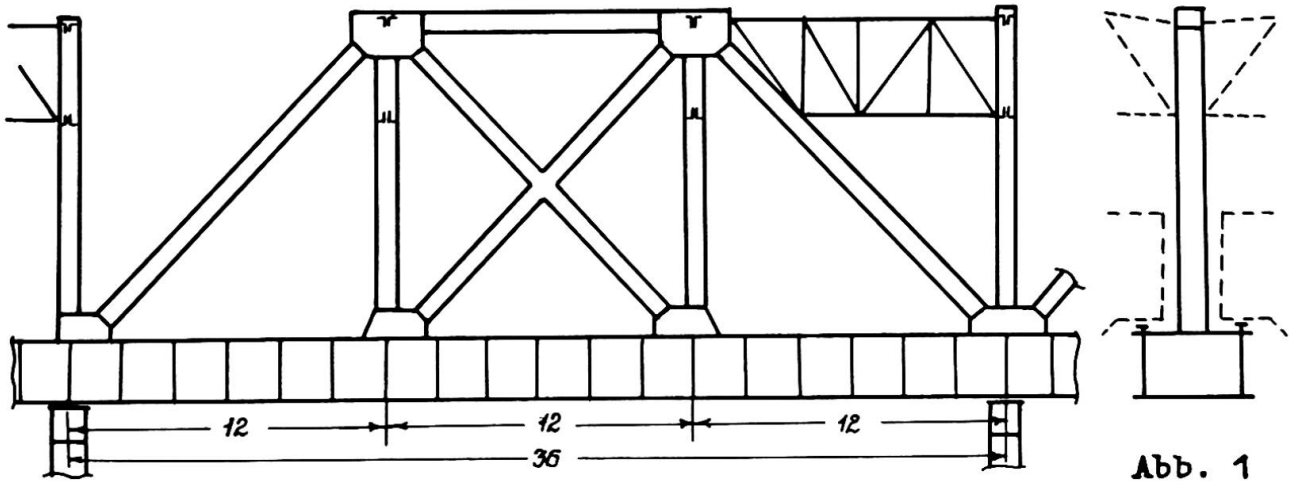

Abb. 1

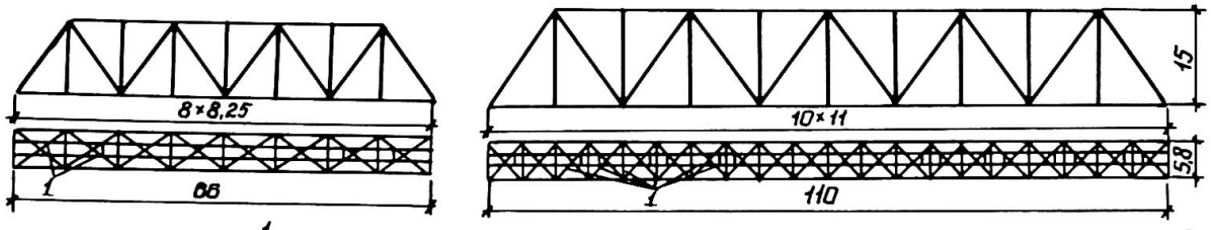

Abb. 2

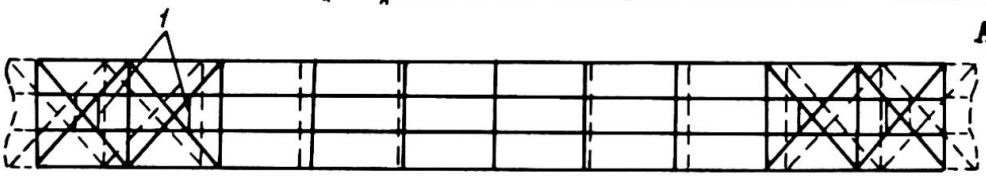

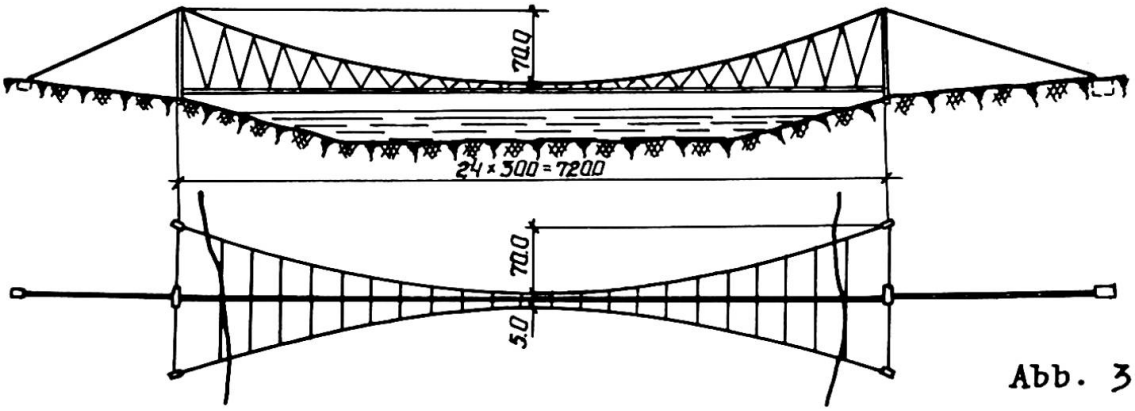

Abb. 3

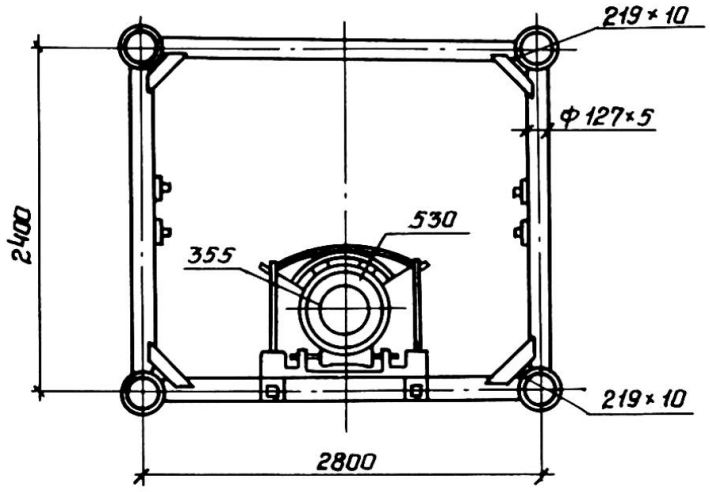

eben nach der Überwindung der Reibungskräfte vergrössert. Demzufolge sind Tragschraubenverbindungen mehr verformungsfähig als Reibungsverbindungen, aber etwas weniger als Verbindungen, die nur auf Quetschen und Scherung beansprucht werden. Im Ausland sind Tragschrauben nur bei minimalem Durchmesserunterschied für Löcher und Schrauben (etwa 0,3 mm) verwendbar. In der UdSSR ist experimentell und theoretisch die Möglichkeit und Effektivität der Verwendung von HV- Tragschraubenverbindungen bei dem Unterschied nominaler Durchmesser bis 3 mm begründet. Die HV-Tragschraubenverbindungen haben ihre praktische Verwendung bekommen, die Schraubenzahl wird dort den Reibungsverbindungen gegenüber im Mittel um 40% vermindert, wobei die aufwendige Bearbeitung aller Kontaktflächen durch eine einfache Bürstenreinigung versetzt wird. 1983 wurde der Bau eines grossen Autobahnbrücke über den Istra mit HV- Tragschraubenmontageverbindungen beendet.

Die geschraubten Schweissverbindungen stellen eine kombinierte Benutzung der Reibungsverbindungen mit HV- Schrauben und dem Montageschweissen dar, was bei der sehr geringen Verformungsfähigkeit der Reibungsverbindungen ganz möglich ist. In der UdSSR werden bei vollwandigen, freivorgebauten Brücken Schrauben-Schweissstösse der Haupttrager mit Reibungsverbindungen für Stege mittels Decklaschen und dem Autoschweissen für Gurte breit verwendet. Die Schraubenstossverbindungen für Stege bestimmen die Einfachkeit des Freivorbaus und der Verzicht auf Schraubenlöcher und auf Decklaschen in Gurtstössen führen zu einer wesentlichen Stahleinsparung.

5. VERFORMUNGSKRITERIEN IN DER FESTIGKEITSBERECHNUNG

Eine wirksame Möglichkeit der Metalleinsparung in der UdSSR ist die Vervollkommnung der Normen- und Berechnungsmethoden von Stahlkonstruktionen. Die Verwendung der Verformungskriterien in der Festigkeitsberechnung führt zu einer höheren wirtschaftlichen Wirkung bei der Verwendung des Prinzips der Funktionsvereinigung, der Verwendung der Gibridstahlträger und der Vervollkommnung der Schraubenverbindungen.

Bei dem Festigkeitsnachweis der Elementenquerschnitte der Stahlkonstruktionen und Stahlbrücken begann es, in der UdSSR das Verformungskriterium begrenzter plastischer Verformungen zu benutzen, was für viele Konstruktionen zu einer grossen Stahleinsparung führt, im Vergleich zu früherem Kräftekriterium des Randfliessens. Als Festigkeitsgrenzzustand gilt jetzt die maximale relative plastische Verformung (im komplizierten Spannungszustand - Intensität plastischer Verformungen), die unter Grenzlasten entsteht und in Grenzen von 0,001 bis 0,004 begrenzt ist, abhängig von Arbeitsbedingungen der Konstruktionen. Diese Begrenzungen schliessen ausserordentliche Restverschiebungen aus und begrenzen so die Neigung, dass im Grenzzustand keine bemerkenswerte Minderung der Kältebeständigkeit, Bruchfestigkeit und anderer Stahleigenschaften im Grenzzustand vorhanden sind; die Begrenzungen im Bereich von 0,001-0,0015 gewährleisten auch die Anpassungsfähigkeit unter beweglichen Belastungen.

Es wurden zwei Festigkeitsberechnungsmethoden nach Kriterien begrenzter plastischer Verformungen ausgearbeitet: unmittelbarer Nachweis maximaler plastischer Verformungen mit Computer-Hilfe und der Nachweis relativer Beanspruchungen, die sich bei der

Einführung tabulierter Ausgleichswerte zu Widerstandsmomenten ergeben, die ihrerseits die begrenzte Entwicklung plastischer Verformungen berücksichtigen. Die Berücksichtigung begrenzter plastischer Verformungen gewährleistet folgende Verminderungen der Querschnittsflächen: bei der Biegung symmetrischer Querschnitte - 3-6%, für asymmetrische Querschnitte und bei der Biegung mit einer Axialkraft - 8-12%, bei der schrägen Biegung und Verdrehung - 12-20%.

Die Verwendung des Prinzips der Funktionsvereinigung, die Präzisierung der Berechnungssysteme, verbunden mit der Computer - Verwendung, und der Übergang zu räumlichen Berechnungssystemen führen zur Feststellung der Überbeanspruchungen in einzelnen Punkten der Bauteilquerschnitte. Bei der Randfliessenberechnung führt das zu einer Erschwerung der Konstruktion, und der Übergang zum Kriterium begrenzter plastischer Verformungen vernichtet vollkommen diese paradoxale Erschwerung.

In bezug auf Schraubenverbindungen ermöglicht das Verformungskriterium des Grenzfestigkeitszustandes in Form der Begrenzung der Schubverschiebung durch einen Grenzwert, Quetschenberechnungen grundsätzlich zu vervollkommnen. In üblicher Form des Spannungsnachweises über Diametralquerschnitt haben diese Berechnungen äusserst bedingten Charakter. Der Übergang zum Verformungskriterium erlaubt in vielen Fällen die erforderliche Schraubenzahl zu vermindern. Das Verformungskriterium ist in HV- Tragschraubenberechnungen schon erfolgreich verwirklicht.

Leere Seite
Blank page
Page vide

Conclusions to Seminar I
Hybrid and Composite Structures

Renaud FAVRE
Professor
Swiss Fed. Inst. of Technology
Lausanne, Switzerland

Five papers were presented orally at this session by Messrs. S. Hamada, Japan; U. Girhammar, Sweden; L. Paulik, France; T. Yamasaki, Japan; and M. Collins, Canada.

It is evident that structures composed of different materials have good prospects in the future. One disadvantage may arise when the use of different materials needs different contractors on the building site. But usually it will be the same contractor who does the whole work.

One of the main problems concerning hybrid structures comes from the connections. As several speakers underlined, the connection between concrete and steel elements, or between wood and concrete or wood and steel elements, needs careful attention by the designer. Actually, most research concerns only the short time behaviour to verify the ultimate resistance of the structure. But there will be many problems in relation with the serviceability and durability, taking into consideration the time effects.

This seminar gave some examples with good slides of actual hybrid structures and laboratory tests. Specially the building possibilities of wood with concrete or steel with concrete, gave rise to many questions during the discussion following each contribution.

Finally it is worth knowing that in Macon, France, a bridge will be tendered for by 8 selected contractors with the obligation to choose a composite girder cross-section with concrete for the slabs and steel for the web or truss. The idea is to promote new ideas and to realize them in the scale 1 : 1.

Leere Seite
Blank page
Page vide